

https://dspace.org/

Investigation of the mechanisms responsible for high speed impact crusher performance

Mokgomola,Tebogo

2022

https://hdl.handle.net/10539/34906

Downloaded from a DSpace repository. https://dspace.org/



UNIVERSITY OF THE
WITWATERSRAND,
JOHANNESBURG

Investigation of the Mechanisms Responsible for High Speed Impact Crusher Performance

MSc Dissertation

Prepared by

Tebogo Mokgomola

812478

Submitted to

School of Chemical and Metallurgical Engineering, Faculty of Engineering and the Built Environment, University of the Witwatersrand, Johannesburg, South Africa

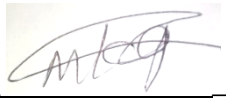
Supervisor(s):

Mr. Kitungwa Kabezya and Dr. Mulenga Bwalya

November 2021

Declaration

I declare that this thesis is my own, unaided work. It is being submitted for the Degree of Master of Science in the University of the Witwatersrand, Johannesburg. It has not been submitted before for any degree or examination in any other University.

Signed______

_15_____ Day of __November____ (Year) __2021___

Abstract

This thesis is an appraisal of developmental work done on an impact crusher. This work covered spans of contributions from a few student projects, whose data is used to evaluate the performance of impact crusher. To do this some drop weight tests were done on two material types, quartz and limestone. Milling kinetics studies were also done on these two materials in a batch ball mill to determine the breakage and selection function. DEM simulation was used to evaluate and compare ball milling crushing mechanism with that of single rotor impact crusher under various operating conditions: rotor speed and feed size distribution.

The results showed crushing or grinding rate increased with rotor speed, as well as the number of repeated passes to re-crush the product. This naturally suggested an improved design by introducing an additional rotor to correspond to two passes on each batch test. To evaluate the design prior to building the re-designed crusher, discrete element method (DEM) simulation was done to generate the data that was used to compare the current design (single-rotor) with the new (double-rotor). According to DEM simulation output, the double rotor crusher has a potential to more than double the performance at relatively lower rotor speed as it shifts the impact energy spectra into more effective breakage region.

Acknowledgements

I would like to acknowledge the following individuals for their contribution to this work either directly or indirectly:

- My supervisors Mr. Martin Kitungwa Kabezya and Dr Mulenga Murray Bwalya for their guidance, support, and all efforts they put in correcting my work and challenging my views. Above all, I am thankful for the bond that has been created.

- Wits merSETA for the funding of this research project.

- Sancho Nyoni, Mohammed Dajee, and Cedric Mvula for conducting all important experiments used in this collaborative work.

- My family, friends, and the Christian action fellowship church (CAF) for all the support, words of encouragement, and prayers.

And most importantly the Lord Jesus Christ for His grace and love that carried me through this journey.

Table of contents

Declaration 1

Abstract 2

Acknowledgements 3

Table of contents 4

List of figures 6

List of tables 8

Nomenclature 10

Chapter 1: Introduction 12

Chapter 2 : Literature review 16

2.1. Crushers and breakage mechanisms 16

2.2. Impact crushers 17

2.2.1. Impact crusher description 17

2.2.2. Types of impact crushers 18

2.2.3. Modelling on classification and breakage functions 20

2.2.4. Modelling on energy per unit mass, capacity, rock properties and shape in impact crushing 22

2.2.5. Effect of shape and size of particles 23

2.2.6. Method (DEM) for Modelling using discrete element impact crushers 28

2.2.7. Impact crushing of harder materials 39

2.2.8. Automatic control of impact crushers 40

2.2.9. Modelling of impact crusher performance 42

2.2.10. Impact energy per unit mass in hammer (horizontal shaft-like) impact crusher 44

2.2.11. Kinematics of hammer rotation 45

2.3. Material property and tests 46

2.3.1. Bond test 47

2.3.2. Selection and breakage function tests 48

2.3.3. Drop weight test 51

Chapter 3 : Lay out Experimental work 52

3.1. Drop weight test 53

3.2. Ball milling 55
3.3. DEM simulation 58
3.3.1. DEM simulation of ball mill impact spectra 58
3.3.2. DEM simulation of impact crusher 58
Chapter 4 : Results and discussion 62
4.1. Drop weight tests 62
4.1.1. Limestone and quartz probability of breakage model parameters 67
4.1.2. Quartz and limestone probability of breakage comparison 67
4.1.3. Specific Threshold energy comparison between limestone and quartz 70
4.2. Ball milling 73
4.2.1. Selection function 73
4.2.2. Breakage function 79
4.3. DEM simulation 86
4.3.1. DEM simulation of ball mill energy spectra Versus impact crusher energy spectra 86
4.3.2. Improving a single rotor impact crusher design by adding a second rotor using DEM simulation 90
Conclusion 97
Recommendations 99
References 100
Appendices 108
Appendix A: Drop weight tests data 108
-19+16mm size class breakage data 109
-13.2+11.2mm size class breakage data 113
-9.5+6.7mm size class breakage data 117
Drop weight probability of breakage parameters modelling 120
Appendix B: Ball milling data 123
Mass distribution and selection function data for ball milling 123
Breakage function data 130

List of figures

Figure 2.1: Horizontal shaft impact crusher 19
Figure 2.2: Vertical shaft impact crusher 20
***Figure 2.3**: Representation of the decomposition of the contact force to normal and tangential components* (Labra et al., 2012) 29
Figure 2.4: Contact interface model (Labra et al., 2012) 30
Figure 2.5: Spring and Dashpot Model between two particles (Stiehm et al., 2016) 32
Figure 3.1: Drop weight Test Apparatus 53
Figure 3.2: 13.2+11.2mm size class of Limestone 53
Figure 3.3: Mill chamber on rollers 55
Figure 3.4: 20 and 30mm balls, quartz and lifters inside the mill 56
Figure 3.5: Single rotor design made up of 4 hammers, particles and the Cone Feeder from DEM 59
Figure 3.6: Double rotor impeller design with a bottom and upper impeller 60
Figure 3.7: Double rotor impact crusher design 60
Figure 4.1: probability of breakage versus no. of breakage attempts for particle size 2 at heights 1 and 3 energy inputs 65
Figure 4.2: Probability of breakage versus Mass to compare Limestone and Quartz and E = 1J and n = 1 68
Figure 4.3: Probability of breakage versus Mass to compare Limestone and Quartz and E = 1.8J and n = 1 69
Figure 4.4: Plot of Threshold energy comparison between quartz and limestone 71
Figure 4.5: Plot of logarithm of weight fraction retained versus time 74
Figure 4.6: Experimental and model selection function values for quartz 76
Figure 4.7: Selection function comparison between quartz and limestone (Mvula, 2018) 78
Figure 4.8: Experimental breakage function versus normalized particle size for size class -13.2 + 9.5mm quartz 81
Figure 4.9: Experiment and model breakage function versus normalized particle size for quartz size class -13.2 + 9.5mm 82
Figure 4.10: Cumulative breakage function comparison between limestone and quartz using model parameters 85
Figure 4.11: Energy spectra for a single rotor impact crusher and ball milling on the same plot for particle size -19.0+16.0 mm (Dajee, 2018) 87
Figure 4.12: Energy spectra for a single rotor impact crusher and ball milling on the same plot for particle size -13.2+11.2 mm (Dajee, 2018) 87
Figure 4.13: Energy spectra showing the effect of adding a second rotor with particle size -19.0+16.0 mm at speed 1040 rpm (Dajee, 2018) 91
Figure 4.14: Energy spectra showing the effect of adding a second rotor with particle size -13.2+11.2 mm at speed 1040rpm (Dajee, 2018) 91
Figure 4.15: Energy spectra showing the effect of adding a second rotor with particle size -13.2+11.2 mm at speed 885rpm (Dajee, 2018) 92
Figure 4.16: Energy spectra showing a single rotor design at 2080 rpm and double rotor design at 885 rpm with a particle size class of -19.0+16.0 mm (Dajee, 2018) 94
Figure 4.17: Energy spectra showing a single rotor design at 2080 rpm and double rotor design at 885 rpm with a particle size class of -13.2+11.2 mm (Dajee, 2018) 94
Figure 1: Selection function graph for -6.7+4.75mm 124

Figure 2: Selection function graph for -3.35+2.8mm 125
Figure 3: Selection function graph for -1.4+1.0mm 127
Figure 4: Selection function graph for -0.85+0.6mm 128
Figure 5: Selection function graph for -0.30+0.212mm 130

List of tables

Table 2.1: Commands to control the size distribution in an impact crusher 41
Table 4.1: Breakage behaviour of size class -13.2+11.2 mm at height 22.2 cm of impact weight.....63
Table 4.2: Cumulative probability of breakage for particle size 2 at height 1 64
Table 4.3: Experimental and Model cumulative probability of breakage 64
Table 4.4: Limestone and Quartz (Nyoni, 2019) probability of breakage model parameters .67
Table 4.5: Probability of breakage versus particle mass comparison between quartz and limestone at E = 1J and n = 1 68
Table 4.6: Threshold energy for quartz and limestone particles 71
Table 4.7: Size distribution results for -13.2 + 9.5mm size class. 73
Table 4.8: logarithm of weight fraction retained divided by product sampled mass versus time.....74
Table 4.9: Selection function values for each size class for quartz. 75
Table 4.10: Experimental and model Selection values for quartz 75
Table 4.11: Austin model selection function parameters 77
Table 4.12: Selection function experiment and model values for limestone and quartz 78
Table 4.13: Breakage function experimental results and model data for size class -13.2+9.5mm 80
Table 4.14: Experiment and model breakage function values for size class -13.2 + 9.5mm..82
Table 4.15: Quartz breakage function model parameters for quartz.....83
Table 4.16: Breakage function model parameters for quartz and Limestone (Mvula, 2018) .84
Table 4.17: Cumulative breakage function for quartz and limestone using model parameters 84
Table 1: Breakage behaviour of Limestone particle size 1 at height 1 109
Table 2: Particle size 1 at height 1 probability of breakage 110
Table 3: Breakage behaviour of particle size 1 at height 2 111
Table 4: Particle size class 1 at height 2 probability of breakage 112
Table 5: Breakage behaviour of Limestone particle size at height 2 113
Table 6: Particle size 2 at height 2 probability of breakage 114
Table 7: Breakage behaviour of Limestone particle size 2 at height 3 115
Table 8: Particle size class 2 at height 3 probability of breakage 116
Table 9: Breakage behaviour of Limestone particle size class 3 at height 1 117
Table 10: Particle size class 3 at height 1 probability of breakage 118
Table 11: Breakage behaviour of Limestone particle size class 3 at height 3 119
Table 12: Particle size class 3 at height 3 probability of breakage 120
Table 13: Modelling probability of breakage data for size class -19+16mm.....120
Table 14: Modelling probability of breakage data for size class -13.2+11.2mm.....121
Table 15: Modelling probability of breakage data for size class -9.5+6.7mm.....121
Table 16: probability of breakage between quartz and limestone with E = 1.8J and n = 1 ..122
Table 17: -6.7+4.75mm selection function mass distribution.....123
Table 18: -6.7+4.75mm selection function graph data.....123
Table 19: -3.35+2.8mm ball milling mass distribution.....124
Table 20: -3.35+2.8mm selection function graph data.....125
Table 21: -1.4+1.0mm ball milling mass distribution.....126
Table 22: -1.4+1.0mm selection function graph data.....126

Table 23: -0.85+0.6mm ball milling mass distribution 127
Table 24: -0.85+0.6mm selection function graph data 128
Table 25: -0.30+0.212mm ball milling mass distribution 129
Table 26: -0.30+0.212mm selection function graph data 129
Table 27: Cumulative breakage function experimental and model data for size class - 6.7+4.75mm 131
Table 28: Cumulative breakage function experimental and model data for size class - 3.35+2.8mm 132
Table 29: Cumulative breakage function experimental and model data for size class - 0.85+0.60mm 133
Table 30: Cumulative breakage function experimental and model data for size class - 0.3+0.212mm 134

Nomenclature

Symbol	Description	Units
DEM	Discrete element method	-
E	Energy	J
ton	tonnes	-
hr	hour	-
min	minutes	-
HIS	Horizontal shaft impact crusher	-
VSI	Vertical shaft impact crusher	-
Eq.	Equation	-
tph	tonnes/hr	-
Q	Volumetric Flowrate	tph
rpm	revolutions per minute	
d	diameter	m
mm	millimetre	-
m	meters	-
t_{10}	breakage index	-
kW h/t	kilowatt-hour per ton	
t	time	minutes
S_{ij}	Selection function	min^{-1}
B_{ij}	Breakage function	-
V	velocity	m/s
M	Mass of impact hammers	kg
xi	Representative particle size	mm
PS	particle size	mm
h	height	cm
E_{X0}	Minimum threshold energy	J
P_b	probability of breakage	-
n	number of breakage attempts	-
x	particle mass	g

g	grams	
g	Gravitational acceleration	m/s^2
P	Cumulative fraction of particles	-
Exp	Experiment	-
Mod	Model	-

Chapter 1: Introduction

Crushing and ball milling are the traditional route used in comminution. Role of the crusher unit is to reduce particles to a size that can be milled, while ball milling is used to produce a finished product with sufficient mineral liberation. However, for some ores other specialised equipment might work efficiently. This might be due to mineralogical characteristics of the ore, or the nature of the product that must be produced (Patnaik et al., 2007; Michaud, 2015). Here we investigated the application of high-speed impact crushing which has been a subject of rising interest in recent years as some (Nikolov, 2002; Patnaik et al., 2007; Gupta, 2011) claim high comminution efficiency can be achieved using this.

Several reports have alluded to impact crushing as being significantly more efficient than most comminution methods. High-speed Impact crushers are cost, time and energy saving. These advantages have made impact crushers to be the most used type of crushers in the last two decades (Nikolov, 2004; Patnaik et al., 2007; Borg et al., 2015).

In impact crushing, solid materials are hit with a sufficient force to make them shatter. This force comes from high speed rotating impact hammers attached to a rotor to create a rotating impeller of impact hammers. According to impact crusher literature, breakage rate is closely linked to the rotor speed, thus when rotor speed is increased more fines are produced. Literature also shows that, most impact crusher work has been conducted using a single rotor impact crusher design (Nikolov, 2002, 2004; Patnaik et al., 2007; Gupta, 2011; Jaatinen et al.,2013).

In this project, a design that involves adding a second rotor to accelerate particle breakage and achieve both higher breakage rate and number of impacts was proposed. Before building the equipment, the discrete element method (DEM) was used to simulate this new design to predict expected performance of the equipment. The two rotors have been designed to run independently, thus the rotors could be both co-rotated and counter rotated. The numerical software such as DEM is widely used to solve many engineering particle-related problems and was used in this project to get a better insight into expected performance of the double rotor impact crusher (Ketterhagen et al., 2009). The DEM version used for the simulation was the commercial PFC3D. DEM is a computer technique used for simulation of solid particles flow in various equipment under controlled conditions allowing the prediction of outputs (Cleary et al., 2014).

Dem simulation records information about contact events occurring and stores them as outputs files. This information from contact events with corresponding energy levels is applied to determine the failure rate of a particle under a stress. Contact events present the number of impacts for a particle occurring at various energy inputs. For particle failure to occur the applied stress should exceed the particle threshold energy required for failure to occur (Bwalya, 2005). To know this energy, single particle fracture tests on Ore samples were conducted using the drop weight test to produce a model that is used to predict the probability of breakage at various energy inputs. Energy spectra is the name given to the information from DEM simulation containing contact events with corresponding energy inputs.

Literature (Nikolov, 2002; 2004) showed that most of the work done on impact crusher modelling focuses on predicting the outcome of product size distribution. Other literature (Patnaik et al., 2007; Gupta, 2011) showed that much work has also been done in understanding the impact crusher performance in relation to machine configuration and operational conditions using experimental work and mathematical modelling. However, not much research has been done on velocity and energy distribution of collisions inside the crushing chamber, and thus the operating mechanisms (or crushing behaviour) in an impact crusher are still not clear (Djordjevic et al., 2003; Nikolov, 2004, Bengtsson et al., 2008). To know this in depths, impact crusher operating mechanism must be known.

Nikolov (2002, 2004) presented performance modelling for all types of impact crushers to predict distribution of the size of the product. This was developed to be applied to different types of impact crushers. Impact energy and ore flowrate were used as input variables to determine the classification and breakage functions. However, the shortcoming of the proposed modelling was, the effect of variation in feed size distribution and different material properties on the product size distribution and energy input were not taken into consideration. This paper has been discussed further in section 2.23 and the model equations in section 2.2.9.

Unland et al. (2008) presented a study to determine the influence of particle shape on impact crusher parameters by testing single particles in a high-resolution impact analysing. The study used seven different feed particle shapes as the input to determine the influence of the feed shape on the crushing parameters by measuring the contact time and force, the energy

transferred, fragment size, and shape distribution as well as the energy used by the crusher. The particles shapes ranged from spheres and cubes to plate -shaped and acicular bodies.

It was found that cubical and spherical particles have the highest contact forces and energy transferred and the lowest contact time. Spherical and cubical particles showed to have the lowest energy utilization. Energy utilization was found to be rising with increased elongation and flatness of the feed particles. Elongated and plate shaped particles had a better fracture probability and energy utilization and with this, the results found using cubic shaped particles can be used as a basis for energy saving in impact crushing (Unland et al., 2008).

Deniz (2011) presented a breakage test method to determine the effect of mean particles and bond work index of three different types of limestone on product size distribution. This method incorporates the self-similar breakage behaviours in laboratory comminution and thus can be used as an alternative to drop weight and twin pendulum tests.

It was found that different classes of limestone also have different breakage behaviours since limestone-I sample was found to be more friable than limestone-II which was more friable than limestone-III. However, the proposed breakage test method did not take into consideration the effect of feed rate, rotor speed, lining design, and impact hammers design. In overall, it was shown that the product size distribution can be different for minerals or rocks with different properties for the same class (Deniz, 2011).

Dajee (2018) investigated the advantage of having a double rotor impact crusher design using DEM simulation by varying rotor speed and feed particle size. The crusher has a vertical shaft with two rotor impellers at one end. The impellers rotate and have direct impact with the particles and thus rotor speed is used for particles breakage. Initially a single rotor impact hammers impeller crusher was used followed by the double rotor impact hammers impeller and the results found from these were compared. It was found that the double rotor impact hammers impeller design achieves more impacts at lower speeds compared to a single rotor impact hammers impeller design.

It is seen from what is discussed above that researchers continue to develop a better understanding of the comminution involved in impact crushers. However, there is no comprehensive unified model that is available. This research is an ongoing exploration to establish evidence for improved performance over conventional milling when applied on the same materials. This investigation was based on experimental work done on a single rotor

impact crusher and DEM simulations were used to determine how a single rotor impact crusher can be improved to increase production at low costs.

Aim:

- To use the Discrete Element Method (DEM) to determine if a double rotor impact crusher design will be a significant improvement over a single rotor impact crusher design.

Objectives:

- To determine the threshold energy required to break quartz and limestone using a single particle test like Drop weight tests and to compare the breakage characteristics of quartz and limestone in drop weight tests and ball milling.
- To investigate if a single rotor impact crusher will be an improvement on ball milling using DEM.
- To evaluate and compare the influence of speed on breakage in ball milling and high-speed impact crusher.

Chapter 2 : Literature review

2.1. Crushers and breakage mechanisms

Crushing is a dry process and is performed in three stages; primary, secondary, and tertiary depending on the next processing stage that follows. Crushers are available in various sizes and capacities ranging from 0.2-1400 ton/hr classified based on factors like the product size and the type of mechanism used. Three different types of crushers are jaw, cone, and impact crushers. Primary crushing usually occurs underground after mining to reduce the particle size of Run-Of-Mine-ore to be suitable for transportation. Types of crushers used for primary crushing are jaw and gyratory crushers. The product from primary crushing is further processed in secondary and tertiary crushers depending on the final desired product size. Crushers used for secondary and tertiary crushing are high pressure roll, cone, and impact crushers. Crushers are chosen based on the stage of crushing and on the size of the desired final product (Patnaik et al., 2007, Ndlovu et al., 2017; Machowski, 2015).

Particle breakage involves different types of mechanisms. These mechanisms can be cost and time saving depending on the type of crusher used and the mineralogy of the ore to be crushed. Dominant mechanisms involved in particle breakage are compression, abrasion, attrition, shear, and impact. Compression and shear are dominant mechanisms in jaw, cone, and gyratory crushers while impact, abrasion, and attrition are dominant in milling. Impact is the dominant mechanism in impact crushers (Patnaik et al., 2007; Gupta, 2011).

There are times when an alternative crusher may be used in place of the traditional cone crushers used. This may be based on the material characteristics or intended product specifications. In recent time, there are researchers who have been suggesting that the impact could enhance the crushing performance (Nikolov, 2004; Borg et al., 2015) The other rival alternative has been high pressure grinding rolls that rely on high pressure comprehension to initiate and propagate cracks efficiently as it has been shown that cleavage fracture can occur in this mechanism (van der Meer et al., 2012).

Due to the use of impact, high speed crushers have advantages over other type of crushers. Impact crushing is relevant to many fields of science and technology. Impact crushers have been applied in mineral, coal, concrete, cement, and chemical industries for a long time. High speed Impact crushers are cost, time and energy saving and because of these advantages they have become the most used type of crushers in the last two decades. Other advantages of impact crushers include high size reduction ratio, even and cubic shaped product particles, and easy modification of product size distribution (Nikolov, 2004)

Despite all these advantages, only recently have impact crushers started receiving attention in terms of modelling and simulation. Only few studies have been conducted to model how parameters such as rotor speed, feed flowrate, feed size distribution, type and size of hammers, shape of particles, material, or ore type, etc. influence energy consumption and production in impact crushers (Gupta, 2006).

Impact breakage occurs when particles, experience rapid impulsive forces causing breakage through the following means:

- **Shattering**: occurs when particle breakage results into multiple fragments due to the energy applied being in excess of the minimum energy required. Typically occurs when force loading rate is rapid (Katubilwa, 2009; Nyabando, 2014).
- **Cleavage**: occurs when particles break along grain boundaries to produce fragments of the same size as a result of the energy supplied being just enough to allow fracture to occur (Katubilwa, 2009; Nyabando, 2014).

A brief review is given on impact crushers that looks at some of the parameters that have been investigated. These include the effect of ore mineralogy, rotor speed, energy, size and shape of particles, and impact hammer or anvil properties on production.

2.2. Impact crushers

2.2.1. Impact crusher description

Impact crushers rely on rapid sharp impulsive blows for the reduction of materials instead of pressure which is used in jaw, cone, gyratory, and high-pressure roll crushers. Gupta (2011) presented that crushing in an impact crusher takes place in a shorter time duration than in jaw and cone and other crushers. This is due to the short time durations of collisions events between the hammer and the particle or, particle and particle. This results in rapid crack propagation within the particles and thus leading to fast failure of particles.

Borg et al. (2015) presented an impact crusher called the Vero Liberator. This is a dry-crushing system and consumes very low energy with high reduction ratios between 200 to >400 in a single pass. This impact crusher has the ability, in some mineral processing circuits to replace several comminution stages, thus saving energy costs. Vero Liberator does not only boost high reduction ratios but also achieves high degrees of particle liberation. This is as a result of high velocity impacts of the hammer blows inflicted onto the ore particles. In jaw and cone crushers, crushing is slow due to the use of compression and shear and thus the magnitude and nature of the forces and energy consumption are higher than those involved in high speed impact crushing (Gupta, 2011).

In an impact crusher, the material is contained in a caging that has openings on the bottom end or side and these openings are in the form of screens so that the desired size of the pulverised material can escape. Impact crushers are usually used for soft materials like, coal, limestone, seeds, or soft metallic ores. The mechanism used in an impact crusher is referred to as impact loading, the applied force time duration is less than the horizontal frequency of vibration of the body. The hammers rotating at a very high speed deliver sharp blows to particles that would lead to particle failure if particle threshold energy is exceeded. The aspect of threshold is discussed when drop weight tests are discussed (Patnaik et al., 2007).

Some impact crusher examples are hammer mills, ball mills, and stamp mills. In hammer mills, heavy metal bars are attached to the edges of horizontal rotating disks by hinges, to crush the material with ball mills using metal balls in rotating cylinders for crushing, and Stamp mills use cans to lift weighed vertical hammers which are dropped by gravity to crush the material (Patnaik et al., 2007). The impact crusher used in this research is a hammer mill type with heavy metal bars attached to a vertical rotor creating an impeller.

2.2.2. Types of impact crushers

Two distinct design types are available: horizontal and vertical impact crusher. They are classified based on the position of the rotor and the shaft. Horizontal shaft impact crushers (HSI) shown in Figure 2.1 have a reduction ratio of about 10:1 to 25:1 and they mainly used to crush extracted minerals, sand, gravels, and most metallic ores. The vertical shaft impact (VSI) crusher shown in Figure 2.2 has a lower reduction ratio of 6:1 to 8:1 compared to that of HSI and is used for sand and gravels. Vertical horizontal impact (VSI) crusher is also used in tertiary mining industries for the size reduction of hard rock materials or ores when a conical shape fine product is the desired goal (Gupta, 2011; Numbi et al., 2014).

Breakage in HSI takes place when the rock material collides with hammer bars that are fixed to the spinning rotor. The shaft rotor is aligned along the horizontal axis. When feed material is introduced into the system, breakage occurs when it hits the rotating hammers of the rotor because of the sudden impact. In VSI the rotor spins at a speed along the vertical axis operating like a centrifugal pump. Breakage occurs when the feed material hits the outer part of the crusher body at high speed and when collisions occur between the rock materials. Both HSI and VSI have performed better in suitable material than other secondary and tertiary crushers such as cone and high pressure roll due to high energy efficiency (Gupta, 2011; Numbi et al., 2014).

Verma et al., (2014) described horizontal shaft impact crushers as crushers that break rock material by impacting the material with hammers or blow bars that are fixed upon the outer cycle of a spinning rotor. In this crusher, the rotor shaft is aligned along the horizontal axis. When the material is fed, it hits the rotating hammers and due to the sudden impact, the material breaks, and further breakage occurs when the material is thrown to the breaking bars/ anvils. These crushers will tend to have a reduction ratio ranging from 10:1 to 25:1. One of the shortcomings of impact crushers include only applicable to soft and less abrasive materials (Evertsson, 2000).

Below are the images showing the difference between horizontal shaft and vertical shaft impact crushers. The images have been presented by (Stedman Company, 2018; Marcotte, 2018)



Figure 2.1: *Horizontal shaft impact crusher*



***Figure 2.2**: Vertical shaft impact crusher*

2.2.3. Modelling on classification and breakage functions

In the work conducted by Nikolov (2002), a model for impact crusher was built based on the standard matrix formulation that includes classification and breakage matrices. For this research, the product size distribution was obtained as a function of the crusher's rotor radius and angular velocity, the feed rate, and the feed size distribution. Only the variations in the product size distribution resulting from changes in rotor velocity and the feed rate were investigated. However, variations in the product size distribution resulting from rotor radius, and the feed size distribution were not taken into consideration. The model developed can also be applied on both hammer and vertical shaft impact crushers with the use of corresponding estimations for the impact energy per unit mass. The model equation has been shown and explained under section 2.2.9. below.

Here the classification functions, and the breakage functions were proposed considering the dynamic character of the impact breakage. Classification also known as selection represents the probability of a particle being broken when certain aggregate of particles is compressed. Example: only a certain portion of particles will be compressed but the classification function shows the probability that a certain particle is broken. Breakage function represents a way in which a particle is broken into smaller fragments (Whiten et al., 1979; Nikolov, 2002).

In this research, the classification function took a form of a cumulative Weibull distribution which incorporated a minimum breakable size of particles depending on the impact energy per unit mass and the feed rate. The cumulative Weibull distribution is made up of two parameters: the shape parameter (β) and the scale parameter (η). The shape parameter

represents the slope of the probability line in a plot and influences the distribution while the scale parameter can stretch the distribution if increased. This is applicable on the classification function since it shows the probability of a particle to be broken. The breakage function was modelled as the sum of two Broadbent-callout distributions. It was assumed that the function depends on impact energy and the feed rate through the expression which shows the proportion of the fine fraction in the product. The expressions showing the classification, breakage, energy per unit mass, proportion of the fine product, and the minimum breakable size were developed and the experiments were run to compare the model predictions with the experimental data for limestone treated in a pilot-plant hammer crusher (Whiten et al., 1979; Nikolov, 2002).

Using two different feed rates (Q = 2 and 7 tph) and three different rotor velocities (w = 540; 720; 900 rpm) it was found that at higher rotor velocities the size distribution of the product becomes finer and this happens when the feed rate and feed size distribution are kept constant. Alternatively, when the feed rate is increased at constant rotor velocity, the product size distribution becomes coarser (Nikolov, 2002).

From the above information, Nikolov (2002) concluded that this model can be used in the prediction of the steady state performance of hammer and vertical shaft impact crusher integrated in complex flowsheets. However, further work must be done to adopt the model for unsteady state operating regimes.

To propose a new classification function Nikolov (2004) extended his research from Nikolov (2002) by presenting an impact crusher model that predicts the product size distribution as a function of rotor strike radius and velocity, material properties, feed size distribution and the feed rate. The model was also based on the standard matrix representation and included the classification and breakage functions. Like the Nikolov (2002) work, the classification was proposed in the form of a Weibull cumulative distribution and the average size of particles undergoing breakage was assumed as a function of the impact energy and the feed rate. This new classification model equation has been shown and explained under section 2.2.9.

In both papers his papers, Nikolov (2002, 2004) used the same approach but the only difference was how the minimum breakable size (d_{min}) was calculated. The Nikolov (2002) equation had the rate constant, maximum breakable diameter (d_{max}) and the intensity factor of the particle-particle interactions while the Nikolov (2004) work had a logarithm called factor

$\beta\ (mm)$ (See Equation 2.31) related to specific particle size depending on both crusher design and the granulate properties.

The Nikolov (2004) model equation (See Equation 2.31) was tested using the same parameters previously used in the Nikolov (2002) model (See Equation 2.29) for two sets of experimental data at different feed rates and rotor velocities to simulate the process to help refine the equation. It was found that parameters such as the fine product fraction (φ) and the shape parameter (k) could not be kept as constants. It was found that the shape parameter (k) depends on the rotor velocity, in other words related to impact energy. Nikolov (2002) did not assume the above parameters as constants but had the breakage function as a sum of two Broadbent-callout distributions and the thus a fine fraction was dependent on the impact energy, feed rate, and the shape parameter (k) depending on the impact energy and the experimental law for the minimum breakable size (d_{min}).

Overall, both predictions agreed that at a fixed feed rate, the product size distribution is finer at higher rotor velocities and when the feed rates are higher at fixed rotor speed, the product size distribution is coarser. It was also found that the impact energy per unit mass in vertical shaft impact crushers is greater than that of horizontal shaft impact crusher. From the work above, it was concluded that, the Nikolov (2002) experimental based functions worked better than the more detailed ones (Nikolov, 2004).

2.2.4. Modelling on energy per unit mass, capacity, rock properties and shape in impact crushing

Bengtsson et al. (2008) introduced the studying of capacity, power, and particle size distribution in vertical shaft impact (VSI) crushers. The study presented the use of feedrate to determine crusher capacity, and velocity, inlet and output flowrate of material in and out of the crusher chamber, to calculate power consumption in an impact crusher.

Input parameters were simulated recording capacity and power consumption for different flow rates and speed. It was found that crusher capacity decreased with increasing speed and power consumption was directly proportional to speed. In conclusion the study was successful in determining power consumption in the crusher (Bengtsson et al., 2008). Power depends on mass flowrate and angular velocity as defined by

$P = M \times \omega$ ..... E.q. 2.1

where: M= Mass flowrate (kg/s)

ω = angular velocity (rad/s)

This model did not take into consideration the underlying mechanisms of rock breakage and does not also predict the product size distribution and a desirable particle shape; thus, improvement is needed to incorporate theses parameters.

Rock material type was taken into consideration and it was concluded that breakage behaviour depends on the rock type. Rocks can be classified as gneiss, graphite etc. but just because some rocks belong to a certain group does not mean that they will have similar characteristics. For example, gneiss rocks contain different mineral quantities and their anisotropy also takes on different values. This shows that it is not easy to assume that a certain model can be used to describe the properties for certain class or group of rock. Rock similarity can only be used as a guide to predict how rocks within a certain class will break (Bengtsson et al., 2008).

On the shape of the product particles, Klingberg (2001) and Bengtsson et al. (2008) all concluded that crusher settings affect the shape of the particles of the product. Klingberg (2001) showed that the properties of a crushed rock can only be improved when crushing parameters are set in a way that the product is as cubical as possible.

Again, under the class of rocks with different properties, Deniz (2011) presented a study in impact crushing to determine the effects of mean particles and bond work index of three different types of limestone on product size distribution. This model equation used incorporates the self-similar breakage behaviours in laboratory comminution and thus could be used as an alternative to drop weight and twin pendulum tests.

The experiments were conducted, and it was found that different classes of limestone also have different breakage behaviours since limestone-I sample was found to be more friable than limestone-II which was more friable than limestone-III. However, the study did not take into consideration the effect of feed rate, rotor speed, lining design, and impact hammers design. Overall, this study showed that the product size distribution is different for minerals or rocks with different properties even though feed size same class was the same (Deniz, 2011).

2.2.5. Effect of shape and size of particles

Unland et al. (2008) discussed sizing and designing of impact crushers. The crushers are sized and designed based on the feed parameters and the desired product parameters. The

feed parameters include: the type of the material to be crushed, the mass flowrate, and the size or diameter and the moisture content of the feed particles while the desired product parameters are the final product particle size and shape distribution. System parameters such as the wear rates of the crusher parts and hammers as well as the specific energy consumption of the crusher must also be taken into consideration.

Sizing of impact crushers cannot be specifically determined and assumed to be the same for every material, but it is mainly based on experience. This is because of the difficulty experienced when measuring certain parameters such as the energy transferred between the particles fed and the impact bars or hammers of the crusher (also known as the contact forces). Another important reason is the lack of systematic investigations, for example: the effect of the particle size feed on crusher parameters is hardly known (Rumpf, 1973; Schönert et al., 1984; Unland et al., 2004).

To solve this problem Unland et al. (2008) studied the influence of particle shape on impact crusher parameters by testing single particles in a high-resolution impact analysing. The experiment involved the use of seven different feed particle shapes as inputs to determine the influence of the feed shape on the crushing parameters by measuring the contact time and force, the energy transferred, fragment size, and shape distribution as well as the energy used by the crusher. The particles shapes ranged from spheres and cubes to plate -shaped and acicular bodies.

A test apparatus and a test program were developed to determine the system and the product parameters. The material used was a Triassic limestone and it was crushed in a hammer crusher with a container and a vibrating feeder. The crusher was consisting of a rotor with two bars of hardened steel connected to a motor. After all simulations, it was shown that the measured parameters were all different based on the shapes of the feed particles. Unland et al. (2008) presented that these differences are due to additional orientation phase of an irregularly shaped particle prior to the main impact.

It was found that cubical and spherical particles have the highest contact forces and energy transfer within the lowest contact time. This suggests the significance of particle shape when testing impact crusher performance. When it comes to the product size distribution, sphere particles recorded the lowest for both the upper diameter and size modulus of a truncated Rosin-Rammler-Sperling-Bennet distribution and there was also no clear trend in respect to the distribution modulus (Wagner, 2005; Unland et al., 2008).

When comparing the fragment shape distributions, it is shown that the particle shape of the feed only has a huge influence of the coarser fragments and hardly on smaller fragments. Cubical, acicular, and plate-shaped bodies showed to have the highest energy utilization compared to other shapes. Energy utilization was found to be rising with increased elongation and flatness of the feed particles. Elongated and plate shaped particles had a better fracture probability and energy utilization and with this, the results found using cubic shaped particles can be used as a basis. Unland et al. (2008) presented that on spherical shapes, central impacts occur while with irregular shapes the impacts are eccentric and results in an angular impulse.

For shape recommendations, it was found that sphere and cubical irregular shaped particles were the most difficult to crush. Plate-shaped or elongated particles can produce small fragments at a low energy utilization compared to cubic and sphere-shaped particles. Stress effect superimposes the energy effect. The contact time of irregularly shaped particles is higher than that of sphere-shaped particles. This is because impact with spherical particles is planar whereas with irregular shaped particles the impact bar collides with the corners and edges of the particle. Then upon particles rotation, planar collision would follow resulting in breakage. Contact time for irregular particles is thus long due to phase orientation (Unland et al., 2008).

However, Unland et al. (2008) did not consider different feed mechanisms such as using a manual feed hopper and did not study the effect of product fineness on energy consumption in more detail. The effect of the radius of the rotor and the mass of the bars was not determined and since they also depend energy consumption by the crusher it would be better determine them when the effect of product fineness on energy consumption is determined. The effect of different material properties was not also determined since only limestone was used. In the experiment to be conducted there will be a different feeding mechanism and two different materials will be used so that a model can be derived for different type of rocks and minerals.

Norazirah et al. (2016) presented the study of how the size and shape of particles affect the breakage characteristics of minerals through the use single breakage experiments in drop weight tests. Different sizes of particles were used along with two different shapes of particles (Flaky, and equidimensional). In this experiment the relationship between specific comminution energy level and the breakage index number (t_{10}) was established based on size

fraction, so that the variation in impact breakage characteristics of different particle shapes can be observed. The following equation first presented by Napier-Munn et al. (1996) was used to establish the relationship above:

$$t_{10} = A \times \left(1 - e^{(-E_{cs} \times b)}\right) \quad \text{Eq. 2.2}$$

Where:

t_{10} = breakage index defined as the progeny percent passing one tenth of the initial mean particle size,

E_{CS} = the specific comminution energy (kW h/t), and

A = Maximum degree of breakage

b = parameter of hardness

The experiments were conducted using different size classes at different particle shapes to observe the breakage characteristics of different shapes at certain particle sizes. The degree of breakage t_{10} obtained from the relationships between t_{10} and t_n-family cures can be used to generate a size distribution which will be used to observe the behaviour of particles during breakage (Özer et al., 2012).

Breakage characteristics of any material depend on physical properties such as shape and size. The shape characteristic is increasingly an important parameter which influences the performance pf particles in mineral processing operations. The breakage process is characterized by two basic functions, selection and breakage function. Selection function (S_i) represents the fractional rate of breakage of particles in each size class and breakage function (B_{ij}) represents the average size distribution of daughter fragments resulting from primary breakage events (Norazirah et al., 2016).

In the past, researchers developed the breakage model to determine the particle size effect on breakage distribution function (Bourgeois et al., 2002; Vodel et al., 2004; Shi et al., 2007). To determine this breakage distribution, the following single particle breakage tests methods were used depending on the breakage mechanism; single impact, double impact and slow compression (Tavares, 1999; Eksi et al., 2011). Researchers used these methods to investigate the relationship between energy input and size reduction based on energy utilization to determine ways to reduce energy costs while increasing production (Mwanga, 2014). The tests methods used are the drop weight test and the pendulum test. The pendulum tests have a

slight advantage over the drop weight since it can provide additional information on the energy used to break a certain particle (Sahoo et al., 2004; Salman, 2007).

The single particle test was conducted using the drop weight procedure. Drop weight tests are represented by a particle resting on a hard surface and is struck by a falling weight (Sahoo et al., 2004). The height of the weight can be changed, and it represents the specific energy input. The breakage characteristics of particles of different shapes at different sizes can be observed when the height and the mass of the falling weight changes.

For breakage to occur, ore particles undergo fracture because of compressive stress applied on a particle until crack propagation occurs. Particles have both micro and macro flaws, and when compressive stress is applied the cracks grow rapidly until fracture occurs. King (2001) represented that before a particle undergoes breakages, deformation occurs storing elastic energy within a particle. This elastic energy assists with crack propagation, and thus it is the minimum energy required for breakage to occur. Energy must be applied to an optimum level to avoid over grinding.

The results from experiments for both sets of flaky and equidimensional particles showed that, the greater the specific comminution energy input, the finer the product. The flaky particles experienced breakage at a faster rate than equidimensional particles. This is because, the cracks tend to propagate easier in flaky particles than in equidimensional particles due to thin cross section. When flaky particles are subjected to tensile stress, they easily break into smaller particles. Equidimensional particles are rigid, and this lowers the point of loading, and thereby reducing compressive forces and hence less fines (Norazirah et al., 2016).

Particle shape has a major influence on how many breakage attempts should be applied to a particle before size reduction occurs and how much fine particles can be produced after breakage. Tavares et al. (1998) presented the study of the influence of particle shape on fracture characteristics using quartz as the testing ore sample. Their finding showed that the strength and stiffness of a particle decreases with the irregularity in shape of the particle. The further the particle is from spherical shape, and the close it is to the flat-like shape the easier it is to break at the first attempt of the drop weight test. In drop weight tests, it was concluded that particles with flaky-like structures produce finer particles while particles with non-flaky structures produce coarse particles. Particles shape does not however, affect fracture energy.

Breakage distributions for flaky particles are higher than those of equidimensional particles for every size fraction and every specific comminution energy input and from this observation it can be concluded that particle shapes do affect the breakage function. The breakage function or appearance value is lower for equidimensional particles because the initiation fracture for homogeneity particle is more complex. At the beginning, micro fibres appear, then cracks will coalesce, and then only through going rupture result. Contact forces deform the particle and cause a stress field within, which in turn initiates cracking if the stress is large (Griffith, 1921; Norazirah et al., 2016).

The effect of size on the relationship between t_{10} and E_{CS} shows that smaller particles required a higher specific energy input for breakage compared to larger particles. The degree of breakage t_{10} increased with particles size as the specific comminution energy increased. In some instances, when the specific comminution energy was 1 $\frac{kWh}{h}$ it was observed that t_{10} for 10 mm size was larger than t_{10} for 6.3mm. This is because breakage in large particles result into larger fragments due to micro-cracks acting as weak zones. The relationship between t_{10} and t_n showed a direct proportional since the increase in one led to an increase in the other and thus t_n can be used to predict size distribution which will result at any known degree of breakage t_{10} (Griffith, 1921; Norazirah et al., 2016)

2.2.6. Method (DEM) for Modelling using discrete element impact crushers

DEM is defined as a computational technique that allows particle flow in various types of equipment to be simulated. It computes the motion of particles as they interact with other particles, and machine surfaces. (Sinnott et al., 2015). This involves the application of Newton's laws to compute particle motion in response to forces when particles interact with each other or solid surfaces, thus dividing DEM to sections of contact forces, modelling and motion equations.

Contact forces

Labra et al. (2012) presented that in DEM simulation, dissipative forces namely normal and tangential frictional forces are modelled using constitutive models presented by Figures 2.3 and 2.5. These dissipative forces are called contact forces and exist when two bodies interact, and contact is detected. The dynamics of particles are modelled using Newton's laws of motion. Dissipative forces are calculated at a point of contact and satisfy Newton's third law of motion for particles i and j between two interacting bodies with the following equation:

$F_i = -F_j$…….. Eq. 2.3

Making $F_i = F$ and decomposing F into normal and tangential frictional forces $F_n$and F_t, F s represented by the following:

$F = f_n n + F_t$…….. Eq.2.4

n represents unit normal vector to particle surface at the point of contact and is defined as:

$n = \frac{x_j - x_i}{||x_j - x_i||}$……. Eq. 2.5

Figure 2.3 shows a constitutive model which represent contact between two bodies and is used to calculate $F_n$and F_t.

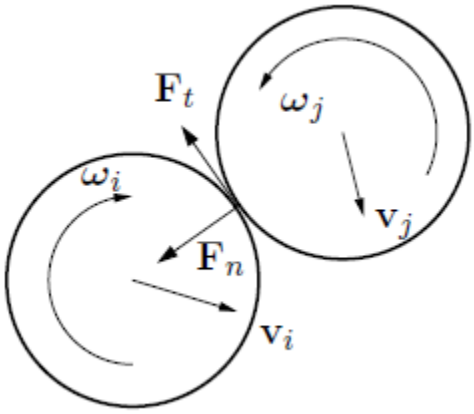


Figure 2.3*: Representation of the decomposition of the contact force to normal and tangential components* (Labra et al., 2012)

Figure 2.4 below represents a model showing contact interface characterized by normal and tangential stiffness (k_n, k_t) with coulomb friction coefficient μ and contact damping coefficient C_n.

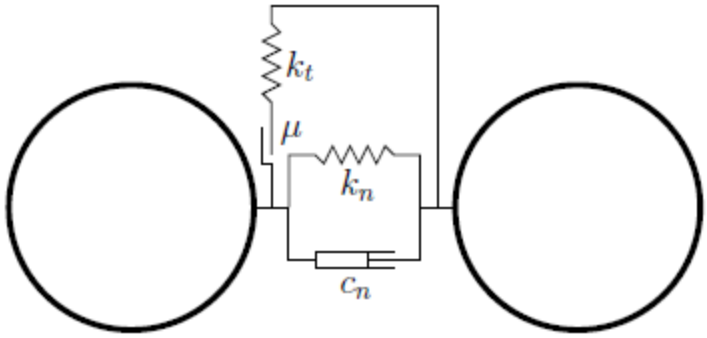


***Figure 2.4**: Contact interface model* (Labra et al., 2012)

Elastic (f_{ne}) and damping (f_{nd}) normal contact forces result from the decomposition of the normal contact force F_n. Damping normal force is used decrease oscillations of contact forces and to dissipate kinetic energy (Labra et al., 2012). Elastic normal contact force (f_{ne}) is defined by Equation 2.6 as it is directly proportional to normal stiffness (k_n) and penetration of two particle surfaces (u_{rn}) defined by Equation 2.7

$$f_{ne} = k_n \times u_{rn} \quad \text{Eq. 2.6}$$

$$u_{rn} = (x_j - x_i) \times n - (r_j + r_i) \quad \text{Eq. 2.7}$$

Where x = particle center, n = normal unit vector defined by Equation 2.5, and r = particle radius.

When there is no collision, no normal tensile forces are allowed and $f_{ne} \leq 0$ and $u_{rn} < 0$ thus $f_{ne} = 0$.

Equation 2.8 defines contact damping normal force, and it assumes the viscosity type (Labra et al., 2012)

$$f_{nd} = c_n \times u_{rn} \quad \text{Eq. 2.8}$$

c_n = damping coefficient which is a fraction of critical damping C_{cr} for a system if two rigid bodies (Taylor, 1992) and

u_{rn} = normal relative velocity between two particle centers defined by Equation 2.9 as follows:

$$u_{rn} = (u_j - u_i) \times n \quad \text{Eq. 2.9}$$

Tangential frictional contact force only appears in the absence of cohesion as it represents tangential reaction F_t which result from friction opposing relative motion at the point of contact between particles (Labra et al., 2012). Equation 2.10 defines relative tangential velocity (v_{rt}) at the point of contact as

$$v_{rt} = v_r - (v_r \times n) \times n \quad \text{Eq. 2.10}$$

Where n = normal unit vector defined by Equation 2.5, and v_r = relative velocity

Non-physical oscillations of the friction force are produced due to the relationship between frictional F_t and relative tangential displacement u_{rt} as a result of passive changes of direction of sliding velocity (Labra et al., 2012). To prevent this, the coulomb friction model was regularized by decomposing tangential relative velocity to two parts: reversible and irreversible parts (v_{rt}^r and v_{rt}^{ir}) and is defined by

$$v_{rt} = v_{rt}^r + v_{rt}^{ir} \quad \text{Eq. 2.11}$$

Using the radial return algorithm, the friction force can be calculated using the trial sate equation defined by Equation 2.12 (Labra et al., 2012). Equation 2.13 is used to check the slip condition $\emptyset^{trial}$ and if $\emptyset^{trial} \leq 0$, the contact is stick and frictional force is equal to trial value,

$$F_t^{trial} = F_t^{n-1} - k_t v_{rt} \Delta t \quad \text{Eq. 2.12}$$

$$\emptyset^{trial} = \left|\left|F_t^{trial}\right|\right| - \mu|f_n| \quad \text{Eq. 2.13}$$

meaning $F_t^{trial} = F_t^n$, otherwise the contact is slip and the friction force is given by

$$F_t^n = \mu|f_n| \frac{F_t^{trial}}{\left||F_t^{trial}|\right|} \quad \text{Eq. 2.14}$$

Constitutive models

There are different types of constitutive models to describe contact between interacting bodies. Two types of models describing elastic response in contact models are linear and non-linear models which re represented by normal and tangential stiffness k_n and k_t (Labra et al., 2012). The most non-linear classical model is defined from the Hertz (1882) theory for an elastic sphere i where normal stiffness is represented by Equation 2.15 as

$$k_n = \left(\frac{2\,G\sqrt{2r'}}{3(1-\nu)}\right)\sqrt{u_{rn}} \quad \text{Eq. 2.15}$$

r' = contact radius

Since the Hertz (1882) model only considers the normal collision, Mindlin et al. (1953) added to the Hertz (1882) model theory by introducing stiffness in the tangential direction (k_t) presented by Equation 2.16 as

$$k_t = \left(\frac{2\,(G^2 3(1-v)r')^{\frac{1}{3}}}{2-v}\right)|f_{ne}|^{\frac{1}{3}} \quad \text{Eq. 2.16}$$

to create what is called Hertz-Mindlin contact model which has so far been used mostly for granular dynamic simulations (Deresiewicz, 1958; Ji, 2006). The Hertz theory does not however work in the case of bonded particles but only works for contacts under compression (Labra et al., 2012).

To solve this matter, Cundall et al. (1979) defined a linear stiffness model that is proportional to particle size and is defined as

$$k_n^i = 4 \cdot E_c r_i \quad \text{Eq. 2.17}$$

This model in Equation 2.17 assumes that when particles are in contact the connection along the line passing through the center of these particles is a result of two springs in series. Each of these springs is has its own stiffness k_n^i defined by Equation 2.17, with E_c representing particle elastic modulus. Figure 2.5 shows a spring and dashpot model:

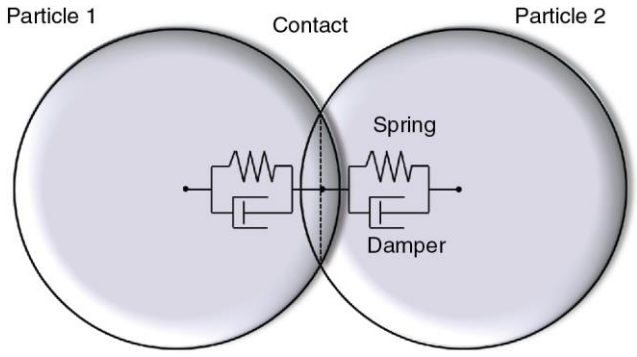


***Figure 2.5**: Spring and Dashpot Model between two particles* (Stiehm et al., 2016)

The Spring and Dashpot model showed in Figure 2.3 illustrates that strain in a particle exists within two elements: spring and dashpot (damper) and this is additive to determine the total strain of the particle (Rashid, 2016). Cundall (1971) proposed the soft contact approach to determine the strain within particles and this allowed the overlap between two approaching entities. This strain is used to calculate the forces between the two particles. From this, the

contact force is a function of material stiffness and the overlap distance between the two approaching entities.

When connection is in series, Equation 2.17 is transformed to

$k_n = \frac{k_n^i k_n^j}{k_n^i + k_n^j}$ …….. Eq. 2.18

Using the radius r of particles i and j with similar numerical properties, contact stiffness in normal and tangential direction is defined by

$k_n = 2E_c r'$ …….…..… Eq. 2.19

$k_t = \frac{k_n}{\mathrm{k}}$ ……...….. Eq. 2.20

With k representing stiffness ratio $\frac{k_n}{k_t}$ (Labra et al., 2012).

This linear model by Cundall et al. (1979) works also in case of bonded contacts for the simulation of cohesive materials. This model has been employed in PFC2D and PFC3D codes (Itasca, 1998). In this project, the type of DEM used is PFC3D which employs the Cundall et al (1979) model.

Equations of motion

A spherical particle's motion namely translational and rotational are described using Newton-Euler equations of rigid body dynamics for particle i with F_i and T_i representing resultant force and moment (Labra et al, 2012). In this section the forces acting on a particle in DEM simulation were visited and defined.

The forces are defined as

$m_i \ddot{u}_i = F_i$ ……..… Eq. 2.21

$I_i \dot{\omega}_i = T_i$ ……... Eq. 2.22

$\ddot{u}_i$ = particle center displacement in a fixed coordinate frame x

$\dot{\omega}_i$ = angular velocity

m_i = Particle mass

I_i = moment of inertia

F_i and T_i are vectors and equal to the sum of all forces and moments loaded on the particle (Labra et al, 2012). The summations are defined as

$$F_i = \sum_{c=1}^{n_c} F_i^c + F_i^{ext} + F_i^{damp} \quad \text{Eq. 2.23}$$

$$T_i = \sum_{c=1}^{n_c} (r_i^c + F_i^c + q_i^c) + T_i^{ext} + T_i^{damp} \quad \text{Eq. 2.24}$$

Where:

F_i^{ext} and T_i^{ext} = external loads

F_i^c = contact force for interacting with neighboring particles and other obstacles

F_i^{damp} and T_i^{damp} = force and torque resulting from damping in the system

r_i^c = vector connecting particle center with point of contact c

n_c = number of particles in contact

q_i^c = torque due to rolling or torsion

DEM simulation and impact crushers literature

In the work carried out by Sinnott et al. (2015), a discrete element modelling (DEM) simulation is introduced for impact crushers. This simulation uses a breakage model to study different types of impact crushers to better understand their level of operation and to demonstrate how that model is possible. From the simulations, estimates of power, product size, throughput rates, and crusher wear were made. The crushers tested are hammer mills, vertical and horizontal shaft impact crushers.

The model used energy absorption threshold to predict the performance of crushers and it was found that it is possible to use the model to predict the performance of a variety of impact-based crushers. Hammer mills and the horizontal shaft crusher were found to be having two or more distinct breakage regions while the Vertical shaft impact only has one breakage region. Using this model, key operational outputs such as power draw, throughput rate and machine wear for different machines can be assessed (Sinnott et al., 2015).

The limitations of this model are that it does not take into consideration different material properties. Different materials have different properties and thus do not have similar motion in any impact crusher.

Yang et al. (2015) introduced the importance of the lifelong endurance of impact hammers used in impact crushing. These hammers are often short-lived due to the high-impact intensity of the collisions. In this study, wear-resistant alloys were welded to the surface of impact hammers to prolong their service life. This allowed the use of discrete element method (DEM) to study the load distribution on each alloy block wear distribution on impact hammers.

The load distribution on the alloys was affected by the structural and manufacturing parameters of the impact crusher while the shape morphology measured the wear distribution of the impact hammer according to impact crushers. In this study, DEM was used to study the impact load on carbon tungsten alloy which was welded on the surface of the impact hammers whilst the effects of rotor speed, feed rate, and particle size on the load distribution were also studied. After simulation, it was found that both load and wear distributions produce similar results. It was concluded that, using optical parameters preserves the life of impact hammers (Yang et al., 2015). However, the limitations of the study were; the effect of different types of alloys and different shapes of hammers were not taken into consideration. Different shapes of hammer exist, and all can have different crushing effects.

da Cunha et al. (2013) presented that despite all attempts to model the performance of the vertical impact crusher (VSI), a comprehensive mathematical description that allows accurate prediction of VSI performance is still lacking. The major reason being that there is limited knowledge on the particle-particle interaction and solid flow mechanism inside the crusher. Past researchers such as Nikolov (2004) and Kojovic (1996) all attempted to model the VSI crusher by estimating the energy transferred to the particles as the kinetic energy at the rotor tip. Using this information and being able to estimate the breakage function in crushers, gave the researchers as great deal of confidence in predicting the performance of the VSI crusher. The problem with these models is that they used the assumption that particles in the crusher are hit with a constant stressing energy and da Cunha et al. (2013) concluded that this was as oversimplification.

To solve the above problem, da Cunha et al. (2013) employed the use of the discrete element method (DEM). This helped in providing a more complete description and additional insights into how VSI crushers are operated. The DEM was applied to simulate the solids flow within a pilot-scale VSI crusher operating under different conditions. The results from the

experiments were used to calculate the residence time distribution of the particles and the collision energy spectrum.

The pilot VSI crusher used consisted of the feed hopper (responsible for distributing the feed material between the fraction that enters the rotor of the machine and the fraction that cascades though the flow gap), crushing chamber, and the rotor. To conduct the experiments, two different feed flowrates were used. The first flowrate in tonnes per hour was under a condition that 100% of the feed goes directly into the rotor and the second flowrate which was double of the first was under the condition that 50 % of the feed material goes directly into the rotor and the remaining 50% goes to the cascade. About residence time, rock particles in VSI crushers are known to be having short residence times due to the high capacity in comparison to the size and chamber volume. This is not the same for every particle since residence time different from particle to particle due to different properties (da Cunha et al., 2013).

From the simulation output of the DEM applied to analyse the residence time distributions of the rock particles from the time they left the feed tube into the crusher rotor to until they left the crushing chamber. It was found that the residence time of the particles inside the rotor is very short and thus the transfer of particles inside the rotor can easily be described approximately as a sequence of a plug flow (0.04 seconds) and a nearly perfectly mixed zone (0.02 seconds). Residence time with no cascade for rocks particles ejected against a ring of steel bars or anvils is lower (about 0.14s) than residence time of particles ejected against a rock bed (about 0.55 seconds). Feeding in the presence of a cascade reduced the residence time of particles thrown from the rotor and the residence time of particles that flow in the cascade was found to be longer (da Cunha et al., 2013).

Energy losses were found to be higher than shear energy losses when the rock particles where propelled against a ring of the hammer bars or anvils. When it comes to shape of the particles and the collision energy spectrum, da Cunha et al., (2013) found that spherical particles have a narrower collision energy spectrum which means that each particle receives collisions within a relatively narrower range of energies. On the other hand, non-spherical particles result in a wider range of values for the energy dissipated in contact, and these are lower than the theoretical kinetic energy of a particle that leaves the rotor (da Cunha et al., 2013).

da Cunha et al. (2013) provided a good application of the discrete element modelling to the operation of the VSI crusher and it is mostly perfect since it tracked the motion of particles from one space to another within the VSI crusher.

Segura-Salazar et al. (2017) introduced the continuation of the modelling of the vertical shaft impact crusher using the model developed by Whiten (1972). Vertical shaft impact crushers are used in the construction industry as alternatives to cone crushers in the production of aggregates due to their good efficiency and the ability to generate more isometric and tougher particles highly desirable in the cement mortars and concrete applications. It was reported that the whiten model has been used as the basis of modelling several important designs of the Vertical shaft impact crusher for further improvements.

Researchers such as Nikolov (2002) proposed the new breakage and classification functions and coupled these functions with the Whiten (1972) model for the calculation of the product size distribution. The functions were then related to important parameters such as the feed rate, rotor radius and its frequency of rotation. However, Nikolov (2002) used the model to predict the performance of the horizontal impact crusher (HSI) and stated that the model can also be applied to VSI crushers but then it was never applied.

Segura-Salazar et al. (2017) also used the Whiten (1972) model and supplemented it with equations that describe the variation of parameter K_3 in the classification function and the parameter t_{10} in the breakage function. Both K_3 and t_{10} were described as the function of the feed rate and the rotor speed. Using breakage and classification functions proposed by Napier et al. (1996) and Kojovic et al. (1998) these models were able to predict the product size distribution and the power consumption in the VSI crusher within the range of conditions studied. However, the feed distributing system did not have a huge effect on the K_3 and t_{10} parameters found in the breakage and the classification functions.

The Whiten (1972) model was proposed for a cone crusher based on the assumption that particles in the crusher could either be broken or dropped off the crusher unbroken, and broken particles could be dropped off the crusher or could be broken further. From this, the Cone crusher was simplified to having a single breakage zone with particles having the probability to enter and re-enter this breakage zone. Particles entering the crusher were characterised by two functions, distribution of the particle after breakage (matrix B or breakage function) and probability of the particle to break (matrix C or classification function)

Breakage matrix (Whiten (1972))

$B = \alpha B_1 + (1 - \alpha) B_2$……Eq. 2.25

Where: B = total breakage matrix

B_1 = product size relative to the of original particle

B_2 = production of fines

α = model parameters

Both B_1 and B_2 have their model equations which were not included in this scope.

Classification matrix (Whiten (1972))

$C(s) = 1 - \left(\frac{s - k_2}{k_1 - k_2}\right)^2$……Eq. 2.26

Where: C(s) = probability of particle with size s entering breakage zone

s = representative size (m)

k_1 and k_2 are model parameters representing size (m)

The classification function used by Segura-Salazar et al. (2017) in DEM simulation is the Whiten (1972) model proposed for direct application by Napier et al. (1996) and Kojovic et al. (1998):

$C(x) = 1 - \left(\frac{K_2 - x}{K_2 - K_1}\right)^{K_3}$…….. Eq. 2.27

Where: x = representative size (m)

K_2 = top size of crusher feed

K_1 = 0 (assuming all particles can be broken)

K_3 = model parameter and equal to 2.3

To test the importance of the feed rate, the DEM simulations were applied. From the simulations it was found that as the feed rate increased, the proportion of material entering the rotor was decreasing while the proportion of material in the cascade flow increased. Again, as the feed rate increased the particles in the cascade flow had lower energy collisions in comparison to those projected by the rotor. Segura-Salazar et al. (2017) concluded that this

might be due to the significant reduction in the K_3 parameter of the classification function as the feed rate increased.

The above experiment was a further improvement on the Whiten (1972) model on the VSI crusher. To date, the Whiten (1972) model has been applied to both the HSI and VSI crushers and any further improvement needed would be to investigate the effect of K_3 of the classification function on the collision energy of the of the articles when the feed rate increases.

2.2.7. Impact crushing of harder materials

Most work on impact crushers involved the use of soft and less abrasive minerals or materials and it was stated that impact crushers cannot be used for crushing hard materials. Despite the advantages such as being energy efficient and having high size reduction ratios, impact crushers have been considered not suitable when it comes to the crushing of relatively harder materials. This may be due to wear that the impact hammers in the mill experience. However, Dey et al. (2013) extended the study by introducing the study of the comminution features in an impact mill.

This study was taken to explore the possibility of using the impact hammer mill for crushing harder materials. The effect of the rotor speed and the material feed rate on the mill efficiency was investigated. The parameters of the hammer mill investigated were the reduction ratio, energy expenditure, product fineness and median size. To perform this experiment, the hammer mill with a 75 mm in diameter rotor shaft mounted with four fixed hammer bars each weighing 2.38 kg each was used. The rotor and the hammers were enclosed in a steel shell which is 1 meter wide with a thickness of 255 mm thick. The material was fed into the mill with the use of an electromagnetic vibratory feeder which used a PLC based control system. Two different types of minerals with different properties were used: iron ore (hematite) and semi-coking coal. It is known from literature that iron ore is hard, and coal is a soft material and there are researchers who used coal as an ore to investigate impact crusher parameters (Dey et al., 2013).

A simulation based on the mill described above was done. The speed of the rotor and the material feed rate were used as variables to study the mill performance. It was found that higher fines production corresponded with high rotor speed, thus favouring high speed of impact mill. As expected, low feed rates also produced a finer product. It was also observed

that fine generation was slower at the beginning for coal and rose sharply after a while, but with coal, the increase is gradual (Fuerstenau et al., 1990, 1995; Dey et al., 2013).

High feed rates resulted in reduced generation of fines due to inadequate comminution of the particles. The fines generated by the hammer mill were observed to exhibit Rosin-Rammler type size distribution. The median size showed an exponential relationship on the number of fines produced while the energy expenditure and the reduction ratio showed linear relationship with slope that was inversely proportional to the bond index of the material. During the crushing process, the importance of the energy expenditure is to create new surfaces and to overcome the elastic strain energy of the cracked surface was demonstrated (Fuerstenau et al., 1990, 1995; Dey et al., 2013).

The main thing this study established was the debunking of the notion that impact crushers cannot be used for crushing hard materials as not being necessary. Dey et al. (2013) showed that impact crushers and mills can be used for the comminution of harder materials when conditions such as feed rate, speed of rotor, and appropriate material is used to manufacture impact hammers.

2.2.8. Automatic control of impact crushers

Automation is a key standard of operating equipment in industry today. Automation also known as automatic control, can self-regulate an industrial process by changing parameters using a controller and requires less human work. Controlling a process means the parameters of a process such as feed rate, temperature, speed etc. are altered, automatically or manually to achieve a desired output. The advantage of automatic control over manual control is that it reduces the risks of human errors. It helps the system in getting the output to the desired value, in short time, with minimal overshoot and little error. The requirement of low labour in automation means that more money and time are saved and therefore automation is the best way to go in the current industrial world (Visioli, 2006)

When it comes to crushers, literature shows that the gyratory crusher has been a subject for control efforts much more than the impact crusher. This is because impact crushers are not usually considered as precision instruments and thus less effort is applied on their automation. To show that it is possible to build a control system for impact hammer crushers Jaatinen et al. (2013) presented a paper to describe a control system that is already in use at a large aggregate plant in the United Kingdom. The paper also describes the future improvements of the control system in the plant. The crusher is used for limestone and its

control is based on measuring the crusher power draw, mass flows and the size distribution of the produced rocks. The product size distribution is estimated with the use of image analysis derived from online camera images.

In a control system, there is a manipulated variable. This is a variable that can be altered to produce the desired product. In this plant, the rotor speed and the impact plate gap of the impact crusher represent the manipulated variables. Out of the two manipulated variables, the rotor speed was considered as the main manipulated variables since it can be adjusted without stopping the feed rate and thus reducing production. Meanwhile on the other hand, breaker plates were considered as the secondary manipulated variable since they can only be adjusted by stopping the feed rate and thus lowering production. For an equipment like a crusher there are many variables that can be used as the manipulated variables in automatic control. The feed rate of material can also be a controlled variable but Jaatinen et al. (2013) stated that the plant condition to keep the feed rate was a constraint that limited further investigation.

In this system, the vibrating feeder is used as the feed mechanism to the hammer crushers with four crusher blow bars and three breaker plates. The size distribution of the product was measured with a Metso Visiorock camera system. This system was perfectly calibrated so that the data observed on the surface was accurately reported. Crushing is controlled by altering the rotation speed of the rotor and the position of the impact breaker plates. It was estimated that during crushing, 60% of the crushing action occurs when the crusher blow bars hit the rocks (kinetic energy from rotation), 30% by rocks hitting the impact breaker plates, and 10% by attrition (rocks hitting each other) (Jaatinen et al., 2013).

In the control system, the other important variable is called the measured variable. This is the product of each process and every controlled variable is altered according to the measured variable so that the desired value can be reached. The measured variable for this crusher control system was the product size or the size distribution. Below is Table 2.1 compiled by Jaatinen et al. (2013) to summarize how a crusher is controlled:

***Table 2.1**: Commands to control the size distribution in an impact crusher*

Commands if product is too coarse…	Commands if product is too fine…
Decrease crusher setting	Increase crusher setting

Increase the rotation speed	Decrease speed
Decrease the feed rate	Increase the feed rate

In every control system, there are disturbances which arise and can change the way a system operates and thus slowing down production. It depends on how a system is tolerable to disturbances and how quickly it can rise to continue producing the desired product. In this plant, the disturbance to look out for was the wear of the blow bars and crusher parts, and the changes in the feed material. When a system is controlled using automation, the target will still have to be met regardless of the disturbances (Visioli, 2006).

This control system was an improvement over the past operating model, and it made it simple for the plant personnel to understand. Before this control system, adjustments on the crusher were done daily but with this system the adjustments are done every 15 minutes. Crusher settings were based on the previous measurements and older logs but with the use of a control system, once production targets are set, the control system will continuously strive to maintain the set target (Jaatinen et al., 2013).

This is clear from work by Jaatinen et al. (2013) that automation on impact crushers is feasible. However, feed rate must be controlled. The control system must consider the feed particle size distribution when determining the final product of the material.

2.2.9. Modelling of impact crusher performance

2.2.9.1. The breakage process model

Nikolov (2004) presented that breakage in impact crushers occurs in a very short time scale due to the dynamic crack propagation, compression, and tensile shock waves traveling through the particles generated by impact. It was also presented that there is a tensile stress that grows within particles and it breaks the particles from within. In 1979, Whiten and White developed a standard size distribution model for core and jaw crushers. Nikolov (2004) discussed that the size distribution model developed in Whiten et al. (1979) was unsuitable for high speed impact crushers since the breakage time, magnitude and nature of forces required and the energy consumption were different and lower than those of jaw and cone crusher.

The following equations were proposed for breakage and classification functions by Nikolov (2002):

2.2.9.2. Classification function

$$C_i(d_i) = 1 - exp\left[\left(\frac{d_i - d_{min}}{d_{min}}\right)^k\right] \text{ …….. Eq. 2.28}$$

Where:

d_{min} = minimum size of particles broken at any operating conditions

k = Shape parameter and,

$C_i(d_i)$ = the probability of breakage for a particle of size d_{min} (mm)

Equation 2.28 above is a cumulative Weibull distribution and it can be derived from physical considerations in relation to brittle solids. The minimum breakable size d_{min} can be calculated as follows:

$$d_{min} = d_{max} \times exp\left\{-\left[c_0 + c_1 \times \ln\left(\frac{Q}{Q_o}\right)\right] \times \left(\frac{E_o}{E}\right)^n\right\} \text{ …… Eq. 2.29}$$

Where:

d_{max} = the maximum particle dimension in the feed (mm)

Q = feed rate (t/h)

E = impact energy per unit mass (kJ/kg)

Q_o = reference feed rate (t/h)

E_o = reference impact energy per unit mass (kJ/kg)

c_1 = intensity of particle – particle interaction

n = material parameter

c_0 = Rate constant.

2.2.9.3. Breakage Function

Consisting of the sum of two broad-bent-callout distributions, the breakage functions was represented as follows:

$$b_{ij}\left(d_i, d_j\right) = 1.582 \times \left\{\varphi\left[1 - exp\left(\frac{d_i}{d_j}\right)^m\right] + (1 - \varphi) \times \left[1 - exp\left(-\left(\frac{d_i}{d_j}\right)^I\right)\right]\right\} \text{ ….. Eq. 2.30}$$

Where:

$i\ and\ j$ = size class

φ = mass fraction of fine product

$m\ and\ I$ = material coefficient

In 2004, Nikolov proposed a new model for the classification function by changing the equation used to calculate d_{min} by representing as follows:

$$d_{min} = \beta\left(\frac{Q}{Q_o}\right)^s\left(\frac{E_o}{E}\right)^n \quad \text{..... Eq. 2.31}$$

Where:

β = specific particle size depending on the crusher design and granulates properties.

s = intensity of particle – particle interaction.

Other parameters have been described in Equation 2.30 above.

In this research the breakage function was represented as the distribution function by Whiten and White (1999) as follows:

$$b_{ij}\left(d_i, d_j\right) = \varphi\left(\frac{d_i}{d_j}\right)^m + (1-\varphi)\left(\frac{d_i}{d_j}\right)^I \text{.....} \quad \text{Eq. 2.32}$$

Parameters have been described in Equation 2.25 above.

After experiments were conducted by Nikolov (2004), it was found that Equations 2.30 and 2.31 assumed φ and k to be constants which is incorrect and thus Nikolov (2004) concluded that equations 2.28, 2.29, and 2.30 are better since they represented φ and k as functions of impact energy per unit mass, feed rate and the experimental law for the minimum breakable size (d_{min}).

2.2.10. Impact energy per unit mass in hammer (horizontal shaft-like) impact crusher

To derive a model for impact energy per unit mass, Attou et al. (1999) made the following assumptions:

1) The mass of rotor is greater than that of a single particle.
2) The kinetic energy of the particles is negligible since the velocity of crushing bar is more important that hat of particles before impact.

From the above, the impact energy per unit mass was given as follows:

$E = 0.5\ (R + 0.5H_b)^2 w^2$……...…….. Eq. 2.33

Where:

R = rotor radius (m)

H_b = height of impact surface of the crushing hammer

w = rotor angular velocity (w^{-1})

2.2.11. Kinematics of hammer rotation

Gupta (2011) presented that hammer rotation is one of the performance parameters used to judge impact crushers. The judgement is based on the following:

1) The fineness of the crushing
2) The life of the hammer

The live span of the hammer depends on the following:

1) The function it is used for and where it is used.
2) The hardness
3) The depth of penetration by material into the hammer faces and
4) The kinetics of hammer rotation.

Verma et al. (2014) presented that the hammers in a hammer crusher are subject to three different types of forces: shear force at the point of fixation, bending frame from the striking of the material, and centrifugal force due to rotation. Different types of sections or shapes can be used to make hammers or blow bars, and that includes s-station, cylindrical bars, and rectangular bars. The type of the bar shape helps in deciding the Impact capacity as well as the strength of the crusher.

Using the above, two equations to calculate the initial and final kinetic energy of the impact crusher were derived as follows:

$T_0 = \frac{1}{2} MV^2$ ……..…..… Eq. 2.34

$T_f = \frac{1}{2}(M + m)U^2$……. Eq. 2.35

Where:

M = Mass of hammer

m = Mass of limestone

V = Velocity of hammer

From the two Equations (2.34 and 2.35) the following was presented:

$$T = \frac{1}{2}\frac{MV^2}{(M+m)} \quad \text{Eq.2.36}$$

In impact crushers, the common energy is the kinetic energy.

The crushing effect was represented as follows:

$$D_m = T_0 - T_f = \frac{1}{2}(MV^2)\left(\frac{M}{M+m}\right) \quad \text{Eq. 2.37}$$

Crushing effect represents the kinetic energy lost due to impact.

Equation 2.37 above shows that when the weight of hammers is beyond the ideal weight, the crushing effect does not improve. This shows that it is important for a low number of hammers in the horizontal shaft impact crusher. From the kinematics of hammer rotation, reducing the number of hammers reduces the cost and the weight of the crusher. Using this, the number of hammers required in an impact crusher can be calculated (Gupta, 2011).

2.3. Material property and tests

To study the crushing efficiency of impact crushers, the properties of the material should be known and there should be tested using material testing processes. In this research, quartz and limestone have been used and thus have been tested to determine breakage properties.

Particle breakage in size reduction processes depends on factors such as size and shape of particles, surrounding conditions, and the mineralogy of the processed ore. Ore mineralogy explains material density and fracture energy while shape and size of particles defines the surface area, which plays a major role in how breakage will occur (King, 2001). Because of this, different materials behave differently under breakage processes.

Fuerstenau et l. (1965) studied the comminution kinetics using quartz and limestone. It was stated that the material property that eased this material selection was the distribution

modulus between the two materials, with quartz having 0.9 and limestone having 0.6. This difference is the one that will ease comminution characteristics differences between the materials.

Another property that provides ease with differentiation is material hardness. According to King (2005) quartz is made of quartzite which gives the mineral a hardness value of 7 on Mohs hardness scale. Due to this quartz toughness, early people used it as an impact tool. Mohs (1812) developed a scale to measure mineral resistance to scratching by other ten minerals. On this scale quartz had a hardness of 7 and calcite a primary mineral of limestone had a hardness of 3 (King, 2005). These differences in hardness makes it easy to differentiate comminution characteristics.

During breakage, materials can be elastic, plastic (ductile), and brittle. Elastic materials experience a temporary change in shape and size when a stress is applied and return to the normal shape and when stress is released. Plastic (ductile) materials undergo a permanent change in shape and size when stress is applied, and brittle materials will break showing a little elastic deformation without a significant plastic deformation. A particle with brittle breakage characteristics, experiences loss of cohesion of the body under stress (Nelson, 2015)

Nelson (2015) presented that minerals such as quartz, olivine, and feldspars are very brittle while minerals such as feldspar, calcite, clay, and micas are very ductile. In this project two minerals, quartz and limestone have been used. Limestone is a sedimentary rock majorly composed of calcium carbonate in form the mineral calcine (Nelson, 2015; King, 2020). This means that in this project, the breakage properties of a brittle material (quartz) will be compared with those of a ductile material (limestone) using the drop weight, selection function, and breakage function tests.

The following tests where used to determine the properties of the materials used in this project. Bond test, selection and breakage function, and the drop weight test. Other testing methods are out of the scope of this project.

2.3.1. Bond test

Bond testing is achieved by using a ball mill to determine the grinding characteristics of the material by using size analysis to determine the amount of size reduction resulting from a controlled energy input.

The following equation was presented by (Michaud, 2013) and is used to determine the bond energy:

$$E = 10.W_i\left(\frac{1}{\sqrt{p}} - \frac{1}{\sqrt{f}}\right)$$ ..... Eq. 2.38

Where: E = Predicted mill energy consumption $\left(\frac{kWh}{t}\right)$

W_i = Work index $\left(\frac{kWh}{t}\right)$

P, f = 80 percent passing sizes for product and feed (μm)

2.3.2. Selection and breakage function tests

Consider a certain number of particle size classes, n and let i represent a certain size class. For any given i, let j be the upper size class to i. Selection function S_{ij}, is defined as fraction of size class j which breaks into size class i at a given time. The breakage function B_{ij} gives the size distribution on how size class j breaks into smaller size classes (McCabe et al., 1993).

The following are the model equations used to find the parameters:

Selection function

In milling, selection function is known as a specific rate of breakage with units of min^{-1}. The importance of selection function is to provide the probability of a particle undergoing breakage in a size reduction unit. The rate of breakage of a material in size class i can be defined in terms of selection function as follows:

$$\frac{dw_i}{dt} = -S_i \cdot w_i(t)$$ .....Eq. 2.39

Where: w_i = weight fraction of size i.

S_i = selection function of size i.

Equation 2.40 follows first order kinetics as established by Austin et al. (1984). After rearranging, this equation and integrating from time 0 to time t and weight 0 to weight $w_i(t)$, the following expression was the result:

$$\int_{w_i(0)}^{w_i(t)} \frac{dw_i}{w_i(t)} = \int_0^t S_i dt$$ ..... Eq. 2.40

Since it is a first order process and S_i does not vary with time. Equation 2.16 can be integrated to:

$$\log(w_i(t)) - \log(w_i(0)) = \frac{-S_j \cdot t}{2{,}303} \quad \text{Eq. 2.41}$$

Using Equation 2.41, the selection function of a material in size lass i can be determined by plotting $\frac{log(w_i(t))}{\log(w_i(0))}$ versus time (min) for first order breakage kinetics which produces a log linear plot with the slope of the line expressed as:

$$Slope = \frac{-S_i}{2.303} \quad \text{Eq. 2.42}$$

Using Equation 2.42, selection function can be found for different size classes and from this variation of selection function with particle size can be determined. Comminution kinetics experiments have shown that with multiple size classes, selection function generally increases with increasing particle size to a certain turning point, usually where the breakage rate is no longer first order. This is known as the abnormal breakage region. The reason for the increase and decrease has been discussed throughout chapter 4 under drop weight and milling results.

An empirical model to predict selection function parameters was established by Austin et al. (1984). Experimental data can be fitted to the model to establish parameters. The selection function model is expressed as:

$$S_i = a \times {x_i}^{\alpha} \times \left\{ \frac{1}{1+\left(\frac{x_i}{\mu}\right)^{\Delta}} \right\} \quad \text{Eq. 2.43}$$

Where: a, μ = constants that are dependent on the milling conditions

Δ And α = constants depending on material properties

S_i = selection function for particle size class i

x_i = representative size for particle size i

According to Katubilwa (2009), the Austin model constants μ and a do not vary with particle size if milling conditions do not change.

Breakage function

Breakage function represents a way in which a particle is broken and distributed into smaller fragments. The importance of this function is to provide the smaller size classes in which a particular larger size will break into in size reduction unit. For example, the breakage function of size j which breaks into size class i is defined by B_{ij} which give a fraction of size

class j broken into size class i (Whiten et al., 1979; Nikolov, 2002). After preforming milling experiments, the size distribution after 30 seconds milling is used to calculate the breakage function of the materials according to Austin et al. (1984).

The Austin et al. (1984) **BII method** which is applied when a single particle size class is milled for a short time, usually 30 seconds can be used to determine the breakage function. Short milling times are employed to minimize the probability of particle re-breakage and thus enabling the cumulative breakage function to be estimated more accurately. For the BII method, the cumulative breakage function is given by:

$$B_{i,j} = \frac{\log\left(\frac{1-P_i(0)}{1-P_i(t)}\right)}{\log\left(\frac{1-P_{j+1}(0)}{1-P_{j+1}(t)}\right)} \quad \text{Eq. 2.44}$$

where:

$B_{i,j}$ = Cumulative fraction of particles passing the top size of size class i due to the breakage of particles in size class j.

$P_i(0)$ = Cumulative fraction of particles passing the top size of size class i in mill feed.

$P_i(t)$ = Cumulative fraction of particles passing the top size of size class i after milling time t.

$P_{j+1}(0)$ = Cumulative fraction of particles passing the top size of size class j+1 in mill feed.

$P_{j+1}(t)$ = Cumulative fraction of particles passing the top size of size class j+1 after milling time t.

Austin et al. (1984), developed an empirical model that can be fitted to experimental data to predict the variation of the Cumulative Breakage Function with the normalized particle size. This empirical function is given as:

$$B_{i,j} = \emptyset \cdot \left(\frac{x_{i-1}}{x_j}\right)^{\gamma} + (1-\emptyset) \cdot \left(\frac{x_{i-1}}{x_j}\right)^{\beta} \quad \text{Eq. 2.45}$$

Where:

$\frac{x_{i-1}}{x_j}$ = normalized particle size

Parameters ϕ, γ and β are depend on material properties and are further explained as follows:

Φ = a parameter which represents the fraction of fines that are produced in a single fracture event. It is a material dependent property and has a value from 0 to 1.

γ = a parameter that is material dependent and has values ranging from 0.5 to 1.5.

β = a parameter that is material dependent. It has values typically ranging from 2.5 to 5.

The cumulative breakage function can then be plotted against particle size to determine the model parameters. The particle size is expressed in the normalized form where:

$$Normalized\ PS = \frac{x_{i-1}}{x_j} \quad \text{..... Eq. 2.46}$$

Where: X_i = Upper size of class where material is broken into

X_j = Upper size of class from which material breaks

Katubilwa (2009) concluded that the cumulative breakage function is assumed to be independent of the initial particle size, and thus it is normalized. The parameters for the above empirical equation can thus be estimated by averaging the values obtained for the grinding of two different particle size classes using the same milling conditions.

2.3.3. Drop weight test

Drop weight tests involve dropping a weight of a known mass from a particular height on a single particle placed on a flat hard surface called an anvil. This is the simplest method used for the investigation of material breakage behaviour (Bwalya et al., 2020). Advantages of using drop weight tests are, short test duration, different size ranges, and a broad range of energy inputs that can be used. (Salman, 2007).

Particles respond differently to external forces due to differences in flaw distributions within particles. Particles that are small have fewer flaws compared to larger particles. Griffith (1921)'s theory of fracture states that particles with more flaws will result in crack propagation faster than particles with less flaws when stress is applied. Flaws act as starting points for crack propagation, and thus when stress is applied large particles will experience fast crack propagation compared to smaller particles. Large particles in milling predominantly undergo breakage due to impact breakage whereas, small particles predominantly break due to attrition (Nyabando, 2014; Lameck, 2006).

To break a particle the energy input must exceed the threshold energy required to break that particle. Bwalya (2005) found that the threshold energy (E_{X0}) was described by the equation:

$E_{X0} = cx^d$ ..... Eq. 2.47

Where: x is the mass of the particle and c and d are constants.

For a particular size, E_{x0} is calculated as the specific threshold energy by dividing its value by the mass (kg) of that particle.

It was observed that particles can break with repeated impact, the higher the energy input, the less breakage attempts were required to cause breakage. An equation that models this phenomenon was found to be as follows:

$P_b = -an^b$ ..... Eq. 2.48

Where: P_b is the probability of breakage, n is the number of breakage attempts, and a and b are constants.

The two equations above can be combined for any energy input and particle size to produce an equation like the one developed by Weichert (1990) written as follows:

$P_b = 1 - e^{(-an^b\left(\frac{E-cx^d}{cx^d}\right)}$ ..... Eq. 2.49

Where a and b are parameters modelling deterioration with each impact, c and d model how threshold energy varies with particle size. x is the particle mass in grams.

Fuerstenau et al., (2003) discussed the concept of elastic energy stored in a particle due to deformation to explain why breakage of particles increase when input energy is increased. When a particle is under a compressive stress, energy is released at the flaw edge when the crack grows. It can also be noticed that some particles had the same size and mass, but their breakage behaviour was different. This is due to flaws distribution within a particle.

To study the crushing efficiency of impact crushers in detail drop weight tests have been conducted and explained.

Chapter 3 : Lay out Experimental work

Quartz and limestone are the materials used in this project and drop weight and ball milling tests have been conducted on these materials to compare the breakage behaviour of these materials using each test and to determine the threshold energies for breakage of various particle sizes of these materials. The effectiveness of impact crushers and ball milling will also be compared using DEM to compare the energy spectra of each crushing method and

how speed affects each method. DEM was used to compare impact energy spectra in ball milling, single rotor impact crusher, and double rotor impact crusher to determine which grinding method is the most efficient.

3.1. Drop weight test

A drop weight test apparatus built at Wits University consists of a rigid steel frame, and an electromagnetic holder with a switch to switch off the electromagnet to release the steel impact weight (1.61kg). The equipment is made up of 1.5m long opposite steel bars with holes that are 8 cm apart to allow the change of drop-weight height. The drop-weight is held up by an electromagnet and is released when the electromagnet is switched off. Figure 3.1 shows a picture of the equipment and the schematic presentation is shown on the right.

Experimental equipment and material



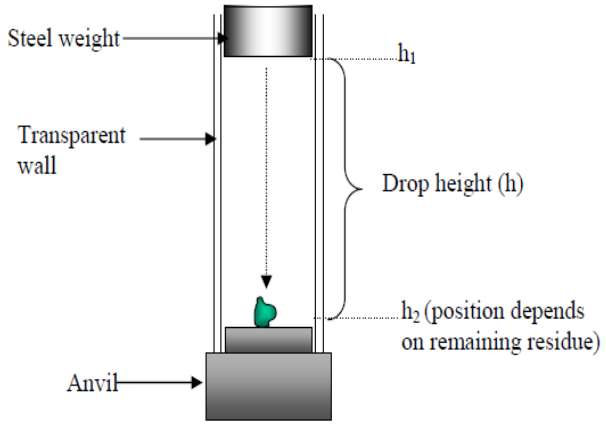




***Figure 3.1**: Drop weight Test Apparatus*

***Figure 3.2**: 13.2+11.2mm size class of Limestone*

Figure 3.2 shows an example of the ore used for Drop weight test experiment.

The drop weight test is used for characterizing particles. It follows a procedure that was developed by Bwalya (2005). This involved

preparation of particles to narrow mass groups. Each group comprised sixty particles which were further subdivided into in three groups of twenty particles of size classes (-19 + 16mm, -13.2 + 11.2mm, and -9.5 + 6.7mm) of limestone. For each group of twenty, breakage was attempted using the following energy levels based on the following heights (cm):

- 22.2cm and 30.2cm for size classes -19 + 16mm and -13.2 + 11.2mm and
- 14.2 cm and 22.2cm for size class -9.5 + 6.7mm.

For the purpose of identification, the samples and drop-weight height are labelled as follows:

- Particle size 1 = -19 + 16mm
- Particle size 2 = -13.2 + 11.2mm
- Particle size 3 = -9.5 + 6.7mm and
- Height 1 = 22.2 cm, height 2 = 30.2cm and height 3 = 14.2 cm

These heights were measured from the bottom of the drop weight tester to the top of the steel weight carrier. To calculate the energy level at each height, Newton's potential energy equation was used.

$E = mgh$ …… Eq. 3.1

Where: m = mass of the steel weight (kg)

g = Gravitational acceleration $(m \cdot s^{-2})$

h = drop height (m) shown if Figure 3.1.

Drop height (h) for each particle was calculated as follows:

$$Drop\ height\ (cm) = height\ from\ bottom\ of\ drop\ weight\ tester\ to\ the\ top\ of\ steel\ weight\ carrier - (particle\ height + steel\ weight\ height + weight\ carrier\ height + Anvil\ or\ base\ height)$$ …… Eq. 3.2

The drop weight height was converted to metres and used in Equation 3.1 to calculate energy. Energy input for the size classes was calculated using the average of the energy from the 20 selected particles for the drop weight test.

The experimental routine involved setting the magnetic weight holder to a specific level from which the drop weight was released to fall on a single particle placed on the anvil. This procedure was repeated on all the twenty particles. Some particles broke while some survived

depending on the energy level. The fraction of broken particles was noted (breakage was defined as 30% of original mass being lost). All the surviving particles where subjected to another drop weight. The broken particles were noted again, and the procedure was repeated on the surviving particles (Bwalya, 2005). From this procedure, the graphs of probability of breakage versus number of breakage attempts were plotted at different energy level in the results section in chapter 4.

3.2. Ball milling

This was conducted on quartz to study the kinetics of milling to obtain the selection and breakage functions, and to further compare the selection and breakage functions with ones found for limestone milled at the same conditions.

Methodology

Equipment

- Ball mill
- Sieve Shaker
- 20 mm and 30 mm by diameter balls
- Spinning riffle
- Sieve screens
- Stopwatch

Visualization of Ball mill equipment



Figure 3.3: *Mill chamber on rollers*



Figure 3.4: *20 and 30mm balls, quartz and lifters inside the mill*

The dimensions of the milling equipment were as follows:

- Length = 250 mm, Diameter = 180mm, lifters length =247mm, and lifters width = 5mm.
- 20mm and 30mm balls were used occupying 50% by mass each.
- Mill fill by balls = 30% with 40% voidage

Mill speed

The variable speed of the mill was based on the critical speed calculated using the following equation presented by Michaud (2015) as $N_c = 42.5 \times D^{-0.5}$ where D is the inside mill diameter (m).

N_c = 100.2 rpm

Mill speeds 60% to 100% less close to the critical speed of the mill were tested and 96rpm was selected as the suitable speed since it provided suitable cataracting in the mill.

Mill speed = 96rpm.

Sample preparation

Six size ranges of quartz (-13.2+9.5mm, -6.7+4.75mm, -3.25+2.8mm, -1.4+1.00mm, -0.85+0.600mm, and -0.3mm+0.212mm) each weighing 1220g were prepared.

The size ranges were found with the use of size range = (Top size)/√2. However, some screens were not available and thus screens close to that number were used.

Experimental procedure

- 1220g of quartz for each size class was prepared
- Each sample was milled for 30 seconds, 1 minute, 2 minutes, and 4 minutes using the stopwatch to measure the mill time.
- The Spinning rifle was used to select a representative sample for each size class to conduct sieve analysis using screens and sieve shake after each milling time.
- From the sieve analysis results, selection and breakage functions were calculated.

To find the breakage function using Austin et al. (1984) **BII method**. The product after 30 seconds milling time for each size class was used. A stopwatch was used to measure the time the mill ran.

3.3. DEM simulation

3.3.1. DEM simulation of ball mill impact spectra

This was conducted to determine the impact spectra of quartz in ball milling. Impact spectra shows the number of impacts at each energy input.

The objective of conducting this experiment was to compare quartz impact spectra in ball milling to quartz impact spectra in a single rotor impact crusher conducted by Dajee (2018) and presented in Chapter 3, 3.3.2.

The DEM version used for the simulation was the commercial PFC3D.

The parameters used are the experimental parameters of the ball milling conducted above:

- Mill dimensions: Length = 250 mm, Diameter = 184 mm,
- Mill lifters dimensions: length =247 mm, width = 5 mm, and number of lifters = 5
- 20mm and 30mm balls were used occupying 50% by mass each.
- Mill fill by balls = 30% with 40% voidage

The size classes used are:

- -19 + 16 mm
- -13.2+11.2 mm

These size classes were selected because Dajee (2018) used the same size classes in single rotor impact crushing. To further the research on comparison between single rotor impact crusher and ball milling, more size classes can be used.

3.3.2. DEM simulation of impact crusher

A crusher to be used has a vertical shaft and consist of two rotating impellers which can rotate in the same direction or opposite directions. This crusher is a new equipment built at Wits University by Dr. Bwalya. Since only a single rotor impeller impact crusher was used before, a simulation in Discrete element method (DEM) had to be conducted to determine whether a double rotor impeller impact crusher would be an improvement of the single impeller crusher or not. The advantage of using DEM is that prediction of the performance of a mill or a crusher can be achieved without doing laboratory work. This can also help in knowing how a certain equipment will operate before doing laboratory work.

Dajee (2018) investigated the advantage of having two impellers in an impact crusher using DEM simulation by varying rotor speed and feed particle size. The crusher has a vertical shaft with two impellers at one end. The impellers rotate and have direct impact with the particles and thus rotor speed is used for particles breakage. Initially Dajee (2018) used a single impeller impact crusher for the simulations and the results were recorded and then a second impeller was used, and the results found from the simulation of the double impeller were compared to those found using a single impeller. The results showed that, a double rotor impeller impact crusher shows a significant improvement on a single rotor impact crusher.

Below is the single rotor impeller impact crusher obtained in DEM:

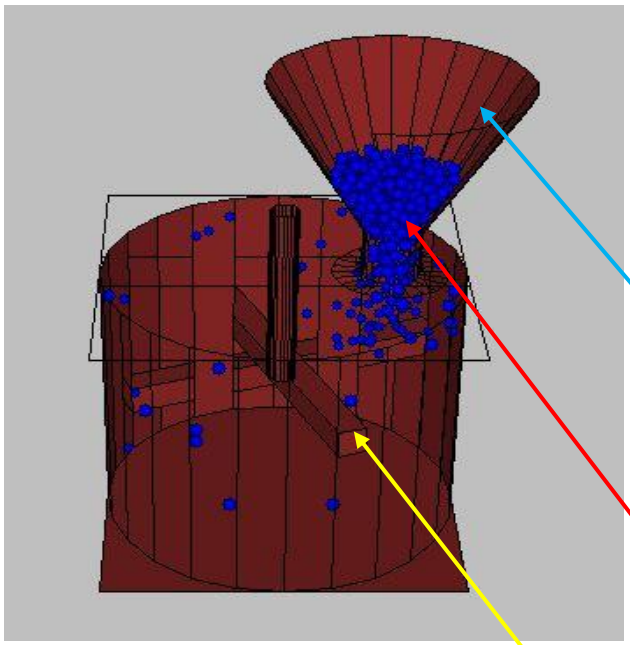


***Figure 3.5**: Single rotor design made up of 4 hammers, particles and the Cone Feeder from DEM*

After simulation with the crusher above, DEM allowed the addition of a second impeller.

Below is the double impeller impact crusher obtained from DEM:

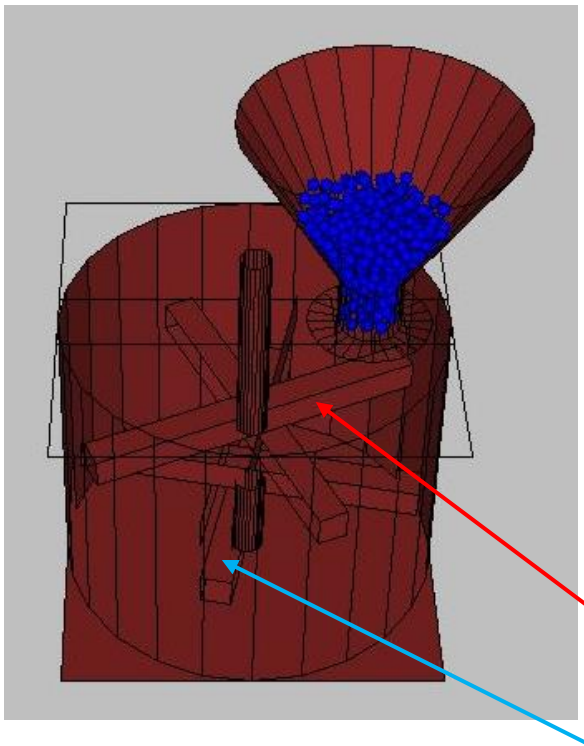


***Figure 3.6**: Double rotor impeller design with a bottom and upper impeller*

Below is the proposed design to be built:

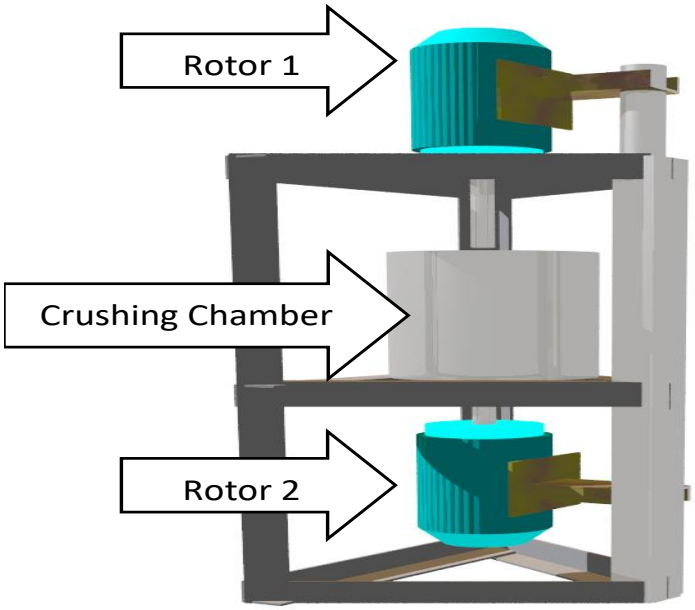


***Figure 3.7:** Double rotor impact crusher design*

The feed mechanism in Figure 3.7 will be a cone feed hopper on top of the crushing chamber.

Figures 3.5 to 3.7 show that, particles enter the crushing chamber through the feeder and crushing occurs when there is impact between the particles and the rotating impellers. This is

a batch impact crusher. Particles enter and are crushed for a certain period and the product is then removed. Impellers are made of the same size with four hammers of the same material and mass. The impellers can rotate in the same or opposite directions and the effect of changing the direction of rotation of impellers to opposite on crushing efficiency will also be investigated and compared to same direction rotation.

Dajee (2018) used the following parameters to determine the impact spectra of the double rotor counter-rotating impact crusher:

- Quartz (particles size ranges of -19 + 16mm and 13.2 + 11.2mm)
- Rotor speeds: 885rpm, 1040rpm, and 2080rpm.
- Simulation running time was 20 seconds

Using DEM simulation, we can compare the expected performance of the double rotor impact crusher with the single rotor impact crusher by comparing the energy intensities represented by DEM spectral outputs of the two simulations.

Chapter 4 : Results and discussion

The material tests involved the comparison of quartz to limestone using the drop weight tester and the batch milling kinetics done in an 18.5cm diameter mill. The batch energy spectra results were compared to that of single rotor impact crusher energy spectra to investigate if impact crushing is an improvement over conventional ball milling using DEM. The results from the single rotor impact crusher were compared to the double rotor impact crusher to investigate if the double rotor impact crusher would be an improvement over the single rotor impact crusher using DEM.

4.1. Drop weight tests

After performing drop weight tests on limestone material with the three size classes mentioned in Chapter 3. 3.1, the results showing the breakage attempts for each particle and the energy input for particle size 2 (-13.2+11.2mm) were recorded in Table 4.1 to give an example of breakage behaviour under different conditions. The results for the rest of the classes were recorded in Tables 1 to 15 in Appendix A. These results in Appendix A were used to calculate the model parameters for Limestone using Equation 2.49. These model parameters have been presented in Table 4.4 and have been used to compare the breakage behaviour of Limestone to that of Quartz.

Breakage behaviour of Particle size 1 at Height 1.

***Table 4.1**: Breakage behaviour of size class -13.2+11.2 mm at height 22.2 cm of impact weight*

-13.2+ 11.2 mm size class at 22.2 cm			
Broken at attempt no.	Particle height (cm)	Total height of the weight fall (h) (m)	Energy for each Particle (J)
1	1,1	0,123	1,942674
1	0,9	0,125	1,974263
1	0,8	0,126	1,990057
2	1,6	0,118	1,863704
4	1,1	0,123	1,942674
1	1,1	0,123	1,942674
3	1	0,124	1,958468
1	0,9	0,125	1,974263
1	1	0,124	1,958468
1	0,9	0,125	1,974263
1	1	0,124	1,958468
1	1,2	0,122	1,92688
1	1	0,124	1,958468
1	1,2	0,122	1,92688
5	1	0,124	1,958468
5	1,3	0,121	1,911086
1	1	0,124	1,958468
1	1	0,124	1,958468
1	1,2	0,122	1,92688
1	0,6	0,128	2,021645
Average Energy (Joules)			**1,951361**

The energy input was calculated using Equation 3.2. The height from bottom of drop weight tester to the top of steel weight carrier was 22.2 cm, steel weight height was 2.3 cm, weight

carrier height was 5.1 cm and Anvil, or base height was 1.4 cm. These parameters were the same for each particle in this test.

From the results in Table 4.1, the cumulative probability of breakage for particle size 2 at height 1 was recorded in Table 4.2 as follows:

Table 4.2: *Cumulative probability of breakage for particle size 2 at height 1*

Breakage no. of Attempts	Probability of breakage
1	0,75
2	0,8
3	0,85
4	0,9
5	1

Table 4.2 shows that as the number of attempts increases the probability of breakage also increases.

Equation 2.49 was used to fit experimental cumulative probability of breakage to find model parameters for the three particles sizes of limestone at the three particle heights. Sum of squares and Excel Solver function were used to find the model fit parameters. Table 4.3 shows a record of the experimental cumulative probability of breakage and the model fit probability of breakage:

Table 4.3: *Experimental and Model cumulative probability of breakage*

Breakage no. of Attempts	Probability of breakage	
	Experimental	Model
1	0,75	0,640055
2	0,8	0,802289
3	0,85	0,880355
4	0,9	0,923572
5	1	0,94937

Figure 4.1 shows the visualization of Table 4.3 on a graph with probability of breakage particle size 2 at height 3 to show how energy input affects probability of breakage with Heights 1 and 3 were converted to energy inputs using Equation 3.1:

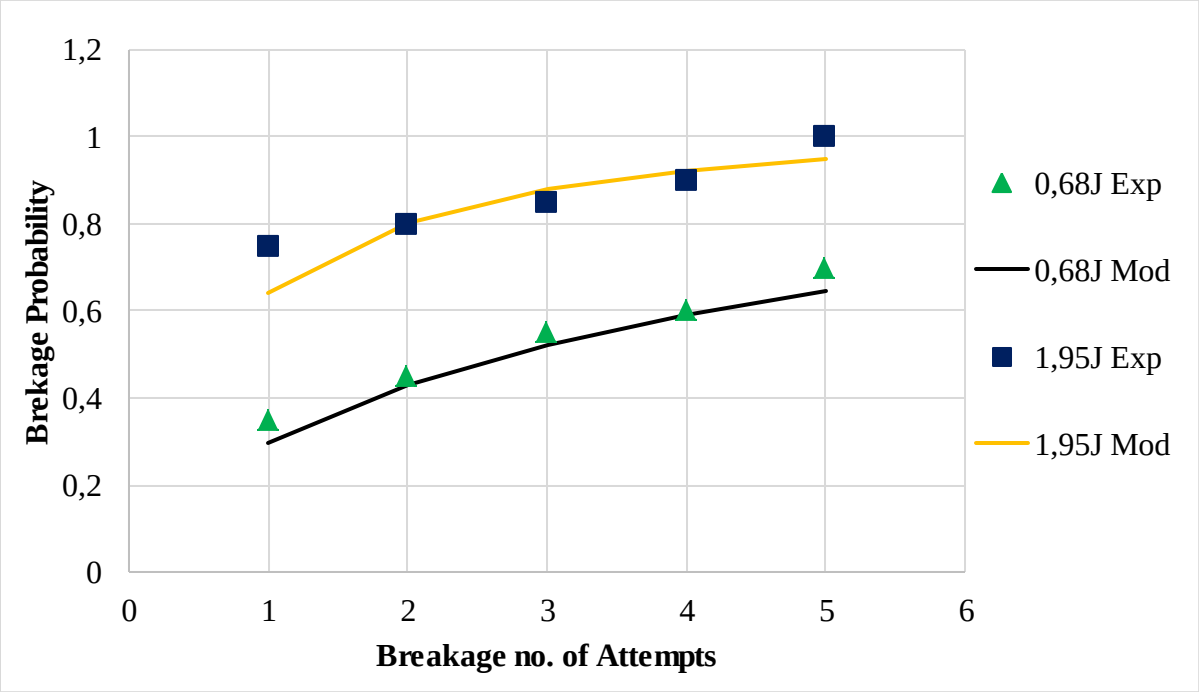


Figure 4.1: *probability of breakage versus no. of breakage attempts for particle size 2 at heights 1 and 3 energy inputs*

Figure 4.1 shows that both the no. of breakage attempts, and energy level (joules) influence the probability of breakage. This general trend observed in Figure 4.1 was found to be the same at various particle sizes and various materials. Kgetjepe (2017) observed the same trend when using Quartz material. That is, increasing breakage attempts increases probability of breakage and the higher the energy input the higher the probability of breakage.

The use of breakage attempts shows that, when energy input is low, the addition of each extra impact increases the probability of breakage. With high energy inputs, the probability of breakage is high, hence few breakage attempts are required. This is in line with Griffith (1921) theory of fracture discussed in Chapter 2, 2.3.3 which states that different particles have different flaws distribution, and these flaws act as starting points for crack propagation which leads to particle breakage.

When energy input is low, breakage occurs due to repeated impact on particles size crack propagation within the particle is slow, thus more impacts are required until breakage occurs.

Equation 2.48 by Bwalya (2005) models this phenomenon by showing that probability of breakage depends on number of breakage attempts.

With energy input, breakage occurs only when the minimum threshold energy Ex_0 is exceeded. Ex_0 defined in Chapter 2, 2.3.3, by Equation 2.47 by Bwalya (2005) as the threshold energy of a given particle mass must be overcome for breakage to occur. Equations 2.47 and 2.48 were combined to produce Equation 2.49 which models probability of breakage and is like the equation developed by Weichert (1990) and modified by Bwalya (2005). Equation 2.49 was used to produce a good fit of the experimental results shown in Figure 4.1 and showed that the probability of breakage depends on energy input and number of impacts.

This behaviour in Figure 4.1 showing how probability of breakage increases with number of impacts. Fuerstenau et al. (2003) discussed the concept of elastic energy stored in a particle due to deformation to explain why breakage of particles increase when number of impacts are increased. When a particle is under a compressive stress, energy is released at the flaw edge when the crack grows. It can also be noticed that some particles had the same size and mass, but their breakage behaviour was different. This is due to variation in flaw distribution within a particle. Particles have micro and macro flaws distributed differently within each particle. Therefore, particles of the same mass and size will break at different energy inputs and number of attempts.

4.1.1. Limestone and quartz probability of breakage model parameters

Table 4.4 presents a record of model parameters for Limestone and Quartz. These parameters were found using the probability of breakage model equation presented by Equation 2.49 and are used because they presented the best model fit for the experimental results i.e. shown by Figure 4.1 for Limestone. The parameters were found using sum of squares and the Excel Solver function to minimize the error between experimental and model results. The quartz results have been compiled by Nyoni (2019) and Table 4.4 shows what was found by him.

***Table 4.4**: Limestone and Quartz (Nyoni, 2019) probability of breakage model parameters*

Model parameters	Limestone	Quartz (Nyoni, 2019)
a	0,029	0,475
b	0,0108	0,719
c	0,011	0,341
d	0,700	0,4005

The parameters presented in Table 4.4 were put into Equation 2.49 to compare probability of breakage between Limestone and Quartz at different praticle sizes (mass (x) = 4 to 12g) and specific energy inputs (E). In Chapter 2, 2.3, the comparison between material properties between quartz and limestone have been compared and their differences makes it easier to use drop weight tests to compare these minerals.

4.1.2. Quartz and limestone probability of breakage comparison

Using the model parameters from Table 4.4, the breakage behaviour of limestone and quartz when energy input (E) = 1.0J, number of breakage attempts (n) = 1 was compared varying the particle mass (x = 4 to 12g) as shown in Table 4.5 and visualized in Figure 4.2:

Table 4.5: *Probability of breakage versus particle mass comparison between quartz and limestone at E = 1J and n = 1*

Mass (g)	Probability of breakage	
	Limestone	Quartz (Nyoni, 2019)
4	0,622519	0,27710842
6	0,668459	0,41986333
8	0,700648	0,52116174
10	0,725184	0,59738972
12	0,744849	0,65689835

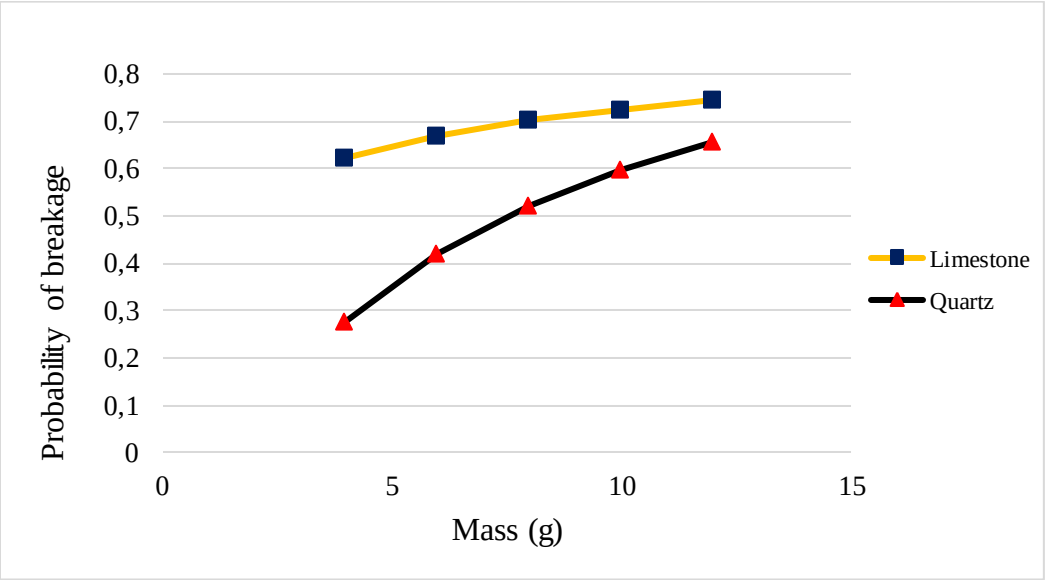


Figure 4.2*: Probability of breakage versus Mass to compare Limestone and Quartz and E = 1J and n = 1*

Now we increased the energy input while keeping n constant. The data used to plot Figure 4.3 was presented in Appendix A by Table 20.

For E = 1.8J, n =1

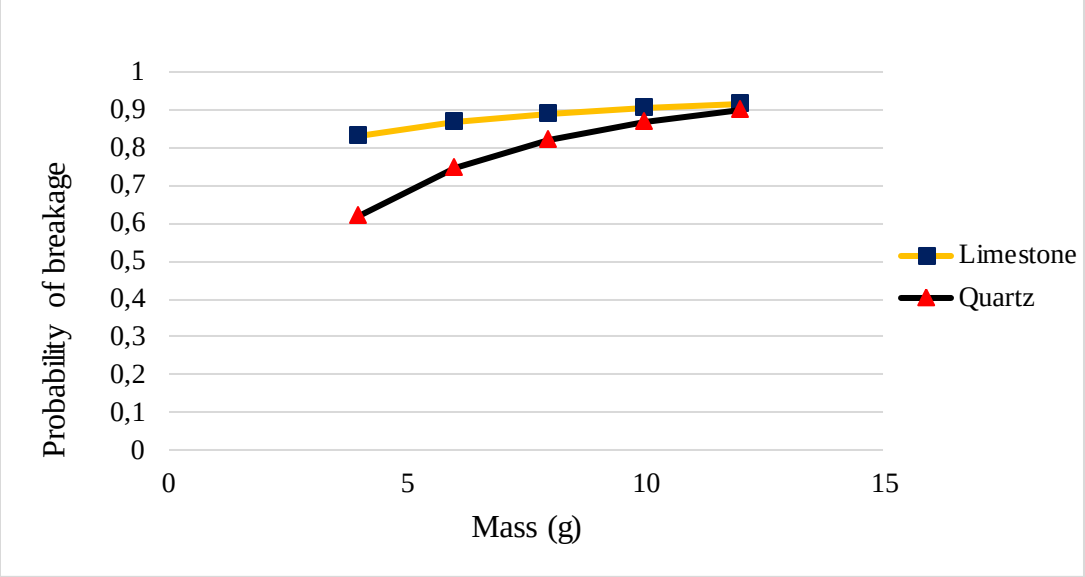


Figure 4.3: *Probability of breakage versus Mass to compare Limestone and Quartz and E = 1.8J and n = 1*

Figures 4.2 to 4.3 represented a relationship between probability of breakage and particle mass calculated by converting particle size using density of the material and average particle size. It was observed that probability of breakage which is a random process, increased with increasing mass for both limestone and quartz. Large particles have showed a high probability of breakage due to the following factors, surface area of a particle for breakage to occur, particle shape, flaw distribution within the particles, and material properties or ore mineralogy.

Bwalya (2005) presented that in drop weight tests, a particle is assumed to be broken if 30% of its original size is broken. According to this theory, large particles have a large surface area for breakage to occur compared to smaller particle. King (2001) presented that shape and size of particles defines the surface area, which plays a major role in how breakage will occur. Breakage also in drop weight tests for a particle can only occur according to the assumption of the person doing the experiments, and thus there is human error interference which might lead to wrong conclusions.

Another factor is particle size, according to the literature by Unland et al. (2008) discussed in Chapter 2, 2.2.5, it was found that the model parameters of an impact crusher differed according to particle shape as irregular particles presented a different orientation phase. It was also found that the most difficult particles to break were sphere and cubical irregular particles whilst plate-shaped or elongated particles were easier to break even at low energy

inputs. This is because flat-shaped like particles same as larger particles compared to small particles have a large surface area for breakage to occur. During impact flat-shaped like particles experience eccentric impacts with sphere shaped experiencing central impacts. The results obtained by Unland et al. (2008) are confirmed by drop weight tests in which flat-shaped like particles are easier to break compared sphere shaped.

Another factor is flaw distribution within a particle discussed in Chapter 2, 2.3.3 by Griffith (1921). Particles have micro and macro flaws within them and are distributed differently even when particles are of the same size and material type. Gilvarry (1961) stated that different particles pertain different crack distributions, and the larger the particle is, the bigger the flaw distribution volume, hence when mass of a particle is increased, probability of breakage increases.

Breakage occurs when a particle is under stress and energy is released within the particle resulting in crack propagation leading to particle fracture. Large particles have more flaws compared to smaller particles and thus large surface area for crack propagation. Griffith (1921) theory of fracture stated that particles with more flaws will result in crack propagation faster than particles with less flaws when stress is applied due to this increased crack propagation surface area. Gilvarry (1961) stated that breakage occurs when crack propagation occurs as a result of pre-existent cracks activated by the applied stress.

The main subject of this test was the material type factor in which limestone and quartz are compared in drop weight tests. Figures 4.2 and 4.3 show that the probability of breakage for limestone to be broken is higher than that of quartz for similar particle masses. This is due to the differences in material properties. In Chapter 2, 2.3, the properties of the two materials were discussed. According to Mohs (1812) hardness scale, quartz is harder than limestone with a hardness of 7 and King (2005) presented that quartz was used as an impact tool by early people due to its hardness. Due to this property, when quartz is under impact it exudes a higher resistance to breakage compared to that of limestone. This property is called material toughness.

4.1.3. Specific Threshold energy comparison between limestone and quartz

Breakage occurs because energy input exceeds minimum threshold energy E_{x0}. E_{x0} defined in Chapter 2, 2.3.3 is the minimum threshold energy of a particle that must be exceeded for a particle to be broken or energy required to initiate any form of breakage (Bwalya et al., 2020). Using Equation 2.47 and model paraments c and d from Table 4.4, the threshold

energies for particles with mass from 4 to 12g were presented in Table 4.6 and visualized in Figure 4.4:

Table 4.6: *Threshold energy for quartz and limestone particles*

Specific Threshold energy (J/kg)		
Mass (kg)	Limestone	Quartz (Nyoni, 2019)
0,004	7,235917481	148,5310699
0,006	6,407169714	116,4796304
0,008	5,877391314	98,02769136
0,01	5,496821104	85,75330817
0,012	5,204238954	76,8743487

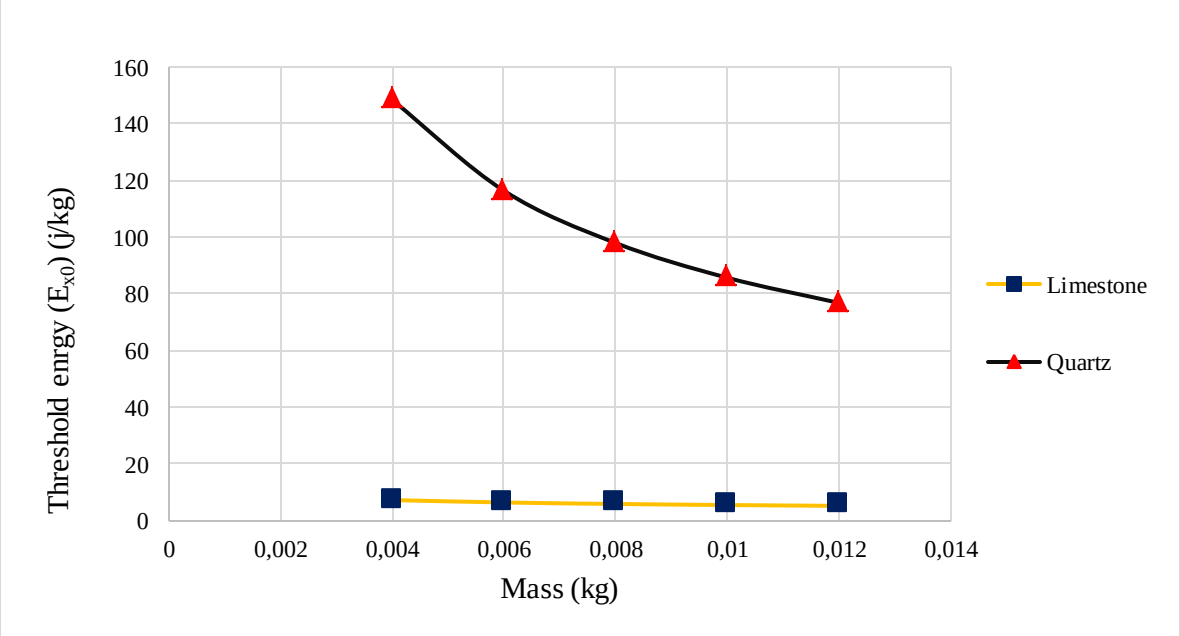


Figure 4.4: *Plot of Threshold energy comparison between quartz and limestone*

It can be observed from Table 4.6 and Figure 4.4 that threshold energy is inversely proportional to particle size. This was discussed in Chapter 2, 2.3.3 by Griffith (1921) and Gilvarry (1961) who attributed this phenomenon to an increase in flaw density when particle size increases. In Chapter 2, 2.2.5 In Chapter 2, 2.2.5 Norazirah et al. (2016) presented that threshold energy decrease with increasing particle size because breakage in large particles

break into larger fragments due to micro-cracks acting as weak zones. King (2001) discussed that before breakage occurs, there is deformation which stores elastic energy within the particle and this energy assists with crack propagation. This elastic energy is called the threshold energy required for particle breakage to occur.

To compare between quartz and limestone, Figure 4.4 shows that quartz is a stronger material with higher threshold energy compared to limestone. This is attributed to the properties of quartz such as hardness and distribution modulus as discussed in Chapter 2, 2.3 by Mohs (1812) that quartz has a hardness value of 7 with limestone having 3. Thus, more energy is needed to break quartz compared to limestone, and as particle size increases, energy required for breakage also steeply decrease for quartz with limestone having a gradual decrease with particle mass.

4.2. Ball milling

4.2.1. Selection function

After conducting milling experimental work at milling times 0.5, 1, 2, and 4 minutes using the procedure described under Chapter 3, 3.2, an example for size class -13.2+9.5 mm of quartz showing size distribution results after each milling time and a plot of $log\left(\frac{w_i(t)}{w_i(0)}\right)$ versus time to find the slope and using Equation 2.42 to find selection function are presented below in Table 4.7 below. The result for the rest of the size classes have been presented in Appendix B by Tables 17 to 26. Size class -13.2+9.5mm has been shown here as just an example of the behaviour of breakage behaviour since the same behaviour was observed for all size classes used in this experiment.

Table 4.7: *Size distribution results for -13.2 + 9.5mm size class.*

- 13.5 + 9.5 mm				
Time (min)	0,5	1	2	4
Aperture size (mm)	Mass retained on upper size class (g)			
9,5	268,45	246,18	204,41	156,33
6,7	34,79			54,56
4,75	5,09			10,53
3,35	1,94			8,44
2,8	1,32			2,3
1,4	2,73			9,04
Pan	8,01	60,82	112,88	64,58
Sieve sample (g)	322	307	318	307
Product mass (g)	1218	1215	1203	1171

In Table 4.7 the results wanted were mass retained on top screen which were used to plot Figure 4.5. w_i (t) represents the mass retained on the top screen after each milling time and w_i (0) represents the sample of the product mass fed into the sieve screens. The sampling was conducted using the spinning rifle.

Dividing mass retained by mass sampled and finding the logarithm, the results versus time were recorded in Table 4.8 and visualized in Figure 4.5 below:

Table 4.8: *logarithm of weight fraction retained divided by product sampled mass versus time*

Time (min)	Ln ((retained mass)/ (Sampled mass))
0,5	0,968501992
1,5	0,961447417
3,5	0,923304467
7,5	0,882155311

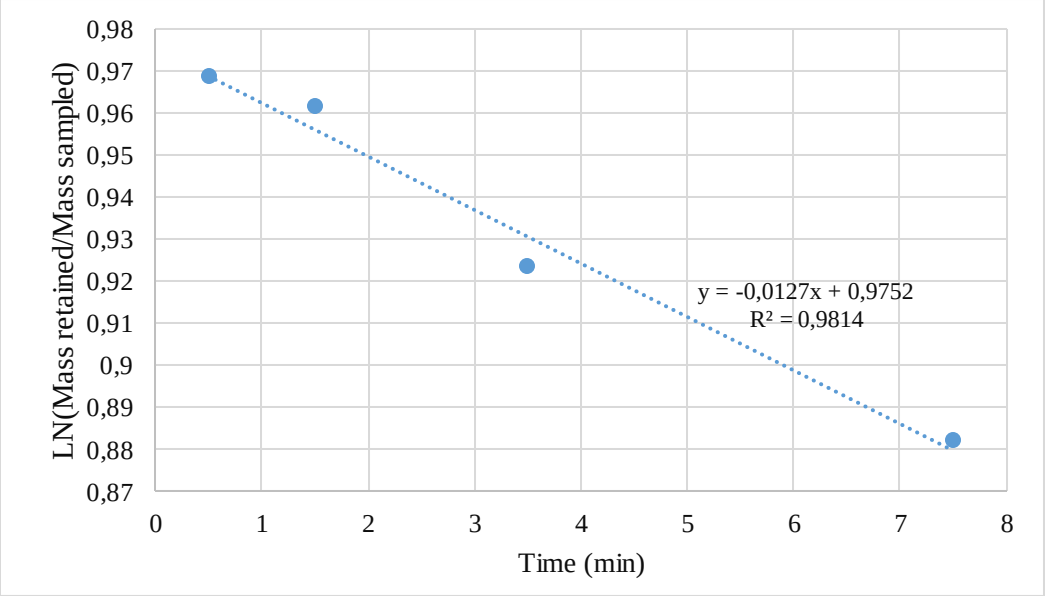


Figure 4.5: *Plot of logarithm of weight fraction retained versus time*

The slope of the graph in Figure 4.5 was used to find the selection function of size class -13.2 +9.5mm using Equation 2.42. The graph like that in Figure 4.5 has been plotted for size classes -6.7 + 4.75mm, -3.25 + 2.8mm, -1.4 + 1.00mm, -0.85 + 0.600mm, and -0.3 + 0.212mm. The plots were shown in Appendix B by Figures 1 to 5, and their slopes were used to find selection function across various size classes for quartz. The results are presented in Table 4.9 below:

Table 4.9: Selection function values for each size class for quartz.

Size class (mm)	Slope	Selection Function
-13.2+9.5	-0,0127	0,0292481
-6.7+4.75	-0,0424	0,0976472
-3.35+2.8	-0,0815	0,1876945
-1.4+1.0	-0,0651	0,1499253
-0.85+0.60	-0,0417	0,0960351
-0.3+0.212	-0,0133	0,14693

Austin et al. (1984) selection function empirical model presented by Equation 2.43 was used to fit experimental selection function data presented in Table 4.9 to find model parameters for quartz. Sum of squares and Excel Solver function were used to find the model fit parameters. Table 4.10 shows a record of the experimental selection function values versus the model fit selection and this data is visualized in Figure 4.6 below:

Table 4.10: *Experimental and model Selection values for quartz*

Screen Sizes (mm)	Quartz selection function (per minute)	
	Experiment	Model
-13.2 +9.5	0,0292481	0,032859078
-6.7 +4.75	0,0976472	0,094718231
-3.25 +2.36	0,1876945	0,189036314
-1.7 +1.25	0,1499253	0,149416577
-0.85 +0.6	0,0960351	0,095200566
-0.3 +0.212	0,0306299	0,032552009

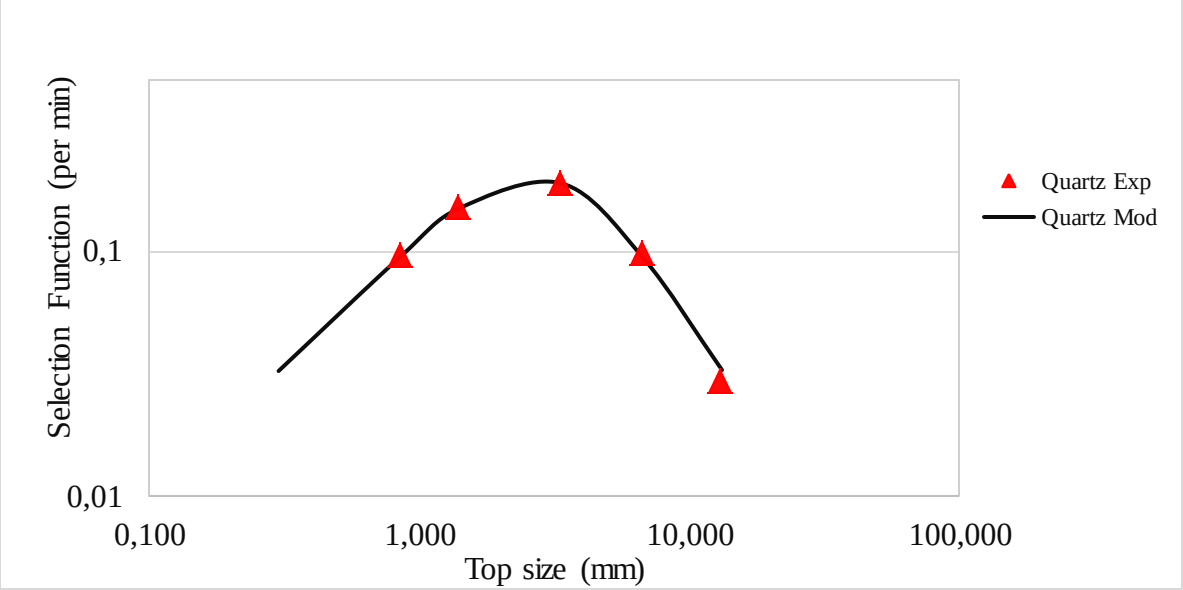


Figure 4.6: *Experimental and model selection function values for quartz*

In Figure 4.6, a log scale on both axis was used and the trend of the graph was in line with Kgetjepe (2017) and Griffith's (1921) theory of fracture since selection function increased with increasing particle size until entering an abnormal breakage region discussed in Chapter 2, 2.3.3, then steeply decreased with increasing particle size. According to Nyabando (2014), abnormal breakage region occurs because particles become too large to completely undergo breakage as they are too big to be nipped and broken effectively by the grinding media (balls). Griffith (1921) and Gilvarry (1961) stated that this is due to increasing flaw density within particles as particle size increases. The effect of particle size increase on selection function is the same on the probability of breakage of particles and this effect has been disused also in Chapter 4, 4.1. This is because the selection function also known as classification function defines the probability of a particle undergoing breakage Nikolov (2004).

Bwalya (2005) introduced the study on how particle size affects the particle strength and fracture energy. Large particles have more flaws compared to smaller particles. As the particle size decreases, the number of flaws also decreases and thus increasing the particle strength and toughness. Flaws act as stress raisers and thus large particles require less energy for crack propagation to occur. Particles of similar size from the same ore will not all have the same breakage behaviour due to differences in flaw distribution within particles.

4.2.1.1. Quartz and limestone comparison using selection function

To understand selection function to a higher, extend the selection function results obtained from quartz were compared to that of the Limestone mineral. This was conducted for the understanding of comminution kinetics. According to Fuerstenau et al. (1965), the differences in distribution modulus between Quartz and limestone makes it easier to observe the differences in comminution characteristics between the two materials.

To conduct this, the model parameters found from fitting the empirical model developed by Austin et al. (1984) presented by Equation 2.43 to experimental data in Table 4.10 and Figure 4.6 were determined for both quartz and limestone. The procedure to determine the parameters has been discussed in Chapter 4, 4.1. The limestone selection function experiments were conducted by Mvula (2018) and the model parameters have been presented in Table 4.11. Using Excel Solver function and sum of squares to minimize the error between the experimental data and the model data, the parameters of the model for both quartz and limestone were found as follows:

***Table 4.11**: Austin model selection function parameters*

Model Parameter	Quartz	Limestone (Mvula, 2018)
a	0,116	0,726
α	1,055	2,61
μ	3,138	1,44
Δ	2,760	4,11

Using the parameters from Table 4.11 and substituting them into Equation 2.43, Table 4.12 shows the selection function data for the experiment and the model for quartz and limestone and the data was visualized in Figure 4.7 where selection function (min^{-1}) was plotted against top size (mm).

Table 4.12: *Selection function experiment and model values for limestone and quartz*

Screen Sizes (mm)	Selection function (per minute)			
	Quartz		Limestone (Mvula, 2018)	
	Experiment	Model	Experiment	Model
-13.2 +9.5	0,0292481	0,032859078	0,0280966	0,068347984
-6.7 +4.75	0,0976472	0,094718231	0,218785	0,188750186
-3.25 +2.36	0,1876945	0,189036314	0,5126478	0,518793351
-1.7 +1.25	0,1499253	0,149416577	0,9294908	0,929030375
-0.85 +0.6	0,0960351	0,095200566	0,426055	0,426428424
-0.3 +0.212	0,0306299	0,032552009		0,031164461

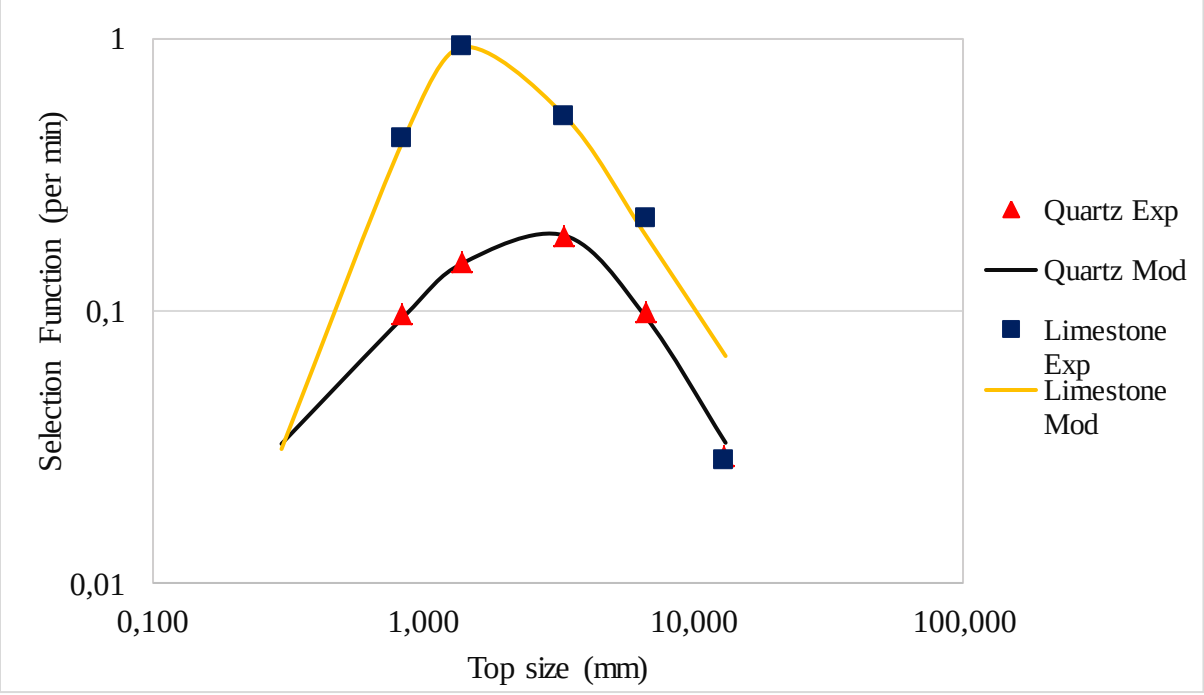


Figure 4.7*: Selection function comparison between quartz and limestone* (Mvula, 2018)

Figure 4.7 shows that the selection function of limestone is higher than that of quartz at various size classes. That is, the probability of breaking limestone under the same conditions as quartz is higher. These milling comminution results agree with the drop weight tests results discussed in Chapter 4, 4.1 that, it is easier to break limestone compared to breaking quartz. According to Fuerstenau et al. (1965) who studied the comminution kinetics using

quartz and limestone, these materials have different properties and material hardness, and distribution modulus are some of the properties which eases differentiating between the comminution characterises.

On Mohs hardness scale, quartz has a hardness value of 7 and limestone has a hardness value of 3. According to King (2005), harder materials like quartz were used by early people as impact tools, thus are not easily broken due to their toughness. Griffith (1921) presented that different materials have different energy distribution within them due to differences in atomic bonding, thus when a particle is subjected to a stress for breakage through collisions with the grinding media and other particles, energy is transferred into the particle. If the transferred energy is greater than the minimum threshold energy E_{x0} discussed in chapter 4, 4.1.3 breakage will occur. In Table 4.6 and Figure 4.4 it was observed using drop weight tests that the specific threshold energy of quartz is higher than that of limestone. This is the importance of drop weight tests as they allow the studying of material properties using single particle tests.

Nelson (2015) presented that quartz is a brittle material and limestone is a brittle-ductile material. Quartz as a brittle mineral has high strength compared to Limestone and it is also harder. Brittle breakage occurs because of flaws and dislocations within minerals. According to Thakur (2019), brittle materials have high strength compared to ductile materials and absorb little energy prior fracture because they are in the absence of plasticity.

4.2.2. Breakage function

After conducting ball milling experiments to determine breakage function, the Austin et al. (1984) BII method (See Equation 2.45) was used and breakage function was determined using the shortest grinding time of 30 seconds to avoid particle re-breakage affecting the breakage function. An example for size class -13.2 + 9.5mm showing how breakage function was found with normalized particle size was presented in Table 4.13 and visualized in Figure 4.8. The goal of this experiment was to find how breakage function varies across various size classes. Therefore, the breakage function results of size classes -6.7 + 4.75mm, -3.25+2.8mm, -1.4 + 1.00mm, -0.85 + 0.600mm, and -0.3 + 0.212mm have been presented in Appendix B, by Tables 27 to 30.

For all size classes used in this experiment, after grinding for 30 seconds sieve analysis was conducted to determine how each size class broke into lower size classes. For example, in Table 4.13 for size class -13.2 + 9.5mm, the lower size classes were -9.5 + 6.7mm, -

6.7+4.75mm, -4.75 + 3.25mm, -3.25 + 2.8mm, and -2.8 + 1.4mm. From this, breakage function was determined as how much of particle size -13.2 + 9.5mm was broken into these lower size classes.

***Table 4.13**: Breakage function experimental results and model data for size class -13.2+9.5mm*

Size class (mm)		-13.2 + 9.5					
Upper size	Lower size	Aperture size (mm)	Mass retained (g)	Mass retained (%)	Cumulative passing (%)	Normalized particle size	Breakage function (Bi,1) (Experiment)
	13,5			0	100		
13,5	9,5	9,5	268,45	83,3695652	16,6304348		
9,5	6,7	6,7	34,46	10,7018634	5,92857143	1	1
6,7	4,75	4,75	5,09	1,58074534	4,34782609	0,7037037	0,336010039
4,75	3,35	3,35	1,94	0,60248447	3,74534161	0,4962963	0,244392368
3,35	2,8	2,8	1,32	0,40993789	3,33540373	0,3518519	0,209871199
2,8	1,4	1,4	2,73	0,84782609	2,48757764	0,2481481	0,186505876
1,4	Pan	Pan	8,01	2,48757764	0	0,2074074	0,13849492
		Sieve sample (g)	322				

Table 4.13 shows the experimental breakage function data of size class -13.2 + 9.5mm. The upper size of each class was divided by 13.2mm to calculate the normalized particle size for each size class. Figure 4.8 shows the normalized particle size versus experimental breakage function below:

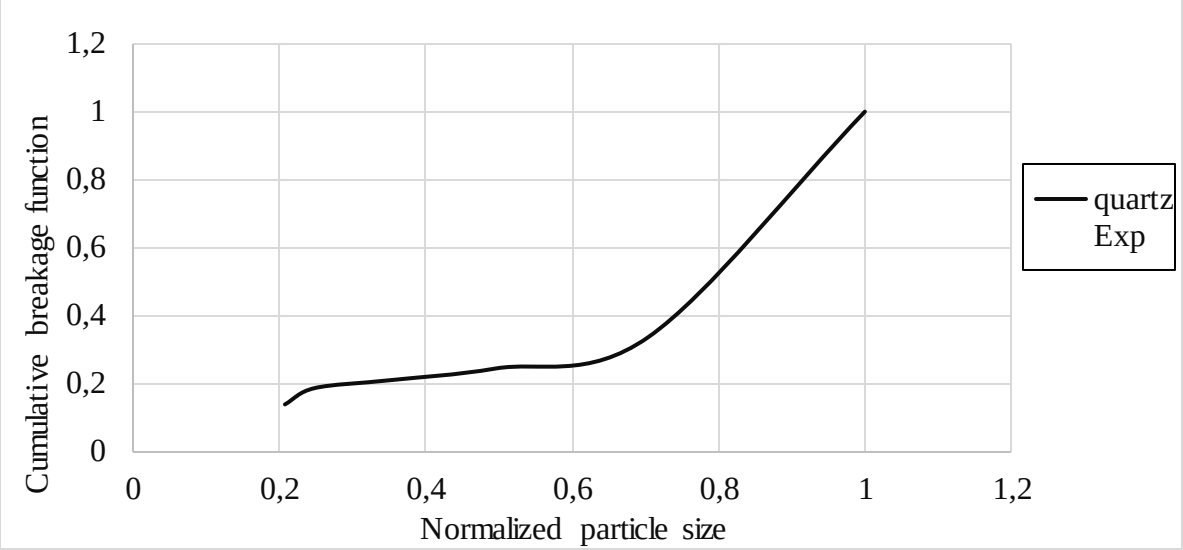


Figure 4.8: *Experimental breakage function versus normalized particle size for size class -13.2 + 9.5mm quartz*

In Figure 4.8 it was observed that breakage function increases with increasing normalized particle size. Equation 2.46 was used to find the normalized particle size and it showed that normalized particle size is directly proportional to increasing particle size. Thus, when the particle size increases the breakage function of that size also increases.

This is because the larger the particle size is, the more fragments are produced into lower size classes, thus the larger the breakage function. According to Norazirah et al. (2016), this occurs because breakage in large particles break into larger fragments due to micro-cracks acting as weak zones. This is also supported by Griffith ‘s (1921) theory of fracture discussed under drop weight tests in Chapter 4, 4.1 and Selection function in 4.2.1, that large particles have more flaws compared to smaller particles thus they have high probability of breakage, selection function and breakage function. This confirms the results regarding particle size increase and breakage as it was observed in drop weight tests, selection function and breakage functions that the larger the particle the large the probability of breakage and higher selection and breakage functions.

The Austin et al. (1984) empirical model presented by Equation 2.45 was used to find the best fit for experimental breakage function results for all size classes to obtain breakage function model parameters for quartz. Table 4.14 and Figure 4.9 shows the variation of breakage function values with normalized particle size for both experimental and model breakage function values for size class -13.2 + 9.5mm. The experimental data has also been shown in Table 4.13.

Table 4.14: *Experiment and model breakage function values for size class -13.2 + 9.5mm*

Normalized particle size	Breakage function (Bi,1) (Experiment)	Breakage function (Bi,1) (MOD)
1	1	1
0,7037037	0,336010039	0,33290584
0,4962963	0,244392368	0,18301823
0,3518519	0,209871199	0,13010645
0,2481481	0,186505876	0,09924028
0,2074074	0,13849492	0,08709663

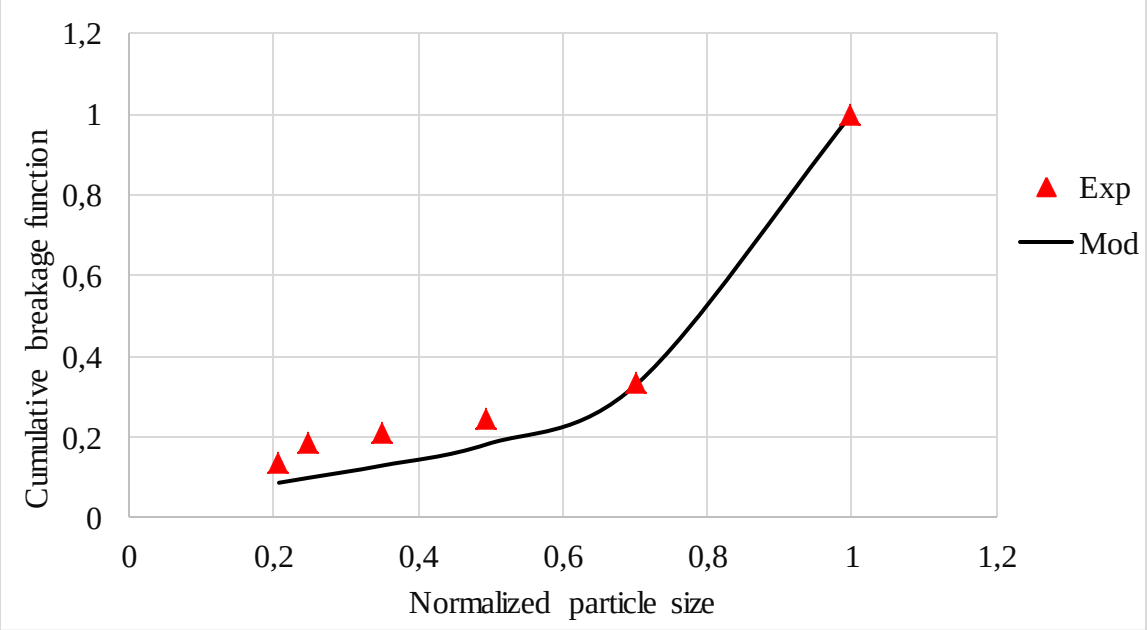


Figure 4.9: *Experiment and model breakage function versus normalized particle size for quartz size class -13.2 + 9.5mm*

Figure 4.9 shows that the empirical model presented by Austin et al. (1984) follows the experimental data trend and provides an acceptable fit since only two points fit and the rest on almost the same range.

The model parameters found by fitting Equation 2.45 to breakage function experimental data were obtained using sum of squares and Excel Solver function to reduce the error between the experimental and model values. These model parameters are shown in Table 4.15 as follows:

Table 4.15: *Quartz breakage function model parameters for quartz*

Parameters	Quartz
β	5
γ	0,70687413
φ	0,26394267

According to Austin et al. (1984), parameter φ represents a fraction of fines produced in a single fracture event and has values between 0 and 1. β and γ are material dependent and usually have the values ranging from 2.5 to 5 for β and 0.5 to 1.5 for γ. The values found in Table 4.15 fell within the defined ranges.

4.2.2.1. Breakage function Model parameters for quartz and limestone

The model parameters in Table 4.15 were determined to allow the comparison of quartz breakage function to that of limestone. Having these parameters for both minerals, Equation 2.45 can be used to predict the behaviours of the breakage function across various size classes to compare quartz to limestone. Comparing quartz to limestone using model parameters has been shown in Chapter 4, 4.1 and 4.2.1 with drop weight and selection function tests. Table 4.16 below shows selection model parameters for quartz and limestone. The limestone experiments were conducted by Mvula (2018) and these are the same results used for selection function in Chapter 4, 4.2.1.

The breakage function model parameters are shown below:

***Table 4.16**: Breakage function model parameters for quartz and Limestone* (Mvula, 2018)

Breakage function Model parameters		
Parameters	Quartz (Mokgomola, 2018)	Limestone (Mvula, 2018)
B	5	4,21
γ	0.707	0,5
φ	0.264	0,315

4.2.2.2. Comparison of quartz and limestone breakage properties using the breakage function

Using the breakage function model parameters in Table 4.16, the variation of cumulative breakage function with normalized particle size for limestone and quartz was recorded in Table 4.17 and compared on the same plot in Figure 4.10 below:

***Table 4.17:** Cumulative breakage function for quartz and limestone using model parameters*

Normalized Particle size	Breakage function (B_i,1)	
	Quartz (Mokgomola, 2018)	Limestone (Mvula, 2018)
1	1	1
0,71969697	0,3513075	0,43882994
0,507575758	0,1882295	0,26398461
0,359848485	0,1325982	0,19836097
0,253787879	0,1009006	0,16093844
0,212121212	0,0885203	0,14619008

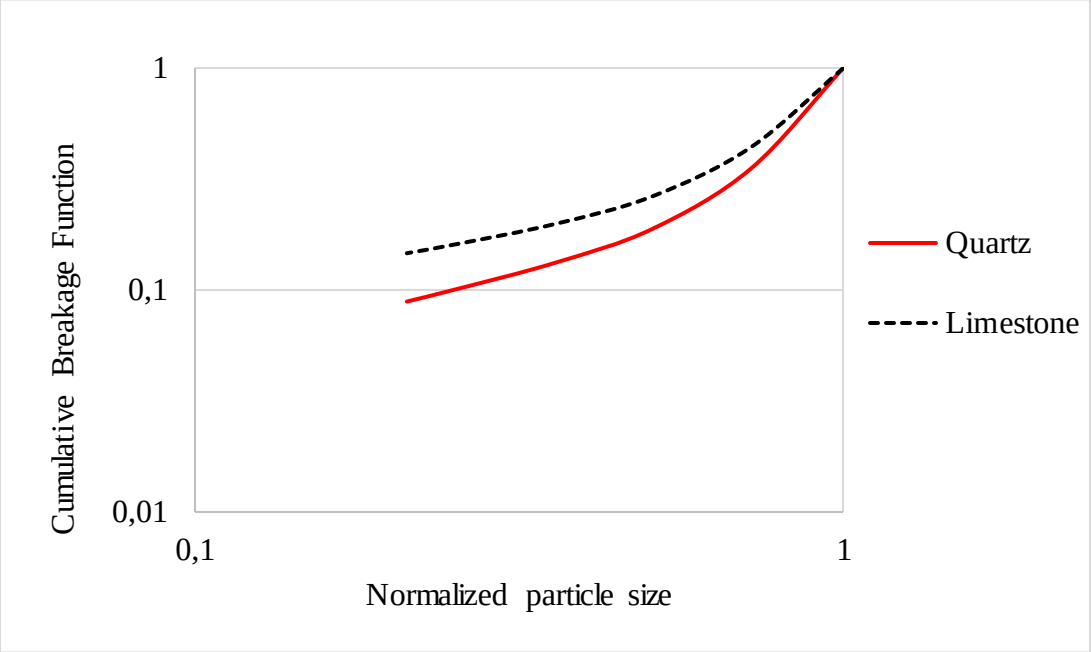


Figure 4.10: *Cumulative breakage function comparison between limestone and quartz using model parameters*

Table 4.17 and Figure 4.10 show that limestone has high breakage function compared to quartz. These results confirm what has been found by drop weight and selection function tests in Chapter 4, 4.1 and 4.2.1. The results imply that a large proportion of material break into smaller size classes when the material used is Limestone. This is consistent with the drop weight and the selection function tests since it was observed that it is easier to break limestone compared to quartz.

This is attributed to the difference in properties between the two materials. Quartz is brittle and is hard with high strength compared to limestone which is brittle-ductile and a softer material. Quartz has a hardness of 7 and limestone a hardness 3 as discussed in Chapter 2, 2.3 (Mohs, 1812; Griffith, 1921; Nelson, 2015).

4.3. DEM simulation

4.3.1. DEM simulation of ball mill energy spectra Versus impact crusher energy spectra

In this section, the results of DEM simulation energy spectra of ball milling experiments presented in Chapter 3, 3.3.1 have been compared to the energy spectra in impact crushing experiments conducted by Dajee (2018) and presented in Chapter 3, 3.3.2. The material used in DEM section to compare single rotor impact rusher to ball mill, and single rotor impact crusher to double rotor impact crusher was quartz. This is because according to Evertsson (2000) and Patnaik et al. (2007) impact crushers are mostly suitable for softer materials like coal and limestone but Dey et al. (2013) stated that under controlled conditions impact crushers can be used to crush hard materials. So, using quartz which is a harder material according to King (2005) as discussed under Chapter 2.3 with Mohs (1812) scale hardness value of 7 these comparisons will provide ease with predicting the behaviour of softer materials like limestone with a Mohs (1812) hardness value of 3 in impact crushers.

As represented in DEM ball milling experimental procedure, size classes -19 + 16mm and -13.2 + 11.2mm were chosen because Dajee (2018) had already used them in DEM impact crusher experiments. Other size classes to increase the scope of the research can be used. This was conducted to compare the effectiveness of single rotor impact crusher to that of ball milling.

Figures 4.11 and 4.12 showed the relationship between number of impacts and energy to compare ball milling number of impacts to impact crusher number of impacts at different rotor speeds of 885, 1040, and 2080rpm. The ball mill had a rotational speed of 96rpm.

Number of impacts versus energy input to compare ball milling and impact crushing on the same plot for -19 + 16 mm quartz size class:

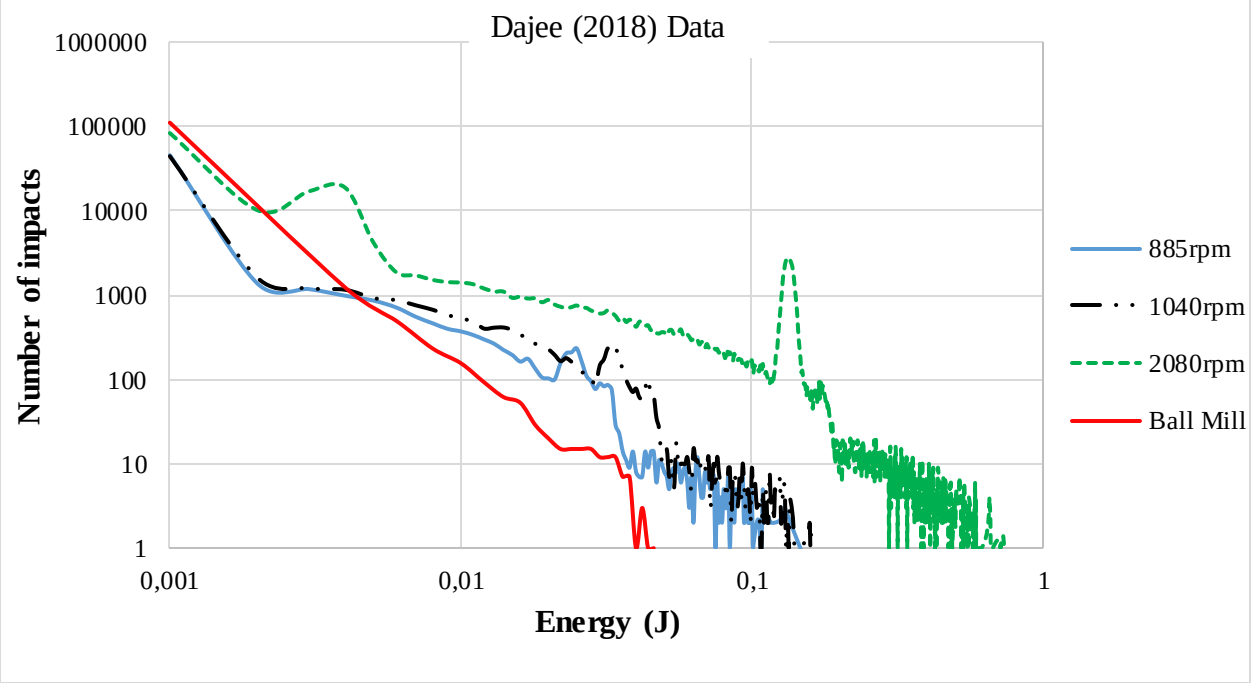


Figure 4.11: *Energy spectra for a single rotor impact crusher and ball milling on the same plot for particle size -19.0+16.0 mm*

Number of impacts versus energy input to compare ball milling and impact crushing on the same plot for -13.2 + 11.2 mm quartz size class:

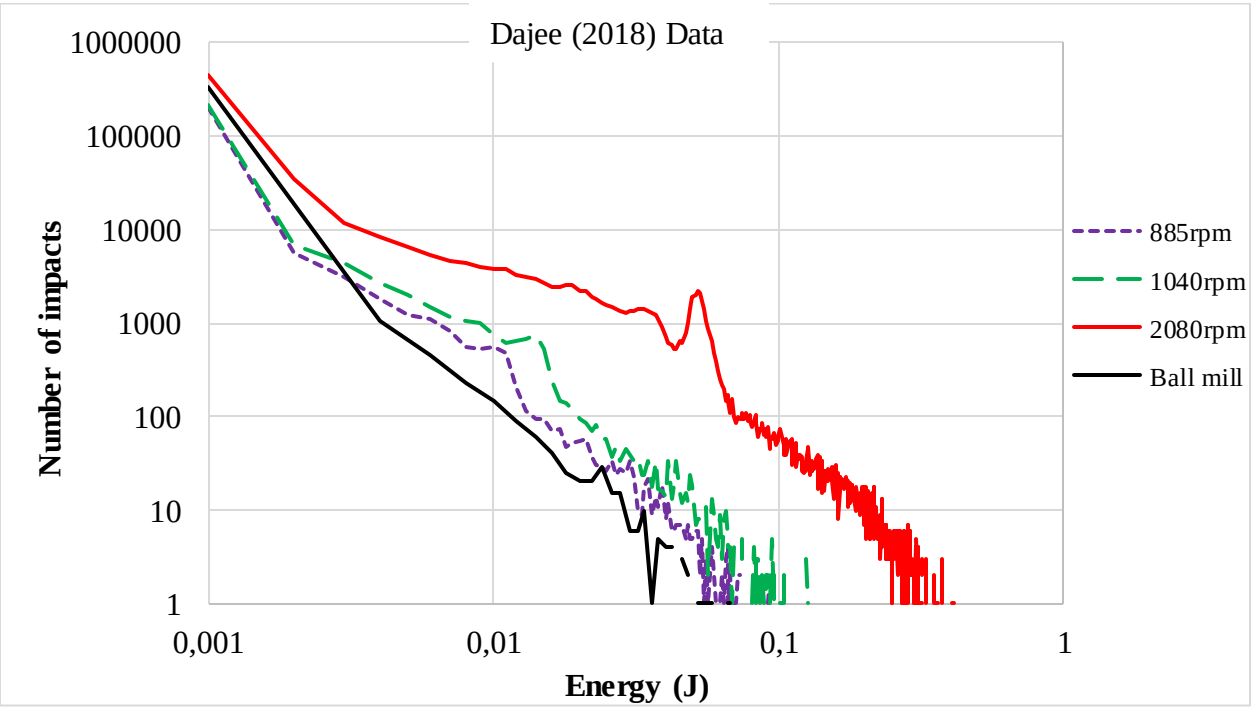


Figure 4.12*: Energy spectra for a single rotor impact crusher and ball milling on the same plot for particle size -13.2+11.2 mm*

Figures 4.11 and 4.12 results compare ball milling and impact crusher performance using the number of impacts and energy input. In Chapter 4, 4.1.3, it was discussed that breakage occurs when energy input is greater than the minimum threshold energy E_{x0}. These figures provided the number of impacts that exist in ball milling and impact crushing when energy input exceeds E_{x0}. Size class -19 + 16mm quartz has an average mass of 10.6g. According to the drop weight test model parameters discussed in Chapter 4, 4.1.1 using Equation 2.49, the E_{x0} of this class was 0.87J with size class -13.2 + 11.2mm having an average mass of 3.6 and E_{x0} of 0.57J.

In Figure 4.11 it can be observed that ball milling had no events above size class -19 + 16 mm which had E_{x0} = 0.87J and the result was the same for size class -13.2 + 11.2mm. With impact crusher events, Figure 4.11 also showed that above 0.87J, rotor speeds of 885rpm and 1040rpm had no breakage events and as the rotor speed increased to 2080rpm, number of impacts increased to approximately10 events. The advantage of impact crushing to ball milling is that the speed can be increased to increases the number of impacts while ball milling speed remains below the critical speed. Critical speed defined in Chapter 3, 3.2 is the speed at which the mill charge begins to centrifuge and is discussed in the next paragraph.

Effect of speed and particle size in ball milling and impact crushing

At low speed inputs, there will be no significant breakage in both ball milling and impact crushing since there will be no energy transferred from the grinding medium to the material for breakage to occur. According to Nyabando (2014) the speed of the mill directly affects the motion of the charge inside the mill; thus, mills must operate at speeds lower than the critical speed. Three behaviours that can happen to the mill charge as a result of mill speed are cascading, cataracting and centrifuging (Nyabando, 2014).

Cascading occurs when mill speed is less than 60% of the critical speed. When this happens, the mill charge rolls down to the toe of the mill and the breakage mechanisms that occur are attrition and abrasion without impact breakage. Cataracting occurs when the mill speed is within a range between 60 % to less than 100% of the critical speed. At this stage, the grinding media rolls to the top of the mill, then falls to the mill charge resulting into breakage (Ajaal et al., 2002; Kasture et al., 2008).

For breakage to occur within a mill, cataracting must occur in the mill. Impact, attrition and abrasion breakage mechanisms are present at this stage. For example, in the milling experiment conducted, the critical mill speed was 100.2rpm and the variable speed used was

96rpm. Centrifuging occurs when the mill speed is greater than the critical speed causing the mill charge to centrifuge on the walls of the mill (Ajaal et al., 2002; Kasture et al., 2008, Lameck, 2006). This was explained to show that, unlike impact crusher, ball mill speed should always remain within a certain range for breakage to occur. This proved that the single rotor impact crusher is a significant improvement on ball milling.

In impact crushing, low speed means particles will escape contact from the impact hammers leading to less production of fragments. When rotor speed increases number of impacts also increase. This is because particle very rarely escape contact from impact hammers and are thus energised with energy that exceeds E_{x0} leading to increasing number of impacts. These energised particles also meet other particles transferring energy and more impacts are generated due to particle-particle collisions and more fragments are produced. This effect of speed increase was in line with the work conducted by Nikolov (2002; 2004) and Bwalya (2005), presented in Chapter 2, 2.2.3 in which it was stated that high size reductions are achieved with increasing rotor speed in impact crushing. High rotor speed increases the probability of breakage of particles.

In the case of impact crushers, particles at high energy in a confined space like the crusher chamber will not lose all energy after a single collision but ricochets across ay surface in the path. From this it can be concluded that an increase in speed of rotor increases the probability of breakage since the energy of impacts in particles increases above the threshold energy of breakage according to Bwalya's model (Bwalya, 2005).

As discussed in Chapter 4, 4.1 and 4.2 regarding particle size and breakage, Figure 4.11 showed that for size class -19 + 16mm, number of impact events at the used rotor speeds are higher compared to those of size class -13.2 + 11.2mm. This is in line with drop weight, selection and breakage function tests in which it was confirmed that increasing particle size increases the probability of breakage due to flaw density within particles. According to Griffith (1921) the larger the particle the larger the flaws which initiate crack propagation when energy input exceeds E_{x0}.

Particle shape does not have an effect since DEM assumes spherical particles. According to Wagner (2005) and Unland et al. (2008), spherical particles have the highest contact forces and energy transfer within the lowest contact time compared to other shapes discussed in Chapter 2, 2.5. During crushing, spherical particles experience central impacts, have the highest energy utilization and most difficult to crush compared to plate-shaped, elongated,

and acicular particles. This information about the behaviour of spherical particles during crushing is the reason why spherical particles are used as the basis in comminution calculations (Unland et al, 2008).

4.3.2. Improving a single rotor impact crusher design by adding a second rotor using DEM simulation

In Chapter 4, 4.1 and 4.2 drop weight, selection and breakage function tests were explored using particle shape and size, material type and energy input to determine how breakage behaviour is affected across these tests. Impact crushing was introduced and compared to ball milling and it was found that impact crushing with a single rotor impact crusher shows a significant improvement over ball milling because of speed.

In this section the question was, will adding a second rotor which can co-rotate or counter rotate with rotor 1 improve the single rotor impact crusher? This was explored using DEM results conducted by a Wits University student named Dajee in 2018. This was conducted to use DEM to predict the behaviour of a double rotor impact crusher and compare it to the single rotor impact crusher design.

All these results were obtained from the energy spectra obtained in DEM. Figures 4.13 and 4.14 show how the number of impacts between particles are affected across the single and the double rotor impact crusher design. Figures 2.2 and 3.5 show a representation of a vertical shaft single rotor impact crusher and Figures 3.6 and 3.7 show a representation of the double rotor impact crusher.

Effect of adding a second rotor

This effect was explored across size classes -19 + 16 mm and -13.2+11.2 mm used in this experiment and across all rotor speeds (885rpm, 1040rpm, and 2080rpm) used in this experiment. However, to show examples of this effect the results for size classes -19+16mm and -13.2+11.2mm at a rotor speed of 1040rpm were shown in Figures 4.13 and 4.14 with the results of size class -13.2+11.2mm at a rotor speed of 885rpm also shown in Figure 4.15 below:

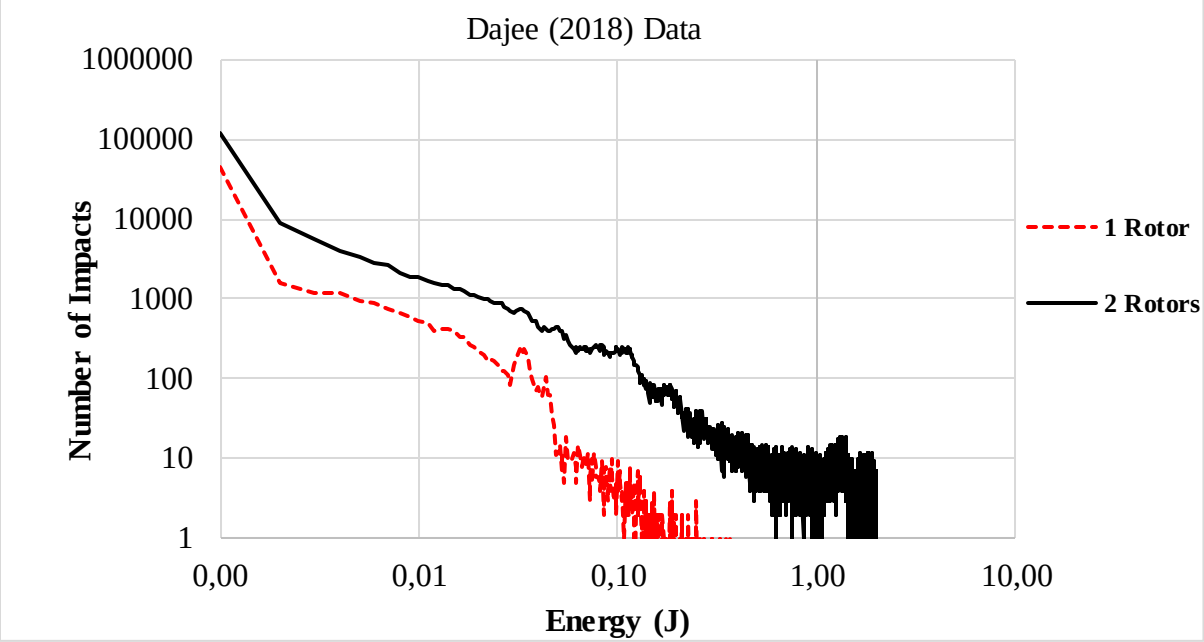


Figure 4.13: *Energy spectra showing the effect of adding a second rotor with particle size - 19.0+16.0 mm at speed 1040 rpm*

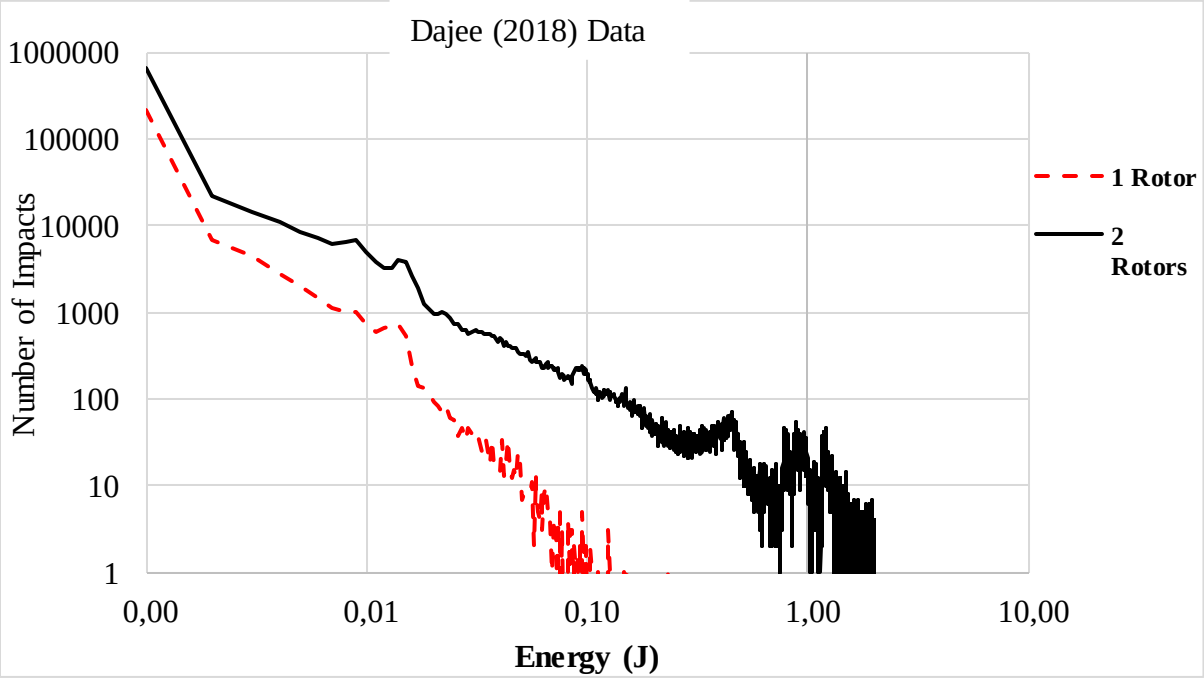


Figure 4.14: *Energy spectra showing the effect of adding a second rotor with particle size - 13.2+11.2 mm at speed 1040rpm*

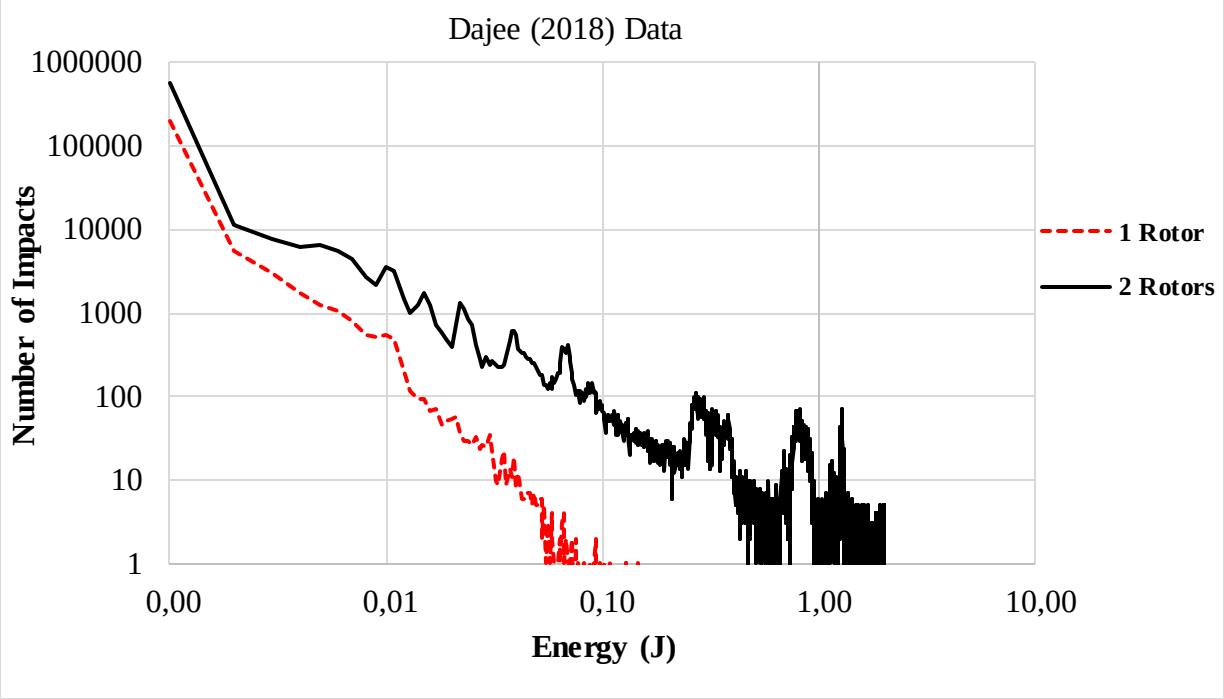


Figure 4.15: *Energy spectra showing the effect of adding a second rotor with particle size -13.2+11.2 mm at speed 885rpm*

For size classes -19+16mm and -13.2+11.2mm, their minimum threshold energies are respectively E_{x0} = 0.87J and E_{x0} = 0.57J discussed in 4.3.1 above. Figures 4.11, 4.12, 4.13, 4.14, and 4.15 showed that a single rotor impact crusher at speeds 885rpm and 1040rpm does not exceed the minimum threshold energies of 0.87J and 0.57J for breakage to occur. At the same speeds but after adding the second rotor, the threshold energy was exceeded and above 0.87J and 0.57J there was impact events as shown by Figures 4.13 to 4.15. This confirms that the addition of the second rotor to a single rotor impact crusher has the same effect and trend across the size classes and rotor speeds used.

When 2 rotors which can rotate in the same direction or counter rotate were used, impact events occurred not because speed was increased but because of doubled relative velocity between the 2 rotors. When particles are fed into this type of impact crusher, the contact between particles and the upper impact hammers transfers energy into particles. These energised particles gain more energy from particle-particle collisions and then they collide with the bottom rotor impact hammers moving at high speed and are energised to overcome the minimum threshold energy leading to collisions. An example of this is comparing a moving object crushing into a stationery object to two moving objects colliding with each other, the latter will result into more fatalities than the first one.

This shows that, having two rotors increases collisions because the bottom rotor acts as a second obstacle to the particles thus particles rarely escape contact from impact hammers. Using a single rotor impact crusher, increasing fines production means after crushing, the product will be crushed again and again until the desired product size distribution is achieved. This consumes time and energy, and even contributes to mass loss of the material due to mishandling while moving from 1 pass to another. With two rotors at work, the production of fines or fragments from first and second passes is achieved with a single pass.

Figures 4.11 and 4.12 showed that when the speed was increased to 2080rpm, the minimum threshold energies of 0.87J and 0.57J were overcome and impact events occurred. This showed that increasing rotor speed increases the breakage rate of particles in a single rotor impeller crusher, but this means that more energy is consumed and thus high operating costs. Adding a second rotor impeller as shown in Figure 4.13 increased the breakage probability by the addition of a second obstacle to the particles without the need to increase the speed.

4.3.2.4. The combined effect

In this section, it was explored how energy can be saved in impact crushing by comparing number of impacts of a double rotor impact crusher design running at a very low speed of 885rpm to the number of impacts of a single rotor design running at a higher speed of 2080rpm.

This was conducted to investigate if the double rotor design can outperform the single rotor design when ran at a lower speed. Figures 4.15 and 4.16 below shows the results for all size classes used in this experiment:

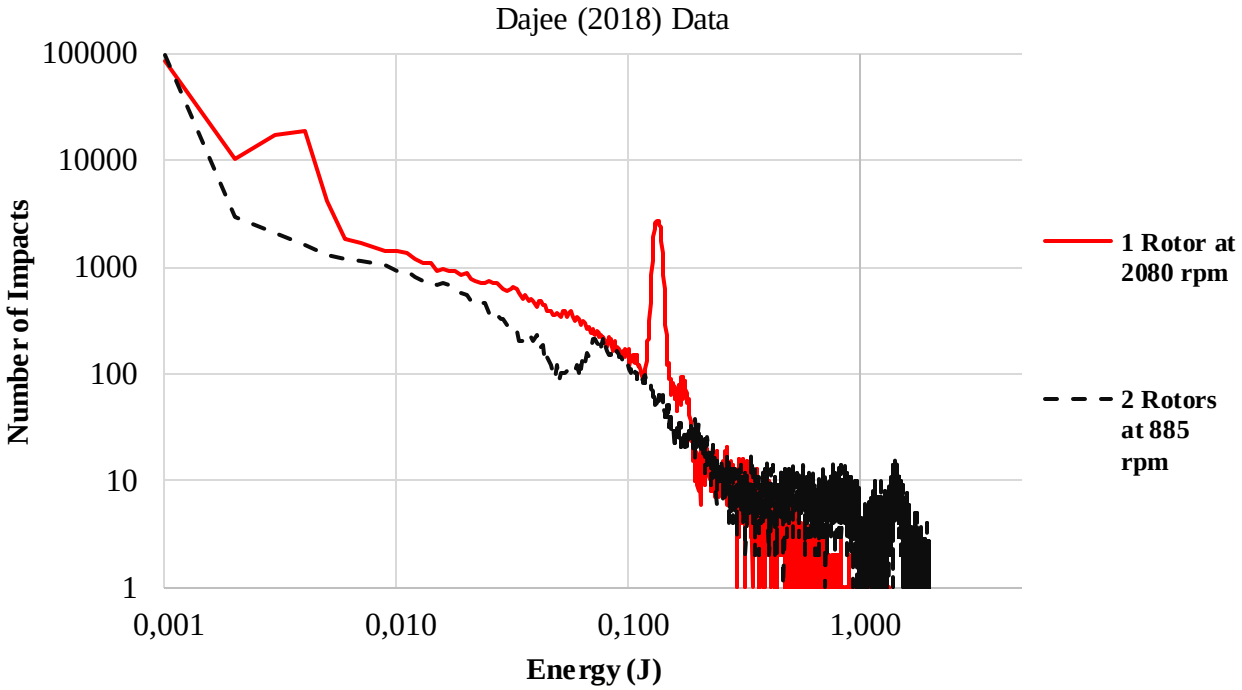


Figure 4.16: *Energy spectra showing a single rotor design at 2080 rpm and double rotor design at 885 rpm with a particle size class of -19.0+16.0 mm*

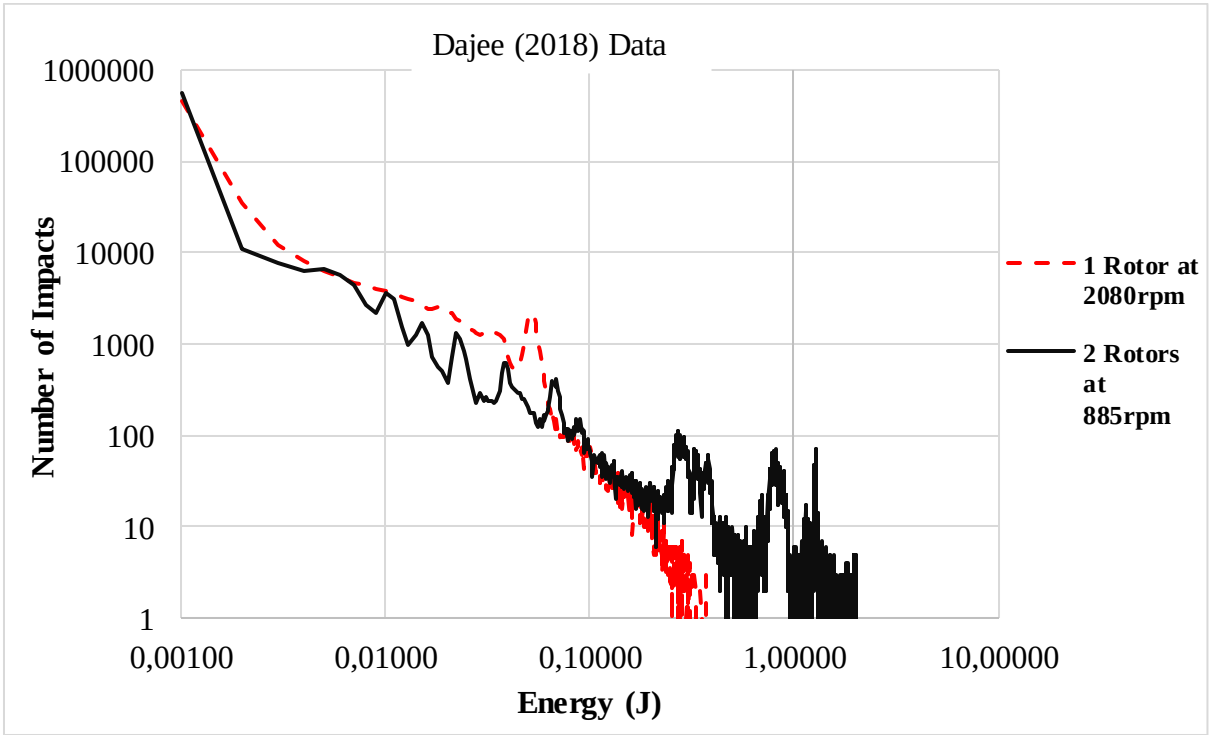


Figure 4.17: *Energy spectra showing a single rotor design at 2080 rpm and double rotor design at 885 rpm with a particle size class of -13.2+11.2 mm*

Figures 4.11 and 4.12 agree that a single rotor impact crusher design can only transfer energy greater than E_{x0} for size classes -19+16mm and -13.2+11.2mm only at a rotor speed of

2080rpm. This means that energy input must be increased to achieve breakage thus leading to increased operation costs. An alternative to this was provided by presenting a double rotor impact crusher with a rotor speed of 885rpm. It was found that for size classes -19+16mm and 13.2+11.2mm presented by Figures 4.16 and 4.17, the double rotor design at the lowest rotor speed of 885rpm outperforms the highest rotor speed of 2080 rpm of a single rotor design.

Figures 4.16 and 4.17 showed that, above the minimum threshold energies for the given size classes, double rotor impact crusher had more impact events even when running at a low speed compared to a single rotor impact crusher even when running at a high speed. The number of impacts is high in double rotor crusher due to increased residence time of the particles within the crusher. The residence time is high due to three ways in which particles can be energised. Particles are energised by contact with the moving upper rotor impact hammers, particle-particle collision, and contact with the moving bottom rotor impact hammers. In single rotor impact crusher, particles can be energised only in two ways which are contact with upper rotor impact hammers and particle-particle collisions.

For these DEM simulations, the residence time set was 20 seconds but for single rotor impact crusher, it was observed that particles settle before the 20 seconds run is complete. However, this was not the case in a double rotor design due to the existence of the second rotor which acted as a second obstacle for the particles maintaining activity in the impact crusher and particles broken by upper rotor impact hammers were broken further by the second rotor increasing the production of fines.

Using a single rotor means that the residence time is small and particles that will escape contact from the impact rotor hammers will not be ground and to achieve the desired particle size, re-grinding should be performed which is time and energy consuming. The addition of a counter-rotating rotor allows the crusher to achieve the desirable results at half the speed of a traditional single-rotor design at a high breakage rate and less power consumption.

From the simulation results shown in Figures 4.16 and 4.17 it was observed that the double rotor impact crusher will provide a significant improvement over the traditional single rotor impact crusher with increased production of fines at low energy requirements and less crushing periods. The double rotor impact crusher from these experiments moved the energy spectra into more effective breakage regions at relatively low speed and energy input.

This new mode of impact crusher will be a Vertical shaft impact crusher shown in Figure 2.2 but with two rotors as shown in Figures 3.6 and 3.7. In Chapter 2, 2.2.2, it was presented by Gupta (2011) that this type of crusher can be used in the tertiary grinding of hard rock material and can also be used to grind sand and gravels.

Conclusion

This project was conducted to investigate if adding a second rotor impact hammer impeller will be a significant improvement over the previous single rotor impact hammer crusher. The effectiveness of the traditional single rotor impact crusher was compared to that of ball milling based on the effect of speed and residence time. DEM simulation was used for these occasions. DEM allowed the prediction of the behaviour of these crushers without doing the actual experiments. The Comminution characteristics of limestone and quartz using Drop weight tests and Ball milling selection and breakage functions were investigated.

DEM simulation showed that the proposed double rotor impact crusher design will have superior grinding capabilities at significantly lower speeds of 885rpm compared to a single rotor impact crusher at higher rotor speeds of 2040rpm. At a lower speed of 885rpm the double rotor impact crusher had more impact events above the threshold energies (0.87J and 0.57J) for size classes -19+16mm and -13.2+11.2mm than the single rotor impact crusher at a high rotor speed of 2040rpm. This proved that the double rotor impact crusher saves production costs. The residence time set for both rotor tests was 20 seconds and the single rotor impact rusher particles settled before the set residence time of 20 seconds. This was found not to be true for the double rotor impact crusher since the added rotor acted as the second obstacle to particles. These DEM results provided design insights before embarking on expensive physical experimental work.

The improved numbers of impacts when an impact crusher was used were compared to ball milling and it was found that the impact mechanism depending on speed is superior to mechanisms in ball milling even when residence time in ball milling was high. Residence time in both crushers was 20 seconds but in the single rotor impact crusher particles settled before the end of 20 seconds which made ball milling have the highest residence time. In impact crushing when rotor speed increased from 885rpm to 1040 rpm number of impacts increased whilst in ball milling the variable speed used of 96rpm had to stay within a certain interval of the critical speed. Impact crushing outperformed ball milling due to increasing rotor speeds while ball milling speeds were constrained to the critical speed of 100.2rpm.

Comminution characteristics between quartz and limestone showed that it is easier to grind limestone compared to quartz. This was confirmed by the results found in drop weight, selection, and breakage function tests. The drop weight tests showed that limestone and quartz had the probability of breakage range from 0.62 to 0.74 and 0.28 to 0.66 for the same

particle mass ranging from 4g to 12g when the breakage attempt was 1. The Selection function of limestone was higher ranging from 0,0312 to 0,068 whilst that of quartz was ranging from 0,0326 to 0,0329. All the values between these ranges of selection function for limestone were higher than those of quartz across the size classes used. Breakage function values of limestone ranged from 0,146 to 1 and for quartz from 0,0885 to 1 across the size classes used for the testing.

This was attributed to the difference in material properties between the two minerals such as hardness, strength and distribution modulus. The hardness value of quartz was 7 and that of limestone was 3. Distribution modulus of quartz was 0.9 and that of limestone was 0.6.

In drop weight tests, increasing energy input and particle size increased the probability of breakage and the minimum threshold energy required for breakage to occur decreased with increasing particle size. This was attributed to flaw density within the particles. Probability of breakage also increased with increasing elongation of the particle which increased the surface area for breakage to occur.

In ball milling, increasing particle size increased the probability of breakage by increasing both selection and breakage functions. The relationship between selection function and particle size is directly proportional until a certain turning point of particle size when abnormal breakage region is reached, then probability breakage starts to decrease with increasing particle size. This occurred because particles became too big to be nipped by the grinding medium for breakage to occur. Breakage function showed a direct relationship with probability of breakage since it is normal for larger particle sizes to produce more fragments compared to smaller particles.

Recommendations

- Wear is usually a key problem with this type of equipment, and it is recommended that a DEM simulation to access the potential wear of the equipment is conducted.
- It is also recommended that once the new impact crusher with double rotor is built, the DEM data used here be revisited and appraised accordingly.

References

Attou, A., Gustein, R. and Clepkens, O. (1999). Modelisation de la fragmentation de matiere solide dans un concasseur `a chocs `an axe horizontal. In: C.T.P. Report TP. 909.99, pp.19-28.

Ajaal, T., Smith, R., & Yen, W. (2002). The Development and Characterization of a Ball Mill for Mechanical Alloying. *Canadian Metallurgical Quarterly*, *41*(1), 7-14. doi: 10.1179/cmq.2002.41.1.7

Austin, L., Klimpel, R., Luckie, P., & Klimpel, R. (1984). *Process engineering of size reduction*. New York: Society of Mining Engineers of the American Institute of Mining, Metallurgical, and Petroleum Engineers.

Bengtsson, M. and Evertsson, C. (2008). Modelling of output and power consumption in vertical shaft impact crushers. *International Journal of Mineral Processing*, 88(1-2), pp.18-23.

Borg, G., & Scharfe, F. (2015). Improved Particle Liberation by High-Velocity Comminution – the new VeRo Liberator. *Cuprum - Czasopismo Naukowo-Techniczne Gornictwa Rud*, *75*, 5-14.

Bourgeois, F., & Banini, G. (2002). A portable load cell for in-situ ore impact breakage testing. *International Journal of Mineral Processing*, *65*(1), 31-54. doi: 10.1016/s0301-7516(01)00057-6

Bwalya, M. (2005). Using the discrete elements method to guide the modelling of semi and fully autogenous milling (Postgraduate). University of Witwatersrand.

Bwalya, M., & Chimwani, N. (2020). Development of a More Descriptive Particle Breakage Probability Model. *Minerals*, *10*(8), 710. doi: 10.3390/min10080710

Cleary, P., & Sinnott, M. (2015). Simulation of particle flows and breakage in crushers using DEM: Part 1 – Compression crushers. *Minerals Engineering*, *74*, 178-197. doi: 10.1016/j.mineng.2014.10.021

Cundall, P. (1971). A computer model for simulating progressive large-scale movements in blocky rock systems. *Proc. Symp. Int. Soc. Rock Mech, Nancy*.

Cundall, P., & Strack, O. (1979). A discrete numerical model for granular assemblies. Géotechnique, 29(1), 47-65. doi: 10.1680/geot.1979.29.1.47

da Cunha, E., de Carvalho, R., & Tavares, L. (2013). Simulation of solids flow and energy transfer in a vertical shaft impact crusher using DEM. *Minerals Engineering*, *43-44*, 85-90. doi: 10.1016/j.mineng.2012.09.003

Dajee, M. (2018). Numerical Simulation of a Single and Double-Rotor Impact Crusher Using Discrete Elemental Method (Undergraduate). University of the Witwatersrand.

Deniz, V. (2011). A new size distribution model by t-family curves for comminution of limestones in an impact crusher. *Advanced Powder Technology*, *22*(6), 761-765. doi: 10.1016/j.apt.2010.10.020

Deresiewicz., H. (1958). Mechanics of granular matter. In Advances in Applied Mechanics. Elsevier, 5, 233-306.

Dey, S., Dey, S., & Das, A. (2013). Comminution features in an impact hammer mill. *Powder Technology*, *235*, 914-920. doi: 10.1016/j.powtec.2012.12.003

Djordjevic, N., Shi, F., & Morrison, R. (2003). Applying discrete element modelling to vertical and horizontal shaft impact crushers. *Minerals Engineering*, *16*(10), 983-991. doi: 10.1016/j.mineng.2003.08.007

Eksi, D., Hakan Benzer, A., Sargin, A., & Genc, O. (2011). A new method for determination of fine particle breakage. *Minerals Engineering*, *24*(3-4), 216-220. doi: 10.1016/j.mineng.2010.08.006

Fuerstenau, D., & Kapur, P. (1995). Newer energy-efficient approach to particle production by comminution. *Powder Technology*, *82*(1), 51-57. doi: 10.1016/0032-5910(94)02891-q

Fuerstenau, D., Kapur, P., & Velamakanni, B. (1990). A multi-torque model for the effects of dispersants and slurry viscosity on ball milling, *International Journal of Mineral Processing, 28* (1), 81–98.

Fuerstenau, M., & Han, K. (2003). *Principles of mineral processing* (1st Ed.). Littleton, Colo.: Society for Mining, Metallurgy, and Exploration.

FUERSTENAU, D., & SOMASUNDARAN, P. (1965). COMMINUTION KINETICS. In *Sixth International MINERAL PROCESSING CONGRESS* (pp. 25-31). Cannes:

PERGAMON PRESS OXFORD. Retrieved from http://www.columbia.edu/~ps24/PDFs/Communution%20Kinetics.pdf

Gilvarry, J. (1961). Fracture of Brittle Solids. I. Distribution Function for Fragment Size in Single Fracture (Theoretical). *Journal of Applied Physics*, *32*(3), 391-399. doi: 10.1063/1.1736016

Griffith, A. (1921). The Phenomena of Rupture and Flow in Solids. *Philosophical Transactions of the Royal Society A: Mathematical, Physical and Engineering Sciences*, *221*(582-593), 163-198. doi: 10.1098/rsta.1921.0006

Gupta, C. (2006). Chemical Metallurgy: Principles and Practice (1st ed., pp. 130-131). John Wiley & Sons.

Gupta, D. (2011). Design and analysis of a horizontal shaft impact crusher. Undergraduate. National Institute of Technology Rourkela.

Hertz, H. (1882). Uber die beruhrung fester elasticher korper (On the contact of elastic solids). *Journal Fur Die Reine Und Angewandte Mathematik*, *92*, 156-171.

Jaatinen, A., & Onnela, T. (2013). Automatic Control of Impact Crushers Based on Visual Measurement of Size Distribution. *IFAC Proceedings Volumes*, *46*(16), 214-217. doi: 10.3182/20130825-4-us-2038.00088

Ji, S., & Shen, H. (2006). Effect of Contact Force Models on Granular Flow Dynamics. Journal of Engineering Mechanics, 132(11), 1252-1259. doi: 10.1061/(asce)0733-9399(2006)132:11(1252)

Katubilwa, F., & Moys, M. (2009). Effect of ball size distribution on milling rate. *Minerals Engineering*, *22*(15), 1283-1288. doi: 10.1016/j.mineng.2009.07.008

Kasture, A., & Wadodkar, S. (2008). *A textbook of pharmaceutical chemistry - I* (pp. 5.9-5.10). Pune: Nirali Prakashan.

Ketterhagen, W., am Ende, M., & Hancock, B. (2009). Process Modelling in the Pharmaceutical Industry using the Discrete Element Method. Retrieved 2 August 2020, from https://www.researchgate.net/publication/5292467_Process_Modeling_in_the_Pharmaceutical_Industry_using_the_Discrete_Element_Method

Kgetjepe, M., & Bwalya, M. (2017). Analysis of a Scale up Theory using a 180 mm and 300 mm batch mills. *Arab Economic and Business Journal*, 1-5.

King, H. (2005). Mohs Hardness Scale: Testing the Resistance to Being Scratched. Retrieved 16 September 2020, from https://geology.com/minerals/mohs-hardness-scale.shtml

King, R. (2001). *Modelling and simulation of mineral processing systems* (1st ed., pp. 132-150). Englewood, Colo.: Butterworth-Heinemann.

Klinberg, A. (2001). *Variationer hos Materialparametrar inom ballasttillverkningen, Lic, Eng*. Dept. Civil and Environmental Engineering, Royal Institute of Technology.

King, H. (2020). Limestone: Rock Uses, Formation, Composition, Pictures. Retrieved 23 January 2020, from https://geology.com/rocks/limestone.shtml

Labra, C., Oñate Ibáñez de Navarra, E., & Rojek, J. (2012). Advances in the development of the discrete element method for excavation processes (pp. 5-14). Barcelona: International Center for Numerical Methods in Engineering.

Lameck, N., Kiangi, K., & Moys, M. (2006). Effects of grinding media shapes on load behaviour and mill power in a dry ball mill. *Minerals Engineering*, *19*(13), 1357-1361. doi: 10.1016/j.mineng.2006.01.005

Lucas, J. (2017). Force, Mass & Acceleration: Newton's Second Law of Motion. Retrieved 19 October 2020, from https://www.livescience.com/46560-newton-second-law.html

Machowski, R. (2015). Comminution: Liberation, Crushing, Grinding. Retrieved from https://www.linkedin.com/pulse/comminution-liberation-crushing-grinding-robert-machowski

Marcotte, E. (2018). What Is A Vertical Shaft Impactor (VSI) Primer? | Stedman Machine Company. Retrieved from https://www.stedman-machine.com/vsi-primer-article.html

McCabe, W., Smith, J., & Harriott, P. (1993). *Unit operations of chemical engineering*. New York: McGraw-Hill.

Michaud, D. (2013). Bond Work Index Formula-Equation. Retrieved 2 February 2020, from https://www.911metallurgist.com/blog/bond-work-index-formula-equation

Michaud, L. (2015). Crushing in Mineral Processing. Retrieved 1 August 2020, from https://www.911metallurgist.com/blog/crushing

Mindlin, R., & Deresiewicz., H. (1953). Elastic spheres in contact under varying oblique forces. *J. Appl. Mech*, *20*, 327-344.

Mohs, F. (1812). *Mohs hardness*. Presentation, Germany.

Mvula, L. (2018). *Grinding and breakage characteristics of limestone for the purposes of comminution modelling* (Undergraduate). University of the Witwatersrand.

Mwanga, A. (2014). *Test methods for characterizing ore comminution behaviour in geometallurgy* (Postgraduate). Luleå University of Technology.

Napier-Munn, T., Timothy, J., Morrell, S., Morrison, R., & Kojovic, T. (1996). *Mineral comminution circuits: their operation and optimisation* (p. 413). Indooroopilly, Qld.: Julius Kruttschnitt Mineral Research Centre, brisbane.

Ndlovu, S., Simate, G., & Matinde, E. (2017). Waste production and utilization in the metal extraction industry (1st ed., pp. 67-68). New York: CRC Press.

Nelson, S. (2015). Deformation of Rock. Retrieved 23 January 2020, from https://www.tulane.edu/~sanelson/eens1110/deform.htm

Nikolov, S. (2002). A performance model for impact crushers. Minerals Engineering, 15(10), 715-721. doi: 10.1016/s0892-6875(02)00174-7

Nikolov, S. (2004). Modelling and simulation of particle breakage in impact crushers. International Journal of Mineral Processing, 74, pp. S219-S225.

Norazirah, A., Fuad, S., & Hazizan, M. (2016). The Effect of Size and Shape on Breakage Characteristic of Mineral. *Procedia Chemistry*, *19*, 702-708. doi: 10.1016/j.proche.2016.03.073

Numbi, B., Xia, X., & Zhang, J. (2014). Optimal Energy Control Modelling of a Vertical Shaft Impact Crushing Process. *Energy Procedia*, *61*, 560-563. Doi: 10.1016/j.egypro.2014.11.1170

Nyabando, M. (2014). *Study of the Effect of Mill Liner Design on the Selection Function During Milling* (Undergraduate). University of the Witwatersrand.

Nyoni, S. (2019). *Beneficiation of low-grade Witbank coal*. Presentation, University of the Witwatersrand, Johannesburg.

Özer, C., & Whiten, W. (2012). A multi-component appearance function for the breakage of coal. *International Journal of Mineral Processing*, *104-105*, 37-44. doi: 10.1016/j.minpro.2011.11.014

Patnaik, S. and Pattnaik, B. (2007). *Design and analysis of impact crushers*. (Undergraduate). National Institute of Technology, Rourkela.

RASHID, A. (2016). *EBB 220/3 MODEL FOR VISCO-ELASTICITY*. Presentation, Universiti Sains Malaysia, Nibong Tebal, P. Pinang Malaysia.

Rumpf, H. (1973). Physikalische Aspekte des Zerkleinerns, Ähnlichkeitsgesetz derBruchmechanik und die Energieausnutzung der Einzelkornzerkleinerung. Aufbereitungstechnik, *2*, 59–71.

Sahoo, R., Weedon, D., & Roach, D. (2004). Single-particle breakage tests of Gladstone Port Authority's coal by a twin pendulum apparatus. *Advanced Powder Technology*, *15*(2), 263-280. doi: 10.1163/156855204773644472

Salman, A. (2007). *Particle breakage* (1st ed.). Amsterdam: Elsevier.

Schönert, K., Harnisch, H., Steiner, R., Winnacker, K. (Eds.). (1984). *Chemische Technologie* (1st ed., pp. 80-93). Carl Hanser Verlag, München.

Segura-Salazar, J., Barrios, G., Rodriguez, V., & Tavares, L. (2017). Mathematical modelling of a vertical shaft impact crusher using the Whiten model. *Minerals Engineering*, *111*, 222-228. doi: 10.1016/j.mineng.2017.06.022

Shi, F., & Kojovic, T. (2007). Validation of a model for impact breakage incorporating particle size effect. *International Journal of Mineral Processing*, *82*(3), 156-163. doi: 10.1016/j.minpro.2006.09.006

Sinnott, M., & Cleary, P. (2015). Simulation of particle flows and breakage in crushers using DEM: Part 2 – Impact crushers. *Minerals Engineering*, *74*, 163-177. doi: 10.1016/j.mineng.2014.11.017

Stedman Company. (2018). HSI Crusher Manufacturer | Stedman Machine Company. Retrieved from https://www.stedman-machine.com/more.html

Stedman Company. (2018). Impact Crushers & Cement Crushers - Rotor Impact Crusher | Stedman Machine Company. Retrieved from https://www.stedman-machine.com/impact-crushers.html

Stiehm, M., Wüstenhagen, C., Grabow, N., & Schmitz, K. (2016). Transient Euler-Lagrange/DEM simulation of stent thrombosis. *Current Directions in Biomedical Engineering*, *2*(1), 299. doi: 10.1515/cdbme-2016-0066

Tavares, L. (1999). Energy absorbed in breakage of single particles in drop weight testing. *Minerals Engineering*, *12*(1), 43-50. doi: 10.1016/s0892-6875(98)00118-6

Tavares, L., & King, R. (1998). Single-particle fracture under impact loading. *International Journal of Mineral Processing*, *54*(1), 1-28. doi: 10.1016/s0301-7516(98)00005-2

Taylor, L., & Preece, D. (1992). Simulation of Blasting Induced Rock Motion Using Spherical Element Models. Engineering Computations, 9(2), 243-252. doi: 10.1108/eb023863

Thakur, A. (2019). Do the brittle materials have lower tensile strength than the ductile ones?. Retrieved 22 September 2020, from https://www.researchgate.net/post/Do_the_brittle_materials_have_lower_tensile_strength_than_the_ductile_ones/5daefbc60f95f126c077c0c1/citation/download.

Unland, G., & Al-Khasawneh, Y. (2009). The influence of particle shape on parameters of impact crushing. *Minerals Engineering*, *22*(3), 220-228. doi: 10.1016/j.mineng.2008.08.008

Unland, G., Wegner, T., Nassyrov, M., (2004). Die Zerkleinerungseigenschaften von grobenEinzelpartikeln bei Prall- und Druckbelastung. Aufbereitungstechnik (5), 47–56.

van der Meer, F., & Maphosa, M. (2012). High pressure grinding moving ahead in copper, iron, and gold processing. *The Journal of the Southern African Institute of Mining and Metallurgy*, *112*, 637-647.

Verma, D., & Hatwar, P. (2014). Design of horizontal shaft impact crusher. *International Journal of Application or Innovation in Engineering*, *3*(1), 82-89.

Visioli, A. (2006). *Practical PID control*. Berlin: Springer.

Vogel, L., & Peukert, W. (2004). Determination of material properties relevant to grinding by practicable lab-scale milling tests. *International Journal of Mineral Processing*, *74*, S329-S338. doi: 10.1016/j.minpro.2004.07.018

Wegner, T., (2005). Prallzerkleinerung grober Einzelpartikel als Auslegungsgrundlage für Rotorprallbrecher. Dissertation, Technische Universität Bergakademie Freiberg.

Weichert, R. (1990). Fracture physics in comminution. *Pre-Prints, 7th European Symposium Comminution*, 3-20.

Whiten, W. (1972). The Simulation of Crushing Plants with Models Developed using Multiple Spline Regression. *JOURNAL OF THE SOUTH AFRICAN INSTITUTE OF MINING AND METALLURGY*, 257-264.

Whiten, W. and White, M. (1979). Modelling and simulation of high tonnage crushing plants. Proceedings of the 12th International Mineral Processing Congress, 2, pp.148-158.

Yang, J., Fang, H., & Luo, M. (2015). Load and wear experiments on the impact hammer of a vertical shaft impact crusher. *IOP Conference Series: Materials Science and Engineering*, *103*, 012041. doi: 10.1088/1757-899x/103/1/012041

Appendices

Appendix A: Drop weight tests data

All heights were in **cm** except the total height of the fall which has been converted to **meters** to calculate energy. For each part, 20 particles were tested and the broken attempt at which a particle was broken was listed. This was then used to determine the probability of breakage.

The energy input in this section was calculated using Equation 3.2. The steel weight height was 2.3cm, weight carrier height was 5.1cm and, Anvil or base height was 1.4cm. These parameters were the same for each particle in these tests.

-19+16mm size class breakage data

Table 1: *Breakage behaviour of Limestone particle size 1 at height 1*

Broken at attempt no.	Height of the weight (cm)	Particle height (cm)	Total height of the fall (h) (m)	Energy for each Particle (J)
1	22,2	1,8	0,116	1,832116
3		1,4	0,12	1,895292
0		1,4	0,12	1,895292
4		1,8	0,116	1,832116
0		1,9	0,115	1,816322
1		1,4	0,12	1,895292
1		1,3	0,121	1,911086
1		1,3	0,121	1,911086
0		2	0,114	1,800527
4		1,8	0,116	1,832116
1		1,1	0,123	1,942674
1		1,5	0,119	1,879498
1		1	0,124	1,958468
3		1,6	0,118	1,863704
1		1,4	0,12	1,895292
2		1,2	0,122	1,92688
1		1,2	0,122	1,92688
2		1,4	0,12	1,895292
2		1,9	0,115	1,816322
0		1,8	0,116	1,832116
			Average energy (J) = 1,877918	

***Table 2**: Particle size 1 at height 1 probability of breakage*

No. Attempts	Probability of breakage
1	0,45
2	0,6
3	0,7
4	0,8
5	0,8

***Table 3**: Breakage behaviour of particle size 1 at height 2*

Broken at attempt no.	Height of the weight (cm)	Particle height (cm)	Total height of the fall (h) (m)	Energy for each Particle (J)
4	30,2	1,8	0,196	3,095644
1		1,8	0,196	3,095644
1		1,5	0,199	3,143026
1		1,4	0,2	3,15882
1		1	0,204	3,221996
1		1,4	0,2	3,15882
0		1,7	0,197	3,111438
0		2	0,194	3,064055
1		1	0,204	3,221996
3		1,6	0,198	3,127232
1		1,5	0,199	3,143026
1		1,1	0,203	3,206202
2		1,2	0,202	3,190408
1		1	0,204	3,221996
2		1,9	0,195	3,07985
1		1,5	0,199	3,143026
1		1,6	0,198	3,127232
0		1,9	0,195	3,07985
1		1,4	0,2	3,15882
1		1,2	0,202	3,190408
			Average Energy (J) = **3,146974**	

***Table 4**: Particle size class 1 at height 2 probability of breakage*

No. Attempts	Probability of breakage
1	0,65
2	0,75
3	0,8
4	0,85
5	0,85

-13.2+11.2mm size class breakage data

***Table 5**: Breakage behaviour of Limestone particle size at height 2*

Broken at attempt no.	Height of the weight (cm)	Particle height (cm)	Total height of the fall (h) (m)	Energy for each Particle (J)
1	30,2	0,8	0,206	3,253585
2		1,1	0,203	3,206202
1		1,3	0,201	3,174614
1		0,9	0,205	3,237791
1		1,4	0,2	3,15882
1		0,9	0,205	3,237791
1		1	0,204	3,221996
0		1,6	0,198	3,127232
4		1	0,204	3,221996
1		0,9	0,205	3,237791
1		0,8	0,206	3,253585
1		1	0,204	3,221996
3		1,3	0,201	3,174614
1		0,9	0,205	3,237791
1		1,1	0,203	3,206202
1		1,1	0,203	3,206202
1		1	0,204	3,221996
3		1,1	0,203	3,206202
1		1	0,204	3,221996
1		1	0,204	3,221996
			Average Energy (J) = **3,21252**	

***Table 6**: Particle size 2 at height 2 probability of breakage*

No. Attempts	Probability of breakage
1	0,75
2	0,8
3	0,9
4	0,95
5	0,95

***Table 7**: Breakage behaviour of Limestone particle size 2 at height 3*

Broken at attempt no.	Height of the weight (cm)	Particle height (cm)	Total height of the fall (h) (m)	Energy for each Particle (J)
0	14,2	1,4	0,04	0,631764
0		1,4	0,04	0,631764
1		1,3	0,041	0,647558
1		0,6	0,048	0,758117
2		0,9	0,045	0,710735
4		1	0,044	0,69494
0		1,2	0,042	0,663352
1		0,9	0,045	0,710735
3		0,9	0,045	0,710735
1		0,8	0,046	0,726529
1		1,2	0,042	0,663352
0		1,1	0,043	0,679146
2		1	0,044	0,69494
3		1,4	0,04	0,631764
5		1	0,044	0,69494
1		1,1	0,043	0,679146
0		0,8	0,046	0,726529
1		1	0,044	0,69494
5		1,1	0,043	0,679146
0		1,2	0,042	0,663352
			Average Energy (J) = **0,684674**	

***Table 8**: Particle size class 2 at height 3 probability of breakage*

No. Attempts	Probability of breakage
1	0,35
2	0,45
3	0,55
4	0,6
5	0,7

-9.5+6.7mm size class breakage data

***Table 9**: Breakage behaviour of Limestone particle size class 3 at height 1*

Broken at attempt no.	Height of the weight (cm)	Particle height (cm)	Total height of the fall (h) (m)	Energy for each Particle (J)
1	22,2	0,9	0,125	1,974263
1		0,7	0,127	2,005851
2		0,7	0,127	2,005851
1		0,8	0,126	1,990057
1		0,6	0,128	2,021645
1		0,8	0,126	1,990057
1		1	0,124	1,958468
1		0,8	0,126	1,990057
1		0,8	0,126	1,990057
1		0,5	0,129	2,037439
1		0,5	0,129	2,037439
1		0,8	0,126	1,990057
2		0,7	0,127	2,005851
1		1	0,124	1,958468
1		0,6	0,128	2,021645
1		0,9	0,125	1,974263
1		0,6	0,128	2,021645
1		0,9	0,125	1,974263
2		0,6	0,128	2,021645
1		0,5	0,129	2,037439
			Average Energy (J) = **2,000323**	

***Table 10**: Particle size class 3 at height 1 probability of breakage*

No. Attempts	Probability of breakage
1	0,85
2	1
3	1
4	1
5	1

***Table 11**: Breakage behaviour of Limestone particle size class 3 at height 3*

Broken at attempt no.	Height of the weight (cm)	Particle height (cm)	Total height of the fall (h) (m)	Energy for each Particle (J)
3	14,2	0,8	0,046	0,726529
3		0,5	0,049	0,773911
1		0,7	0,047	0,742323
3		0,8	0,046	0,726529
1		0,9	0,045	0,710735
1		0,8	0,046	0,726529
1		0,9	0,045	0,710735
1		0,6	0,048	0,758117
2		1	0,044	0,69494
1		0,7	0,047	0,742323
4		1	0,044	0,69494
2		0,9	0,045	0,710735
1		0,7	0,047	0,742323
3		0,9	0,045	0,710735
1		0,5	0,049	0,773911
1		0,9	0,045	0,710735
5		0,8	0,046	0,726529
3		0,8	0,046	0,726529
4		0,9	0,045	0,710735
4		0,7	0,047	0,742323
			Average Energy (J) = **0,728108**	

***Table 12**: Particle size class 3 at height 3 probability of breakage*

No. Attempts	Probability of breakage
1	0,45
2	0,55
3	0,6
4	0,95
5	1

Drop weight probability of breakage parameters modelling

This was conducted by fitting the probability of breakage model equation presented by Equation 2.49 in Chapter 2, 2.3.3 on experimental data to obtain model parameters.

***Table 13**: Modelling probability of breakage data for size class -19+16mm*

-19+16mm					
No. Attempts	Probability of breakage (experiment)		Mass (x) (g)	Probability of breakage (Model)	
Energy (J)	1,88	3,15		1.88	3.15
1	0,45	0,65	10,378	0,442914098	0,625647876
2	0,45	0,75		0,604686607	0,789588402
3	0,45	0,8		0,703484795	0,870189077
4	0,45	0,85		0,770593956	0,915638173
5	0,45	0,85		0,818780636	0,943223794

***Table 14**: Modelling probability of breakage data for size class -13.2+11.2mm*

-13.2 +11.2mm					
No. Attempts	Probability of breakage (Experiment)		Mass (x) (g)	Probability of breakage (Model)	
Energy (J)	0,68	1,95		0,728	2
1	0,35	0,75	3,52	0,29818988	0,640055206
2	0,45	0,8		0,42977109	0,802288859
3	0,55	0,85		0,520866083	0,880355055
4	0,6	0,9		0,589789588	0,92357188
5	0,7	1		0,644344917	0,949370433

***Table 15**: Modelling probability of breakage data for size class -9.5+6.7mm*

-9.5+6.7mm					
No. Attempts	Probability of breakage (Experiment)		Mass (x) (g)	Probability of breakage (Model)	
Energy (J)	0,73	2		0,73	2
1	0,45	0,85	0,995	0,503481267	0,853997315
2	0,55	1		0,67065962	0,95275271
3	0,6	1		0,76655798	0,981651105
4	0,95	1		0,828283461	0,992109821
5	1	1		0,870501141	0,996366697

The data from Tables 13 to 15 was used to find the probability of breakage parameters for limestone shown in Table 4.4 in Chapter 4, 4.1.2. Sum of squares and the excel solver function were used on the data above to find model parameters.

The data below was used to plot Figure 4. In Chapter 4, 4.1.2. The data shows the probability of breakage between quartz and limestone.

Table 16: *probability of breakage between quartz and limestone with E = 1.8J and n = 1*

Mass (g)	Probability of breakage	
	Limestone (Mokgomola, 2018)	Quartz (Nyoni, 2019)
4	0,830830286	0,618671033
6	0,866070179	0,743360988
8	0,88856062	0,818319625
10	0,904459467	0,867027802
12	0,916411826	0,900292199

Appendix B: Ball milling data

Mass distribution and selection function data for ball milling

This included mass retained and the logarithm of the mass retained which were plotted against time to find the slope used to determine the selection function. The equation used to find selection function using slope has been presented by Equation 2.42.

-6.7+4.75mm mass distribution and selection function data

Table 17: *-6.7+4.75mm selection function mass distribution*

-6.7+ 4.75mm				
Time (min)	0,5	1	2	4
Aperture size (mm)	Mass retained (g)			
4,75	267,76	136,04	95,48	38,86
3,35	29,98			28,34
2,8	7,11			10,12
1,4	10,74			32,96
1	1,84			17,78
0,85	0,98			8,7
Pan	6,77	164,64	207,84	151,53
Sieve sample (g)	325	301	304	289
Product mass (g)	1220	1216	1208	

Table 18*: -6.7+4.75mm selection function graph data*

Time (min)	Ln ((retained mass)/ (Sampled mass))
0,5	0,966504153
1,5	0,860847037
3,5	0,797427796
7,5	0,645903608

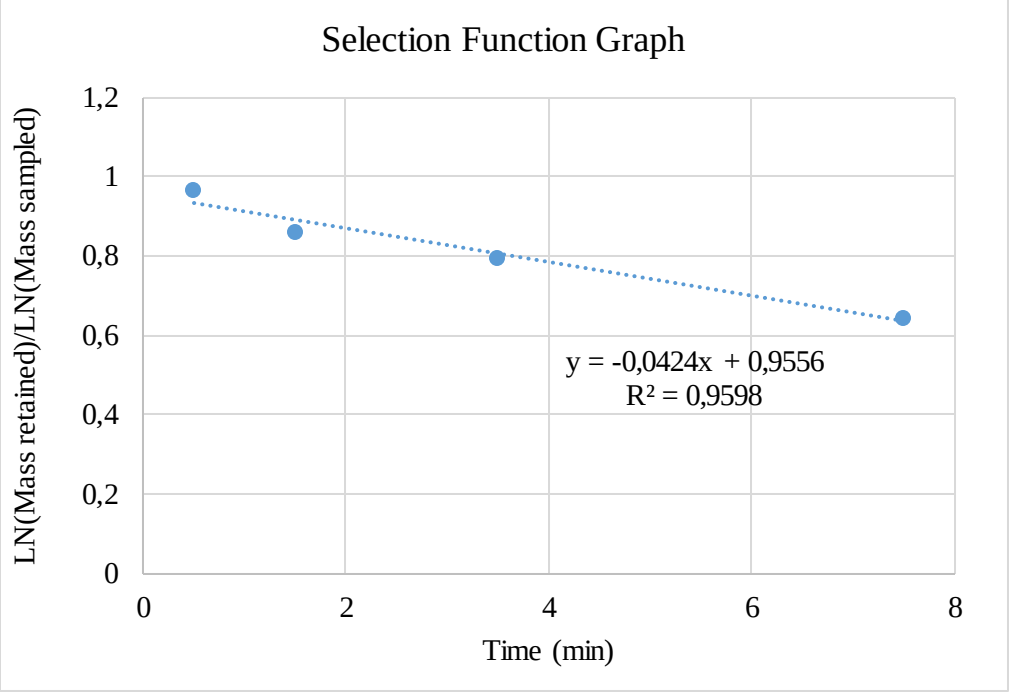


Figure 1: *Selection function graph for -6.7+4.75mm*

-3.35 + 2.8mm mass distribution and selection function data

Table 19*: -3.35+2.8mm ball milling mass distribution*

-3.35 + 2.8mm				
Time (min)	0,5	1	2	4
Aperture size (mm)	Mass retained (g)			
2,8	59,23	30,77	15,81	3,43
1,4	45,23			19,43
1	5,47			11,2
0,85	1,96			5,88
0,6	3,26			14,19
0,5	1,42			8,17
Pan	5,15	87,05	101,23	51,13
Sieve sample (g)	122	118	117	114
Product mass (g)	1220	1197	1175	1143

***Table 20**: -3.35+2.8mm selection function graph data*

Time (min)	Ln ((retained mass)/ (Sampled mass))
0,5	0,849585822
1,5	0,718249153
3,5	0,579702188
7,5	0,260242529

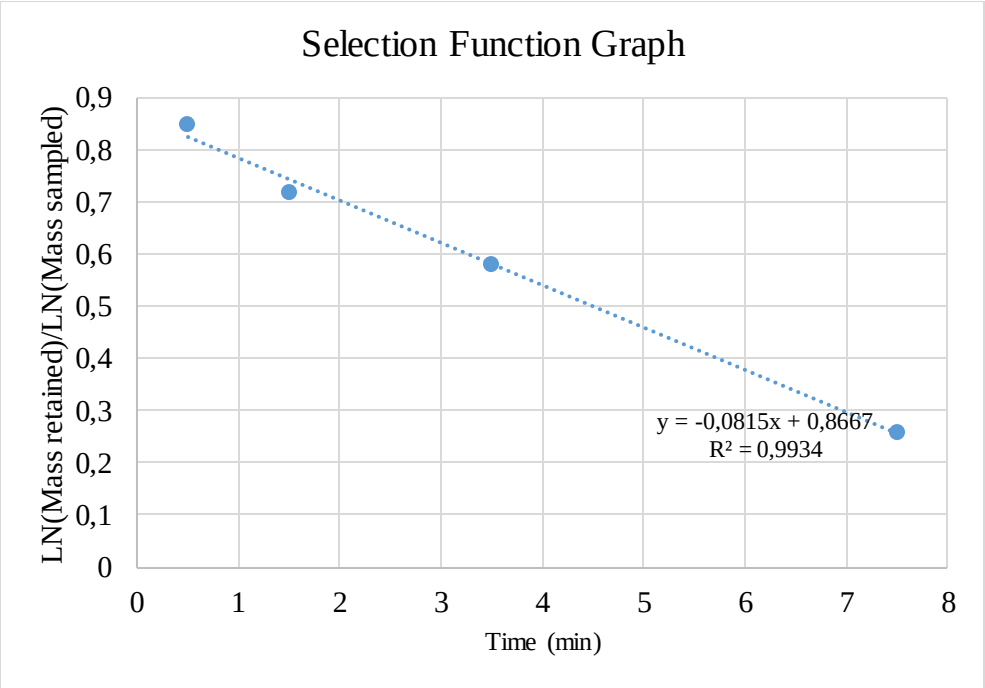


***Figure 2**: Selection function graph for -3.35+2.8mm*

-1.4+ 1.0mm mass distribution and selection function data

Table 21*: -1.4+1.0mm ball milling mass distribution*

-1.4 + 1.0mm				
Time (min)	0,5	1	2	4
Aperture size (mm)	Mass retained (g)			
1	78,38	63	33,37	9,09
0,85	21,79			11,14
0,6	10,14			25,42
0,5	2,72			13,6
0,355	2,72			17,51
0,3	0,96			7,06
Pan	3,12	46	83,48	33,5
Sieve sample (g)	120	119	117	118
Product mass (g)	1218	1211		

Table 22*: -1.4+1.0mm selection function graph data*

Time (min)	Ln ((retained mass)/ (Sampled mass))
0,5	0,911034217
1,5	0,866923555
3,5	0,736566396
7,5	0,462653703

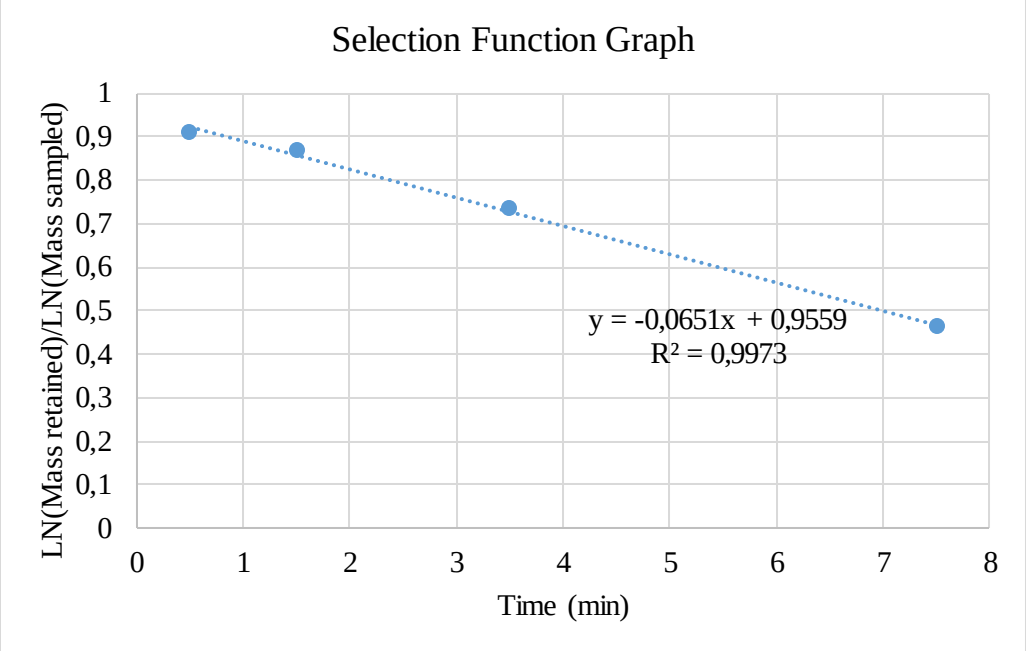


***Figure 3**: Selection function graph for -1.4+1.0mm*

-0.85+ 0.6mm mass distribution and selection function data

***Table 23**: -0.85+0.6mm ball milling mass distribution*

-0.85 + 0.60mm				
Time (min)	0,5	1	2	4
Aperture size (mm)	Mass retained (g)			
0,6	84,37	73,79	49,23	21,1
0,5	28,31			23,69
0,355	8,25			27,1
0,3	1,56			9,62
0,25	0,94			8,09
0,18	1,28			11,82
Pan	1,61	44,56	69,24	20,09
Sieve sample (g)	126	118	118	122
Product mass (g)	1218	1213	1202	1182

***Table 24**: -0.85+0.6mm selection function graph data*

Time (min)	Ln ((retained mass)/ (Sampled mass))
0,5	0,917070587
1,5	0,901594542
3,5	0,816759753
7,5	0,634733489

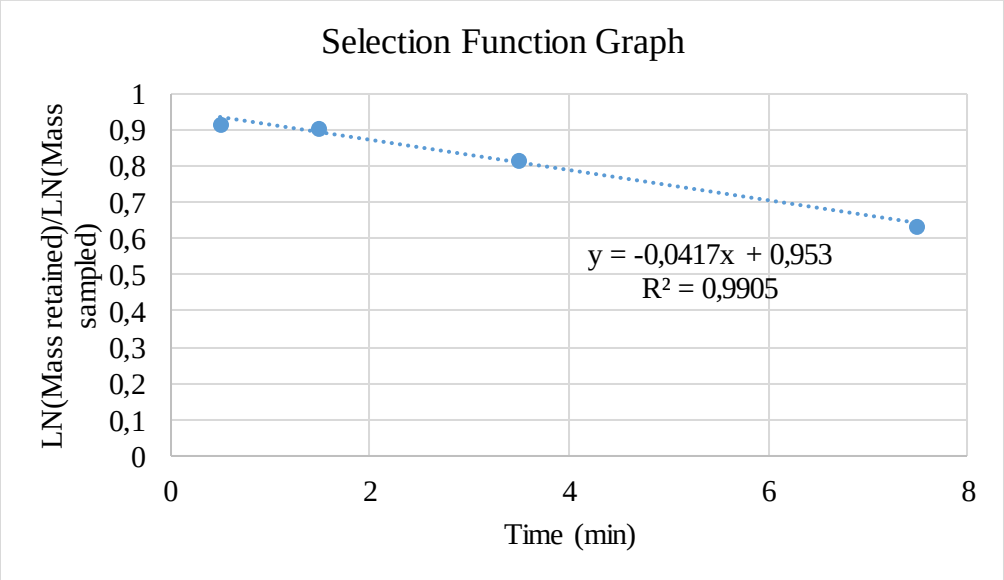


***Figure 4**: Selection function graph for -0.85+0.6mm*

-0.30+ 0.212mm mass distribution and selection function data

***Table 25**: -0.30+0.212mm ball milling mass distribution*

-0.3+ 0.212mm				
Time (min)	0,5	1	2	4
Aperture size (mm)	Mass retained (g)			
0,212	78,54	68,73	60,51	49,91
0,18	17,18			17,79
0,15	9,77			14,69
0,106	6,31			14,04
0,075	3,64			7,94
0,053	2,51			6,4
Pan	2,63	46,01	54,24	9,54
Sieve sample (g)	121	115	115	121
Product mass (g)	1216	1204	1177	1157

***Table 26**: -0.30+0.212mm selection function graph data*

Time (min)	Ln ((retained mass)/ (Sampled mass))
0,5	0,90988295
1,5	0,891516606
3,5	0,864671723
7,5	0,815344487

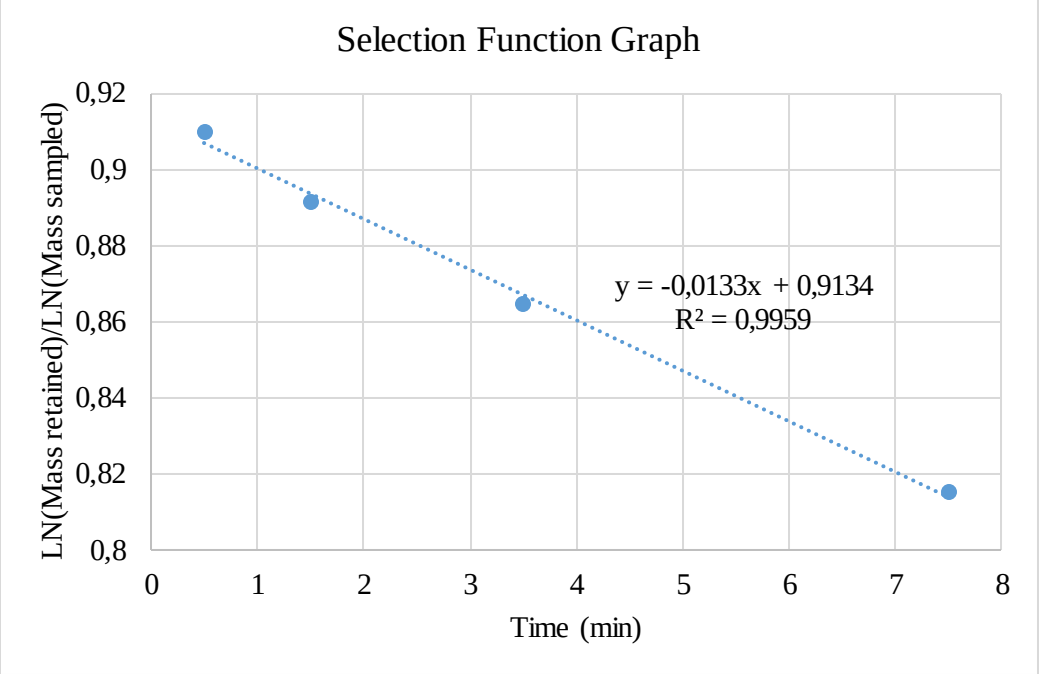


***Figure 5**: Selection function graph for -0.30+0.212mm*

Breakage function data

Breakage function data for all size classes

This is for size classes -6.7 + 4.75mm, -3.25+2.8mm, -1.4 + 1.00mm, -0.85 + 0.600mm, and -0.3 + 0.212mm of quartz. This data was used to find the breakage function model parameters and to determine the breakage function of quartz across various size classes. A size lass of -13.2+9.5mm results have been presented in Chapter 4, 4.2.2 as an example to show the breakage function behaviour of quartz. The model parameters found using these results have been presented in Table 4.15 in Chapter 4, 4.2.2.1.

Table 27: *Cumulative breakage function experimental and model data for size class - 6.7+4.75mm*

- 6.7 + 4.75mm								
Size class (mm)		Time (min)	0,5					
Upper size	Lower size	Aperture size (mm)	Mass retained (g)	% Mass retained	% Cumulative passing	Normalized size	Breakage function (Bi,1) (Exp)	Breakage function (Bi,1) (MOD)
	6,7			0	100			
6,7	4,75	2,8	267,58	82,33231	17,66769			
4,75	3,35	1,4	29,98	9,224615	8,443077	1	1	1
3,35	2,8	1	7,11	2,187692	6,255385	0,70895522	0,453736	0,47307559
2,8	1,4	0,85	10,74	3,304615	2,950769	0,5	0,332272	0,26410127
1,4	1	0,6	1,84	0,566154	2,384615	0,41791045	0,154068	0,21068704
1	0,85	0,5	0,98	0,301538	2,083077	0,20895522	0,124147	0,12269794
0,85	Pan	Pan	6,77	2,083077	0	0,14925373	0,108282	0,10426431
		Sieve sample (g)	325					

Tables 26 to 29 show the mass retained from experimental data after 0.5 minutes. This mass retained was used to calculate the breakage function and an empirical model was used to fit the experimental data. All these have been presented in these tables. Using sum of squares and the solver function to reduce the error between experimental data and model data, the model parameters were determined and were presented in Table 4.15.

***Table 28**: Cumulative breakage function experimental and model data for size class -3.35+2.8mm*

-3.35+2.8mm								
Size class		Time (min)	0,5					
Upper size	lower size	Aperture size (mm)	Mass retained (g)	% Mass retained	% Cumulative passing	Normalized size	Breakage function (Bi,1) (Exp)	Breakage function (Bi,1) (MOD)
	3,35			0	100			
3,35	2,8	2,8	59,23	48,54918	51,45082			
2,8	1,4	1,4	45,51	37,30328	14,14754	1	1	1
1,4	1	1	5,47	4,483607	9,663934	0,8358209	0,211101	0,215605325
1	0,85	0,85	1,96	1,606557	8,057377	0,41791045	0,140651	0,129865484
0,85	0,6	0,6	3,26	2,672131	5,385246	0,29850746	0,116256	0,101550312
0,6	0,5	0,5	1,42	1,163934	4,221311	0,25373134	0,076609	0,090175785
0,5	Pan	Pan	5,15	4,221311	0	0,17910448	0,059688	0,069906994
		Sieve sample (g)	122					

***Table 29**: Cumulative breakage function experimental and model data for size class -0.85+0.60mm*

-0.85 + 0.60								
Size class		Time (min)	0,5					
Upper size (mm)	Lower size (mm)	Aperture size (mm)	Mass retained (g)	% Mass retained	% Cumulative passing	Normalized size	Breakage function (Bi,1) (Exp)	Breakage function (Bi,1) (MOD)
	0,85			0	100			
0,85	0,6	0,6	84,12	66,7619	33,2381			
0,6	0,5	0,5	28,28	22,44444	10,79365	1	1	1
0,5	0,355	0,355	8,21	6,515873	4,277778	0,70588235	0,282691	0,263443785
0,355	0,3	0,3	1,56	1,238095	3,039683	0,58823529	0,108207	0,142368
0,3	0,25	0,25	0,94	0,746032	2,293651	0,41764706	0,0764	0,060862967
0,25	0,18	0,18	1,28	1,015873	1,277778	0,35294118	0,057429	0,04776624
0,18	Pan	Pan	1,61	1,277778	0	0,29411765	0,031829	0,040871271
		Sieve sample (g)	126					

***Table 30**: Cumulative breakage function experimental and model data for size class -0.3+0.212mm*

-0.3+ 0.212								
Size class		Time (min)	0,5					
Upper size	lower size	Aperture size (mm)	Mass retained (g)	% Mass retained	% Cumulative passing	Normalized size	Breakage function (Bi,1) (Exp)	Breakage function (Bi,1) (MOD)
	0,3			0	100			
0,3	0,212	0,212	78,62	64,97521	35,02479			
0,212	0,18	0,18	17,28	14,28099	20,7438	1	1	1
0,18	0,15	0,15	9,85	8,140496	12,60331	0,70666667	0,539202	0,473230288
0,15	0,106	0,106	6,32	5,22314	7,380165	0,6	0,312439	0,332612141
0,106	0,075	0,075	3,64	3,008264	4,371901	0,5	0,177814	0,224548635
0,075	0,053	0,053	2,58	2,132231	2,239669	0,35333333	0,103681	0,106263215
0,053	Pan	Pan	2,71	2,239669	0	0,25	0,052535	0,050422089
		Sieve sample (g)	121					

a